HEAT TRANSFER AND PRESSURE DROP IN TAPE GENERATED SWIRL FLOW

Robert F. Lopina
Arthur E. Bergles

DSR 70281-47

Engineering Projects Laboratory
Department of Mechanical Engineering
Massachusetts Institute of Technology

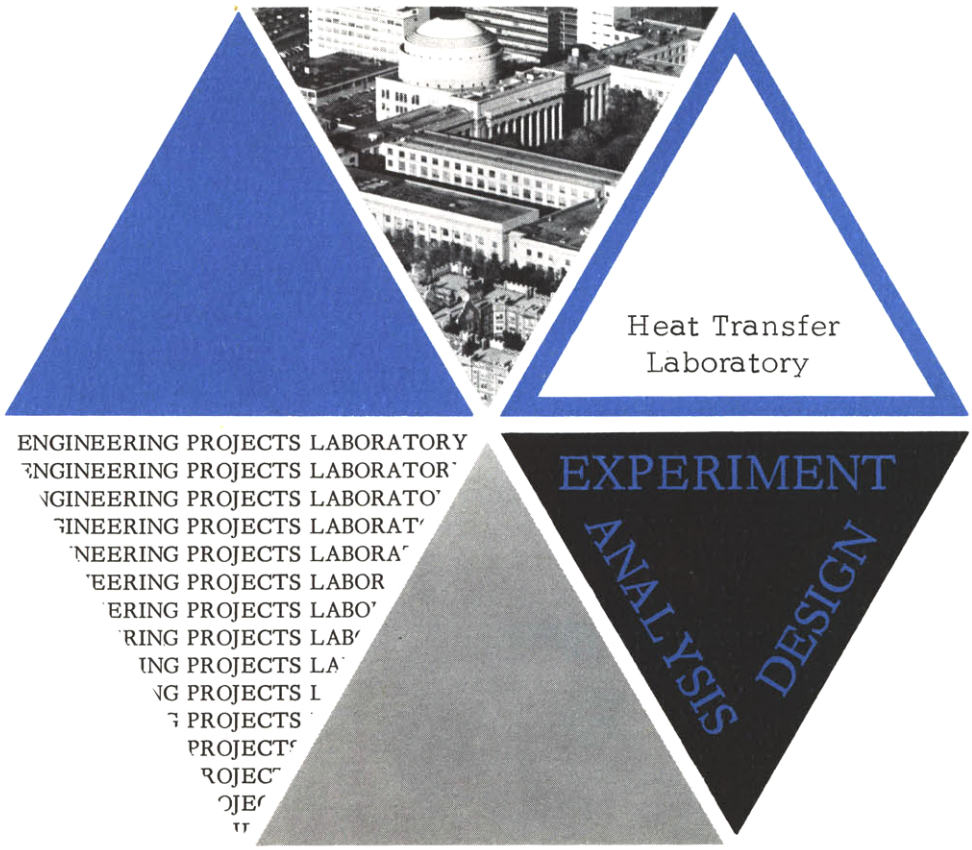

TECHNICAL REPORT NO. 70281-47

HEAT TRANSFER AND PRESSURE DROP IN TAPE GENERATED SWIRL FLOW

by

Robert F. Lopina
Arthur E. Bergles

for

Massachusetts Institute of Technology

National Magnet Laboratory

Sponsored by the Solid State Sciences Division

Air Force Office of Scientific Research (OAR)

Air Force Contract F44620-67-C-0047

D.S.R. Project No. 70281

June, 1967

Department of Mechanical Engineering

Massachusetts Institute of Technology

Cambridge, Massachusetts 02139

ABSTRACT

The heat transfer and pressure drop characteristics of water in tape generated swirl flow were investigated. The test sections were electrically heated small diameter nickel tubes with tight fitting full length Inconel tapes of twist ratios from 2.48 to 9.2 inside diameters/180° of tape twist. Heat transfer coefficients and friction factors were determined for non-boiling forced convection heating and cooling while overall pressure drop information and curves of heat flux versus wall superheat were determined for surface boiling conditions.

Improvements in heat transfer for equal flow rates of up to 85% were observed for the non-boiling swirl flows with heating, but the improvement with cooling was substantially less. Compared on the basis of equal pumping power, improvements in heat transfer of up to 35% were observed for the tighter tape twists. A method for predicting the heat transfer coefficient for non-boiling swirl flows was developed. It was based upon the theory that the improvement was due primarily to: 1) the increased flow path created by the tape, 2) the increased circulation created with heating due to the buoyancy effect set up by the large centrifugal force present, and 3) the fin effect of the tape. The experimental results of this and previous swirl flow investigations were in good agreement with the analytical prediction.

The surface boiling characteristics of swirl flow were found to be similar to those observed in straight flow. The boiling curves for various velocities were asymptotic to a fully developed line at high wall superheats, and the visually observed point of incipient boiling and the transition to the fully developed boiling asymptote were predictable by conventional straight flow methods. It was concluded, therefore, that the dominant surface boiling heat transfer mechanism was similar for both swirl and straight flow.

For non-boiling swirl flows, the decrease in the pressure drop with heating was slightly less than is usual with straight flows, while the increase in the pressure drop with surface boiling was substantially less. A method for predicting the difference in each case is presented.

Acknowledgments

This study was supported by the National Magnet Laboratory of the Massachusetts Institute of Technology which is sponsored by the Solid State Sciences Division of the Air Force Office of Scientific Research.

Professors Peter Griffith, George S. Springer, and John S. Maulbetsch gave generously of their time to discuss various aspects of the program throughout the investigation. The recommendations of Professor Warren M. Rohsenow and of Mr. Michael G. Cooper, visiting lecturer from Cambridge University, are also gratefully acknowledged.

The tubes were redrawn over the twisted tapes by Mr. Fred French of the F. W. French Tube Co., and Mr. Fred Johnson of the M.I.T. Heat Transfer Laboratory assisted with construction details. Machine computations were done on the IBM 7094 Computer at the M.I.T. Computation Center.

Miss Peg Bradley typed the final manuscript.

R. F. Lopina's studies at M.I.T. have been supported by the United States Air Force Institute of Technology and the Air Force Academy.

We wish to express our thanks to all concerned.

TABLE OF CONTENTS

	Page
TITLE PAGE	i
ABSTRACT	ii
ACKNOWLEDGMENTS	iii
TABLE OF CONTENTS	iv
LIST OF FIGURES	vi
NOMENCLATURE	viii
CHAPTER I: INTRODUCTION	
1.1 General Description of Augmentative Techniques	1
1.2 Previous Research on Tape Generated Swirl Flow	3
1.2.1 Forced Convection Heat Transfer	7
1.2.2 Boiling Heat Transfer	12
1.2.3 Pressure Drop and Friction Factors	14
1.3 Purpose of Study	15
CHAPTER II: EXPERIMENTAL PROGRAM	16
2.1 Scope of Research	16
2.2 Description of the Test Loop	17
2.2.1 Hydraulic System	18
2.2.2 Power Supply	19
2.2.3 Instrumentation	20
2.3 Description of the Test Sections	23
2.3.1 Test Section for Heating of Swirl Flows	23
2.3.2 Visual Exit Section for Surface Boiling Observations	25
2.3.3 Test Section for Cooling of Swirl Flows	26
2.3.4 Insulated Tape Test Section	26
2.4 Experimental Procedure	27
2.4.1 General Loop Operation	27
2.4.2 Operating Procedure for Heating Runs	28
2.4.3 Operating Procedure for Cooling Runs	29
2.5 Data Reduction Procedure	29
2.5.1 Heating Runs	29
2.5.2 Cooling Runs	30
CHAPTER III: PRESENTATION AND DISCUSSION OF NON-BOILING FORCED CONVECTION HEAT TRANSFER RESULTS	32
3.1 Observed Effects	32
3.1.1 Tape Twist Effect on the Heat Transfer Coefficient	32
3.1.2 Effect of Variations in ΔT_f on the Heat Transfer Coefficient	33

Errata for 70281-47

p. 32 Third line from bottom: Eq. (4) should be Eq. (3)

p. 33 Second line: Eq. (4) should be Eq. (3)

p. 49 Second paragraph, first line: Fig. 25 should be Fig. 23

p. 51 Eq. (32) should read

$$(q/A)_{inc} = 15.60\ P^{1.156}\ (T_w - T_{sat})^{2.30}\ P^{-0.0234}$$

p. 68 Third paragraph, first line: Eq. (35) should be Eq. (39)

Fourth paragraph, first line: Eq. (51) should be Eq. (59)

p. 70 Fourth line from bottom: Fig. 32 should be Fig. 33

p. 71 Fifth line: y = 1.18 should be y = 1.81

p. 83 Sixth line: Eq. (1.9) should be Eq. (1.10)

p. 87 Eighth line from bottom: Fig. 3 should be Fig. 7

p. 92 Listing of functional relations, q/A, etc. should be indicated as (3.1)

p. 94 Second line from bottom: Eq. (3.6) should be Eq. (3.9)

Fig. 28 Ref. 5 should be Ref. 6

3.1.3 Difference Between Average and Local Nusselt Numbers 34
3.1.4 Effect on the Heat Transfer of Heating Versus Cooling 34
3.1.5 Fin Effect of the Tape 35
3.1.6 Tube Wall Temperature Variation with Length 36
3.2 Formulation of Prediction Method 39
3.3 Application of the Prediction Method 45
3.3.1 Data of this Investigation 45
3.3.2 Water Data of Other Investigations 45
3.3.3 Air Data of Other Investigations 47

CHAPTER IV: PRESENTATION AND DISCUSSION OF SURFACE BOILING HEAT TRANSFER RESULTS 49
4.1 Comparison of Boiling in Swirl and Straight Flow 49
4.2 Inception of Boiling 50
4.3 Effect of Peripheral Pressure Variations on Inception 52
4.4 Transition to Fully Developed Boiling 53
4.5 Probable Heat Transfer Mechanism with Fully Developed Surface Boiling 54

CHAPTER V: PRESENTATION AND DISCUSSION OF PRESSURE DROP RESULTS 56
5.1 Contributions to the Total Pressure Drop for Swirl Flow 56
5.2 Non-Boiling Friction Factors 58
5.3 Surface Boiling Pressure Drop 62

CHAPTER VI: CONSTANT PUMPING POWER COMPARISON 68

CHAPTER VII: CONCLUSIONS 72
7.1 Non-Boiling 72
7.2 Surface Boiling 73

REFERENCES 74

APPENDIX 1 Basic Swirl Flow Equations 81

APPENDIX 2 Details of Data Calculation Procedure 86

APPENDIX 3 Error Analysis 92

APPENDIX 4 Derivation of Fin Effect Equations 97

APPENDIX 5 A Note on the Definition of the Heat Transfer Coefficient 102

FIGURES 105

LIST OF FIGURES

Fig.

1 Schematic Layout of Experimental Facility

2 Typical Test Section for the Heating of Swirl Flows

3 Visual Exit Section for Surface Boiling Observations

4 Counterflow Heat Exchanger for the Cooling of Swirl Flows

5 Computer Printout for a Typical Run

6 Wilson Plot for Cooling Data Reduction

7 Temperature Dependence of Resistivity for Nickel Tubing

8 Temperature Dependence of Thermal Conductivity for Nickel Tubing

9 Average Nusselt Numbers for Heating with Swirl and Straight Flows

10 Average Nusselt Numbers for Heating with Swirl Flow

11 Local Nusselt Numbers for Heating

12 Average Nusselt Numbers for Cooling

13 Dependence of Heat Transfer Coefficient on Temperature Difference

14 Experimental Determination of the Tape Fin Effect

15 Theoretical Prediction of the Tape Fin Effect

16 Comparison of Average Nusselt Numbers for Insulated and Non-Insulated Twisted Tapes

17 Tube Wall Temperature Profiles for Various Heat Fluxes

18 Graphical Representation of the Swirl Flow Heat Transfer Prediction Method

19 Comparison of Predicted and Observed Average Nusselt Numbers

20 Comparison of the Experimental and Predicted Nusselt Numbers for the Water Data of Smithberg and Landis (10)

21 Comparison of the Experimental and Predicted Nusselt Numbers for the Air Data of Smithberg and Landis (10)

22 Comparison of the Experimental and Predicted Nusselt Numbers for the Air Data of Koch (9)

23 Surface Boiling Data for Water in Swirl Flow, $y = 3.15$

24 Heat Flux versus Wall Superheat, $y = 2.48$

25 Composite of Fully Developed Surface Boiling Data

26 Typical Peripheral Pressure Variation

27 Nonboiling Friction Factors for Isothermal and Heated Conditions

28 Comparison of Isothermal Swirl Flow Friction Factors

29 Correlation of Isothermal Swirl Flow Friction Factors

30 Overall Pressure Drop for Surface Boiling of Water in Swirl Flow

31 Comparison of the Surface Boiling Pressure Drop for Swirl and Straight Flow

32 Constant Pumping Power Performance of Present Swirl Flow Systems

33 Constant Pumping Power Comparison Including Data of Previous Investigations

NOMENCLATURE

a = centrifugal acceleration

A = area

A_c = flow cross sectional area

A_x = tube cross sectional area

B = fin constant defined in Eq. (4.15)

c_p = specific heat at constant pressure

d = density in Eq. (2.7)

D = diameter

D_h = hydraulic diameter

E = test section voltage

f = Fanning friction factor

F = fin effect multiplier

g = local acceleration of gravity

g_c = gravitational constant

G = mass velocity

h = heat transfer coefficient

I = test section current

k = thermal conductivity

k_o = thermal conductivity at 0°F

L_h = axial heated length

L_p = axial length between pressure taps

m = fin constant defined in Eq. (4.11)

P = pressure

Q = volume flow rate (w/ρ)

q = rate of heat transfer

q_{cc} = centrifugal convection heat transfer rate

q_f = fin heat transfer rate

q_{sc} = spiral convection heat transfer rate

q/A = heat flux

r = radius

R = electrical resistance of test section

R = gas constant

T = temperature

U = overall heat transfer coefficient

V_a = mean axial fluid velocity

V_s = resultant swirl velocity at tube wall

V_t = tangential fluid velocity

W_x = uncertainty in an arbitrary quantity

w = mass flow rate

Wi = internal heat generation rate per unit volume

y = tape twist ratio = inside diameters/180° of tape twist

α = geometric parameter defined by Eq. (1.7)

α_k = temperature coefficient of thermal conductivity

α_ρ = temperature coefficient of electrical resistivity

β = volumetric coefficient of thermal expansion

γ = fin effect parameter

ΔT_f = wall minus bulk temperature difference

ΔT_{sat} = wall superheat

ΔT_{sub} = degrees of subcooling

δ_f = tape thickness

δ_w = tube wall thickness

ϵ = material roughness

ϵ = fin parameter defined by Eq. (4.17)

ρ = fluid density

ρ = electrical resistivity

ρ_o = electrical resistivity at 0°F

μ = dynamic viscosity

ν = kinematic viscosity

DIMENSIONLESS GROUPS

Nu = Nusselt number = hD/k

Pr = Prandtl number = $c_p\mu/k$

Re = Reynolds number = $G\,D/\mu$

Gr = Grashof number = $\dfrac{V_s^2 \beta \Delta T_f D_h^3}{r_i \nu^2}$

SUBSCRIPTS

a = straight tube condition

adb = adiabatic condition

B = boiling condition

b = bulk fluid condition

cc = centrifugal convection

ex = test section exit condition

f = tape characteristic

FC = non-boiling forced convection condition

h = based on the hydraulic diameter

h = based on the heated length

i = inside tube condition

in = test section inlet condition

inc = incipient boiling condition

iso = isothermal condition

NB = non-boiling condition

o = outside tube condition

o = constant power straight flow condition

P = constant power comparison

s = swirl flow condition

sat = saturated fluid condition

sc = spiral convection

t = tangential

w = tube wall characteristic

x = local condition at a point

All fluid properties are evaluated at the bulk temperature unless otherwise indicated.

Chapter I

INTRODUCTION

1.1 General Description of Augmentative Techniques

In recent years, the requirement for more efficient heat transfer systems has stimulated interest in augmentative heat transfer methods. Artificially roughened surfaces, extended surfaces, inlet vortex generators, vibration of the surface or fluid, application of electrostatic fields, and the insertion in tubes of objects such as twisted tapes, coiled wire or spinners are a few examples of such augmentative techniques. Existing systems can often be improved by using an augmentative method, while in other applications, such as the design of heat exchangers for use in space vehicles, an augmentative scheme may be mandatory in order for the system to function properly in a zero gee environment, and meet the size limitations imposed. Increases in cost, weight, and pumping power are frequently associated with a given augmentative method, and the designer must, therefore, make a careful study in order to determine the net improvement available from such a method. A detailed survey and evaluation of the many augmentative methods presently employed is given by Bergles and Morton (1)*.

Devices which establish a swirl in the fluid in order to increase the heat transfer coefficient and critical heat flux are particularly

---

*Underlined numbers in parentheses refer to references listed beginning on page 74.

attractive augmentative schemes for forced convection systems. They can be readily used to improve the performance of existing systems, and because of the high centrifugal force fields, the results of experiments made in the normal one gee environment are directly applicable in the environment of outer space.

The maximum centrifugal accelerations are obtainable with a tangential slot or spiral ramp vortex generator at the inlet to a heated test section. Gambill and Greene (2) attained the unusually high heat flux of 54.8×10^6 Btu/hr ft^2 with a tangential slot vortex generator at the inlet to a very short test section (I.D. = 0.191 in., L/D = 2.94). The estimated angular velocity of the fluid at the test section inlet was 20,000 RPM representing a centrifugal force at the tube wall of approximately 100,000 gees. However, the swirl created by inlet vortex generators decays rapidly as the fluid moves downstream (3, 4) and hence, the practical applications of such devices are limited.

Swirl flows generated by twisted tapes running the entire length of the heat transfer tube appear to offer significant benefits since improvements in heat transfer and critical heat flux are obtainable at relatively low cost. They also could be easily employed to improve the performance of existing systems. The prime disadvantage to twisted tapes is, of course, the increased pressure drop which accompanies their use. Therefore, the pumping power required is greater for a swirl flow than for a straight tube flow of the same velocity.

An economic comparison between a swirl and a straight flow system can be made on the basis of equal pumping power. That is, a swirl flow system will be more efficient if for the same pumping power it has a higher heat transfer coefficient.

1.2 Previous Research on Tape Generated Swirl Flow

Many investigations have been made to determine the heat transfer and pressure drop characteristics one obtains for various fluids in tape generated swirl flow. The first such investigation appears to have been reported by Royds (5) in 1921. He found that the cooling rate for air could be noticeably improved by inserting a twisted tape in a tube. Since then, investigators have examined the effect of twisted tapes on the heat transfer and pressure drop for water, ethylene glycol, flue gases, and air in forced convection heating and cooling. A limited amount of data is also available for the surface boiling and bulk boiling of liquids in swirl flow. A comparison of these results is made by Gambill and Bundy (6) and Bergles and Morton (1). Tables I and II summarize the range of variables examined in past swirl flow investigations for liquids and gases, respectively. In these tables, a "tight" tape fit is said to exist when there is no measurable gap between the tape and tube wall; whereas a "snug" tape fit exists when a gap of less than 0.01 in. is present.

Table I

Previous Research on the Tape Generated Swirl Flow of Liquids

Investigator	Reference	Fluid	D_i-in.	y	Tape Fit	Nonboiling h_s Heating	Nonboiling h_s Cooling	Boiling	Pressure Drop
Blatt and Adt	16, 17	Water Freon 11	0.15-0.50	2.50-∞	Tight			Bulk	X
Feinstein and Lundberg	14	Water	0.250	2.00-6.00	Tight			Subcooled	X
Gambill et al.	12	Water	0.136-0.25	2.30-12.03	Tight	X		Subcooled	X
Gambill and Bundy	13	Ethylene Glycol	0.136-0.25	2.30-12.03	Tight	X	X	Subcooled	X
Ibragimov et al.	15	Water	0.473	2.12-4.57	Tight				X
Judd	25	Isopropylated Santowax	0.48	2.6-7.3	Snug	X			
Kreith and Margolis	8	Water	0.53	2.58-7.3	Snug	X	X		X

Table I (continued)

Previous Research on the Tape Generated Swirl Flow of Liquids

Investigator	Reference	Fluid	D_i-in.	y	Tape Fit	Nonboiling h_s Heating	Nonboiling h_s Cooling	Boiling	Pressure Drop
Smithberg and Landis	10, 11	Water	1.382	1.81-∞	Snug	X			X
Viskanta	18	Water	0.3125	2.50-5.0	Snug				X

Table II

Previous Research on the Tape Generated Swirl Flow of Gases

Investigator	Reference	Fluid	D_i-in.	y	Tape Fit	h_s Heating	h_s Cooling	Pressure Drop
Colburn & King	7	Air	2.625	2.67-3.05	loose		X	X
Evans & Sarjant	3	non-luminous gases	3.00	2.9-5.9	loose		X	X
Koch	9	Air	1.97	2.45-11.0	tight	X		X
Kreith & Margolis	8	Air	0.53	2.58-7.3	snug	X		X
Royds	5	Air	2.00	Below 10	unknown		X	X
Seymour	19	Air	0.87	1.8-14.0	tight	X		X
Smithberg & Landis	10, 11	Air	1.382	1.81-∞	snug	X		X

1.2.1 Forced Convection Heat Transfer

The mechanisms effecting the heat transfer in forced convection swirl flow have not been clearly defined as a result of the investigations noted in Tables I and II, and no correlation has as yet been presented that correctly accounts for all observed effects. This is in part due to the difficulty in obtaining accurate experimental data for the swirl geometry. The following conclusions may be drawn, however, as a result of these investigations.

1) For a constant Reynolds number the swirl flow heat transfer coefficient, h_s, increases for tighter tape twist (lower y values).

2) For both heating and cooling, h_s is greater than the comparable straight tube coefficient, h_a; however, the improvement is less for cooling than for heating (8, 13).

3) A dependence of h_s on the centrifugal body force and ΔT_f is indicated by the results of Gambill et al. (12, 13) and Kreith and Margolis (8) but the magnitude of this effect has not been determined. This effect can be characterized by a Grashof number based upon the centrifugal acceleration at the tube wall (see Appendix 1 for the derivation of the basic swirl flow formulas). This is

$$Gr = \frac{\pi^2}{2y^2}\left(\frac{V_a D_h}{\nu}\right)^2 \left(\frac{D_h}{D_i}\right)\beta\,\Delta T_f \qquad (1)$$

or

$$Gr = \frac{4.94}{y^2} \cdot Re_h^2 \cdot \left(\frac{D_h}{D_i}\right)\beta\,\Delta T_f \qquad (2)$$

This effect will be referred to as the centrifugal convection effect.

4) The improvement in h_s is due in part to the tape fin effect, however, investigations with just a straight tape in a tube indicate the maximum gain attributable to this fin effect is about 25% (8, 10, 11).

5) In general, the improvement in heat transfer for both liquids and gases in swirl flow is of the same magnitude for equal Re and tube/tape geometry, and the variation in h_s with Re is similar for both fluids (9, 10, 11, 12, 13, 19). The data of Kreith and Margolis (8) represent the only exception to this conclusion. They report an increase in h_s over h_a of more than 300% for the heating of water, but for the heating of air the improvement is only 75%. An examination of the original data of Margolis (26) indicates that an error was perhaps made in construction of the Wilson plot used in the reduction of their water heating data.

For forced convection swirl flow, several types of correlations have been developed to explain the trends noted above. The simplest form as presented by Gambill et al. (12),

$$\frac{h_s}{h_a} = 2.18\, y^{-0.090} \qquad (3)$$

correlates the increase in h_s over h_a as a function of only the tape

twist. This equation presumes that h_s varies exactly as h_a for variations in Re and Pr. It fails to account for variations in h_s, for changes in the fin effect or centrifugal effect, and it does not predict the decrease in h_s for cooling as opposed to heating. As pointed out by Gambill (12), equations of this form are limited in their application and should be used only if the geometry and operating conditions of the system of interest to the designer are identical to those upon which the equation is based.

A more accurate correlation that accounts for both the centrifugal convection and the tape twist effects was also presented by Gambill et al. (12) for their water data.

$$\frac{h_s}{h_a} = 1.65 \left(\frac{10^2 \; (\rho \beta \Delta T_f)^{\frac{1}{2}}}{y} \right)^{0.084} \qquad (4)$$

Equation (4) was later modified as follows (13) to best correlate their water and ethylene glycol data:

$$\left[\frac{(Nu)_i}{(Re)_{i,a}^{0.89} \; Pr^{0.6}} \right] = 0.00675 \left[\frac{(\rho \beta \Delta T)_f \; V_a^2}{y^2 \; D_i} \right]^{0.0344} \qquad (5)$$

where ρ is in lbm/ft^3, V_a in ft/sec, and D_i in ft.

Equation (5) correlates the 103 data points for heating of references (12, 13) with an average deviation of ± 12%. It failed to correlate their 24 data points for cooling of ethylene glycol which still, however, had heat transfer coefficients greater than the conventional straight tube values. Such an equation also overlooks possible variations in the fin effect on the heat transfer.

A more detailed model for the prediction of h_s was developed by Smithberg and Landis (10, 11). They theorized that the swirl flow heat transfer could be found by adding the axial flow heat transfer predicted from conventional correlations and the heat transfer associated with "super mixing" of the warmer boundary layer fluid and the cooler fluid in the swirling core. They also presented a method of accounting for the tape fin effect. The super mixing contribution is expressed as a function of the friction factor predicted from their isothermal flow field model. The applicable equations are:

$$f = 0.464\sqrt{f}\left(\frac{1}{2y}\right)^2 + \frac{0.0498}{Re_h}\left(\frac{\pi D_i^2}{8\ y\ A_c}\right)\left[1125 \ln (Re_h\sqrt{f} - 3170)\right] + 0.046\ Re_h^{0.2} \qquad (6)$$

where A_c = free flow cross sectional area, and

$$Nu_i = \frac{Re_h\, Pr}{1 + \frac{350}{Re_h f y}\left(\frac{D_h}{D_i}\right) Pr^{0.731}} \times$$

$$\frac{25.4}{y\, Re_h \sqrt{f}} + \frac{0.023}{Re_h^{0.2} Pr^{2/3}}\left(\frac{D_i}{D_h}\right)\left(1 + \frac{0.0219}{f(1/2y)^2}\right)^{\frac{1}{2}} \quad (7)$$

The use of Equation (6) is cumbersome in that it is an implicit friction factor relation. Since Equation (7) is based on the isothermal friction factor, it fails to properly account for the centrifugal convection effect and cannot explain the difference observed for the heating and cooling of swirl flows. The use of isothermal swirl flow observations for developing a heat transfer model is questionable when one considers the large buoyancy forces which can be set up in the heated case.

Considering the large number of parametric variables appearing to influence swirl flow and the experimental problems associated with obtaining good heat transfer data, it is not surprising that attempts to predict the data have met with limited success. These prior investigations have served to point out the need for a further study in order to delineate the mechanisms effecting forced convection swirl flow and lead to a more generalized prediction method. While a snug and a tight tape fit might be expected to give the same results if the difference in fin effects is considered, a loose or undersized tape would not tend

to create as large a centrifugal acceleration and one would expect that the mechanisms influencing the heat transfer would also differ. The data and correlations obtained with the loose tapes were, therefore, omitted from this discussion.

1.2.2 Boiling Heat Transfer

For two-phase swirl flows created by boiling at the tube wall, the bubbles formed at the surface of the heated tube are surrounded by the rapidly rotating liquid of higher density. The centrifugal acceleration force acting on the liquid is, therefore, greater than that acting on the bubbles, and hence, a radial transport of the bubble from the wall towards the center of the tube occurs. Since any liquid present in the tube tends to migrate towards the heated wall and force the vapor bubbles away from the wall, a greater critical heat flux is attainable for swirl flows than for comparable axial flows. This increase in critical heat flux has been observed by several investigators (12, 13, 14, 27, 28, 29, 30), and as one might expect, the magnitude of the improvement appears to be directly proportional to the centrifugal acceleration at the tube wall (6, 31).

Little reliable data exists, however, on the heat transfer coefficient for the boiling of water in swirl flow. Gambill et al. (12) and Feinstein and Lundberg (14) appear to have presented the only available surface boiling data obtained in conjunction with their investigation of burnout heat fluxes, while Blatt and Adt (16) have presented

the only bulk boiling data. The results of these investigators are in poor agreement and insufficient data exists in order to draw definite conclusions as to the effects of tape twist, velocity, or subcooling on the boiling heat transfer rate. The marked increase in heat flux which one normally observes at the inception of boiling for water flowing in a straight tube has not been noted for water in swirl flow.

The extremely high wall superheats ($\Delta T_{sat} = 175°F$ for $q/A = 10^6$ Btu/hr ft^2, $\Delta T_{sub} = 200°F$, P = 50 psig, V_a = 49 ft/sec) reported for straight tube boiling by Feinstein and Lundberg raised doubts as to the validity of their data. They employed electrically heated test sections made of Inconel X and calculated their tube wall temperature drop considering the variation in thermal conductivity of the tube with temperature. In an analysis of their data reduction procedure, it was found that an error was made in their evaluation of the integrated thermal conductivity variation with temperature, $\int k(T)dT$, (14, 32). This led to large errors in their calculated inside wall temperature. After making the appropriate corrections, it was found that practically all of their reported surface boiling data was in fact non-boiling. The study by Blatt et al. (17) also appears to be in error in the calculation of the tube wall temperature drop. They used a condensing steam heating system but failed to account for the temperature drop across the stainless steel tube wall. This would cause a negligible error in their reported wall superheats for Freon-11, but could lead to errors as

much as 30°F for their higher heat flux water data.

1.2.3 Pressure Drop and Friction Factors

As noted in Tables I and II, a vast amount of data on swirl flow friction factors is presently available. Gambill and Bundy present a comparison of this data in Reference (6) and it can be seen that for liquids and gases rather close agreement exists between the data of various investigators. Their recommended correlation is

$$(f_s - f_a)_h = \frac{0.0525}{y^{1.31}}\left[\frac{(Re)_h}{2000}\right]^{-n} \qquad (8)$$

where $n = 0.81 \exp\left[-1700\ (e/D_h)\right]$

This equation predicts the isothermal friction data of References (6, 7, 8, 9, 13, 18) with a maximum deviation of 33%. An earlier correlation scheme of Gambill et al. (12) considered the increase in the friction factor for tape generated swirl flow to be caused by the increased surface area per unit length seen by the moving fluid (characterized by the hydraulic diameter) and the increased velocity of a fluid particle at the tube wall due to the spiral flow path (see Appendix 1). The relation between the straight tube friction factor and the swirl flow case is then

$$\frac{f_s}{f_a} = \frac{\left(4y^2 + \pi^2\right)^{3/2}}{8y^3} \qquad (9)$$

The early ORNL water data (12) was correlatable within ± 20% by Equation (9) and Seymour (19) reported his air data could be correlated within ± 7% by this equation.

Equation (6) which was developed analytically by Smithberg and Landis (10, 11) predicts their isothermal air and water data within 16% and the air data of Koch (9), and Margolis (26) within 10%.

While a large amount of reasonably well correlated data is available for isothermal swirl flow pressure drop, little data has been presented on the difference between the isothermal and heated pressure drops for non-boiling forced convection and the pressure drop with surface boiling swirl flows.

1.3 Purpose of Study

In order to better explain the phenomena of swirl flow heat transfer the goals of this study were defined to be:

1. Delineate the mechanisms present in forced convection swirl flows by taking data under carefully controlled conditions and from these data develop, if possible, a more universally applicable method for predicting the associated heat transfer coefficients.

2. Obtain reliable surface boiling heat transfer and pressure drop data, and compare the boiling inception points with conventional straight tube boiling data.

3. Carefully evaluate the usefulness of tape generated swirl flow as an augmentative heat transfer technique.

Chapter II

EXPERIMENTAL PROGRAM

2.1 Scope of Research

A comprehensive investigation was made of the forced convection, non-boiling, heat transfer coefficients and pressure drop for both the heating and cooling of water in swirl flow. The heat transfer characteristics for swirl flow surface boiling of water were also determined and visual observations of the bubble motion present with such boiling were made. The range of variables investigated and the design of the electrically heated test sections were dictated primarily by the capabilities of the low pressure test loop used for this study. The basic test section and system variables were as follows:

Tubing: Nickel, INCO alloy 200

Wall thickness = 0.0125 in., Roughness = 11.0 μ in.(cla)

Straight test section, D_i = 0.198 in.

Swirl test sections, D_i = 0.1935 in.

Heated L/D: 69-76

Calming L/D: 20 (minimum)

Tapes: Inconel, INCO alloy 600

Thickness = 0.0135 in., Roughness = 11.8 μ in. (cla)

y values: 2.48, 3.15, 3.52, 5.26, 9.2

Inlet Temperature: 50-200°F

System Pressure: 30-100 psia

Re_i: $8 \times 10^3 - 1.3 \times 10^5$

Maximum Heat Flux Attained: 3.5×10^6 Btu/hr ft^2

2.2 Description of the Test Loop

2.2.1 Hydraulic System

The test-loop used in this study was located in the M.I.T. Heat Transfer Laboratory and was designed and constructed in 1961 (32). A schematic layout of the facility is shown in Fig. 1. For corrosion resistance, the fittings and pipings are made of brass and stainless steel, while rayon reinforced rubber hose is used for making any required flexible connections. It is a closed loop low pressure system with circulation of the distilled water provided by a Fairbanks-Morse, two-stage regenerative pump (260 psig discharge pressure at 3.6 gal/min) driven through a flexible coupling by a 3 hp Allis Chalmers induction motor. A Fulflo filter is installed at the pump inlet, and a Greer accumulator charged with nitrogen to an initial pressure of 40 psig is at the pump outlet to dampen any pressure fluctuations. A Jamesbury ball valve is used to isolate the accumulator from the loop at shutdown. After the accumulator the flow splits into the by-pass line and the test section line.

In the test section line, fluid flows through a Fischer-Porter flowrator followed by a preheater, thence through a Hoke metering

valve and the test section, after which it merges with fluid from the by-pass line. The fluid then flows through a heat exchanger and returns to the pump. The preheater consists of four Chromalox immersion heaters of approximately 6-kw each. Three of these heaters are controlled by "on-off" switches located on front of the test panel, while the fourth can be varied to provide from 0 to 6 kw by means of powerstat auto-transformer mounted on the test bench. Quick action, 1/4 turn Jamesbury ball valves are installed before the inlet to the flowrator and after the exit from the test section to permit quick isolation of the test section in the event of a burnout or sudden leak. The exit valve was also used to adjust the test section exit pressure.

Flow through the by-pass line is controlled by a ball valve on each side of which there is a 300 psig pressure gage. Pump operating pressure and hence the pressure upstream of the test section needle valve is controlled by this valve.

The heat exchanger is a counterflow type with system water flowing in the inner tube and city water flowing in the outer annulus. Because of seasonal temperature variations, the minimum operating temperature is approximately 50°F in the winter and 80°F in the summer. Except for input power levels above approximately 50 kw, the heat exchanger maintained a constant pump inlet temperature.

A Fulflo filter is installed on the city water line to reduce scale formation in the heat exchanger.

The distilled water was continuously deionized by passing a portion of the flow through a series of four mixed-bed resin demineralizer cartridges installed in a Barnstead "Bantam" demineralizer unit. The conductivity as indicated by a PM-19 Barnstead Purity meter was maintained above 2.0 megohm-cm for all runs. To minimize the dissolved gas in the system a 4.7 gal degassing tank with five electrical heaters (3-220 vac and 2-110 vac) is provided. This tank also served as a surge tank and provided make-up water to the system during operation. A 15 gal stainless steel supply tank is located directly above the degassing tank and it was filled from the standard 5 gal bottles by a small Hypro pump. Sight glasses were provided on both the supply tank and the degassing tank in order to assist in maintaining proper fluid levels.

For the cooling experiments, an additional city water line was used to provide cooling water for the counterflow heat exchanger which surrounded the test section.

2.2.2 Power Supply

Electrical power is supplied to the test section for the heating experiments by two 36 kw Chandrysson direct current generators connected in series. Each generator was rated at 12 volts and 3,000

amperes. A portable power control console permitted coarse or fine voltage control from 0 to 24 volts. A water cooled shunt is installed in parallel with the test section and protects the generators against the shock of a sudden open circuit. Power is transmitted from the main bus to the test section by water cooled power leads. Each power cable was connected through a braided copper connector to a brass test section holder. Each holder consisted of two segments of 3/8 in. brass plate which, when bolted together, clamped to the test section power bushing. To insure good electrical contact between the test section bushings and the holders, the inner surface of the holders were lined with a thin layer of high temperature soft solder. For these experiments, the test section exit power lead was at a positive potential, and for electrical isolation, rubber hose connected the exit plenum chamber to the main loop.

2.2.3 Instrumentation

Instrumentation was provided to monitor the fluid pressure and temperature conditions throughout the system. All fluid temperatures were measured by 30 gage, copper-constantan thermocouples made from the same reel of Leeds and Northrup duplex wire. Calibration checks were performed on three thermocouples selected at random. The deviations from the N.B.S. standard thermocouple tables, however, were negligible and further corrections were deemed

unnecessary. The thermocouples were connected to a common ice bath through one of two Leeds and Northrup 12 position thermocouple selection switches and the millivolt output indications were read on a Minneapolis-Honeywell, Brown recorder with ranges 0-6, 5-11, 10-16, 15-21, and 20-26 millivolts. The recorder was calibrated before and during the investigation. The test section inlet and exit bulk temperatures were measured by thermocouples installed directly in the fluid stream in the inlet and exit plenum chambers. The thermocouples were introduced at these locations through Conax fittings equipped with lava sealants. Prior to taking data, two thermocouples were inserted in the exit plenum with an axial separation of approximately two inches, and simultaneous temperature readings for varying insertion depths were taken. Agreement between the readings was sufficient to insure that the mixed mean temperature could be indicated by a single thermocouple. A thermocouple was also installed in the degassing tank to monitor the tank temperature during degassing, and another was at the pump discharge to insure that the water entering the demineralizers was below the recommended limit of 140°F. Details of the test section instrumentation will be discussed later.

Fischer-Porter flowrators with overlapping ranges from 15 to 4,000 lbm/hr were used to measure the flow rate. At the beginning of this investigation the calibration of each tube-float combination was

checked against the initial calibration curves obtained in a prior investigation (33) and periodic spot checks were made throughout this study.

All pressures at the points indicated on Fig. 1 were read on Bourdon-type gages. The test section inlet and exit pressures were measured with Helicoid 8-1/2 in. gages with a specified accuracy of $\pm$ 1/4% of full scale. At the onset of the investigation, the inlet 200 psig gage and the exit 100 psig and 60 psig gages were calibrated on a dead weight tester and adjusted to within 0.1 psig over their range. They were also checked against each other at various static pressure levels during each series of runs. A manometer system consisting of two 60 in. Meriam U-tube manometers in parallel were also used to accurately measure the test section pressure drop. One manometer was filled with mercury and the other with Meriam Fluid No. 3 (S.G. = 2.95). The reported pressure drop for a given run was always measured by the most sensitive available method. That is, for very low pressure drops the Meriam fluid manometer reading would be taken, whereas for high pressure drops, the difference between the inlet and exit gage readings was used.

The power to the test section was determined from its voltage drop and current. The voltage drop for early runs was read directly on a Weston multiple range D.C. voltmeter with a specified accuracy of $\pm$ 1/2%, and for later runs it was read from a Digitec digital voltmeter accurate to 0.02 volts. The current was obtained by using the

Brown recorder to measure the voltage drop across an N.B.S. calibrated shunt (60.17 amp/mv) in series with the test section.

2.3 Description of the Test Sections

The tapes used for this investigation were fabricated by suspending 80 to 120 pounds of weights on the end of a sheared strip of Inconel (0.0135 in. thick) which was supported at the top by a clamp. The weights were then turned to produce the desired tape twist. To insure uniform contact between the tape and the tube wall, the nickel tubes were redrawn over the twisted tapes. The redrawing was performed by the F. W. French Tube Co. of Newtown, Connecticut. The tape width, tube dimensions, and size of the drawing die were such that the redrawing caused a 1-2 mil penetration of the tape into the tube wall.

X-rays were made of all tube-tape assemblies at the M.I.T. Radiographic Laboratory in order to check on the uniformity of the tape twist and tube wall penetration and to assist in locating the wall thermocouples and pressure taps. In order to examine various aspects of swirl flow, several types of test sections were required. The characteristics of each type will now be examined.

2.3.1 Test Section for Heating of Swirl Flows

Figure 2 is a cross section of a typical test section used to measure the swirl flow heat transfer coefficients and pressure drops for heat addition in the forced convection and surface boiling regimes.

Power was supplied through the brass bushings at each end, and the heated length was defined to be the distance between the inner faces of these bushings.

The pressure taps were 0.0135 in. holes located at a circumferential point 90° from the tube-tape juncture. They were positioned by the aid of X-rays within the first 540° of tape twist as measured from either end to permit deburring of the drilled hole.

Since D.C. heated test sections were used, the tube wall thermocouples had to be insulated from the tubes in order to prevent an erroneous temperature indication. To minimize the radial heat loss from the test section and make accurate thermocouple indications possible, a guard shield surrounded the entire test section. It was constructed from a brass tube which had a single thread-like groove cut in its outer wall. At the third points, it was partially severed to provide three variable temperature segments. A nichrome heater wire insulated in glass sleeving was then placed in the spiral groove for each segment. Two thermocouples were fastened directly to the guard shield inner wall in each segment and three A.C. variacs were used to adjust the inner wall temperature of the guard ring segments to match the test section outer wall temperature in the corresponding length. The guard shield was centered by means of screws at each end and the space between the tube and shield was filled with asbestos insulation.

Six thermocouples were spaced uniformly along the axis of the tube and insulated from the tube wall by a single layer of Scotch Electrical Tape No. 27. The junctions were located at the 90° circumferential point relative to the tape and the leads were then bound radially around the tube with another layer of tape. To avoid conduction errors, sufficient lengths of all thermocouples were left inside the guard shield. To check the accuracy of the guard shield system, two thermocouples were placed directly on the tube wall and water from 100-300°F was circulated through the test section. When the shield temperature was adjusted to equal the temperature indicated by the directly fastened thermocouples, it was found that the six thermocouples insulated from the tube wall were reading within one degree of the two that were directly fastened.

2.3.2 Visual Exit Section for Surface Boiling Observations

To positively ascertain that boiling was occurring in swirl flow and to observe the bubble trajectories, a visual exit section was designed whereby the flow could be observed at the immediate exit of the heated length. Figure 3 shows the details of this test section. The inside diameters of the glass tube and the test section differed by at the most 1.5 mil. The silastic gasket which sealed the glass tube to the exit power connection also allowed for the differences in thermal expansion between the glass and the metal.

2.3.3 Test Section for Cooling of Swirl Flows

In order to determine the heat transfer coefficients for cooling of swirl flows, a counterflow concentric tube heat exchanger depicted in Fig. 4 was employed. The inner tube consisted of a test section used in the heating investigation from which the power bushings and pressure taps had been removed. The heated length was defined to be the distance between the bottom flats of the Conax fittings located at each end of the heat exchanger.

Three 36 gage, iron-constantan thermocouples were recessed in the tube wall and held in place by a drop of epoxy to permit measurement of the local cooling heat transfer coefficients, and to serve as a check on the overall values obtained by conventional heat balance methods.

2.3.4 Insulated Tape Test Section

In order to determine the fin effect of the electrically heated tapes, a special insulated tape test section was fabricated. The tape used for this assembly was twisted from a 10 mil strip of copper in the manner previously described. The twisted tape was then coated with a 2 mil thickness of an organic material called "apcoat." This material has thermal and electrical properties similar to teflon but is stronger and more resistant to abrasion. It was applied with a special spray process by the Applied Plastics Corp. of Norwood, Mass. The tape was sized to fit tight in a nickel tube without the tube being redrawn

over it. An X-ray of the completed tape-tube assembly indicated the gap between tube and tape was no greater than approximately 2 mils at any point. Continuity checks were also made before and after the series of runs with this test section to insure that the tape was electrically insulated from the tube.

2.4 Experimental Procedure

2.4.1 General Loop Operation

After the test section was installed, the loop and degassing tank were filled with water from the supply tank and air was bled from all the high points of the system. The degassing tank was then brought to a boil while water was circulated through the loop and ion exchanger with the heat exchanger on. If heating runs were planned, the generators were also started and allowed to warm up. The degassing tank vent was closed when the tank began to boil and the pressure in the tank was allowed to increase to a level of from 6 to 15 psig. This placed the pump inlet above atmospheric pressure, and prevented air from being sucked in around the pump seals. Degassing was then accomplished by by-passing a portion of the cool loop water into the top of the vigorously boiling degassing tank. The degassing tank was periodically vented to permit the vapor and gases to escape. Continuous degassing was done in this manner during all runs. Forced convection, non-boiling data was not taken until the gas content as indicated by a Winkler analysis was below 1.8 c.c. air/liter (assuming

1 c.c air/liter = 2.9 c.c. O_2/liter). For the boiling runs, however, degassing was continued until the gas content was below 0.2 c.c. air/liter. A pressure of from 220 psig to 260 psig was maintained at all times on the upstream side of the Hoke metering valve to prevent system-induced instabilities.

2.4.2 Operating Procedure for Heating Runs

For each series of runs with heat addition, isothermal pressure drop data was first obtained by varying the water temperature by means of the preheaters for several different flow rates and measuring the overall test section pressure drop. Pressure drop data was also obtained during each heating run.

When the desired flow rate, system pressure, and water inlet temperature were established, the power was applied to the test section. If a particular bulk temperature was required at a specified point in the test section, the inlet temperature was decreased the required amount as the power was increased. At each power setting, the segments of the guard shield were adjusted so their inner wall temperatures were within 2°F of the average of the corresponding test section outer wall temperature. At equilibrium, data were recorded concerning the test section flow rate, inlet and exit fluid temperatures, current, voltage drop, outer wall temperatures, and pressure drop. From 10 to 45 minutes were required per run in order to establish equilibrium at the desired flow conditions and record the data.

2.4.3 Operating Procedure for Cooling Runs

The data for cooling of the test section was obtained in a manner similar to that for heating; however, the guard shield and test section power were not required. The flow rate and inlet and exit temperatures of the cooling water were recorded in addition to the test section flow rate, inlet and exit fluid temperatures, and wall temperatures.

2.5 Data Reduction Procedure

2.5.1 Heating Runs

A Fortran II computer program was written to facilitate the data reduction and present it in a useful form. It was run on the IBM 7094 computer in the M.I.T. Computation Center. A sample printout for a typical run is shown in Fig. 5 and details on the calculation procedure are presented in Appendix 2. Similar records of all data obtained in this investigation are on file in the M.I.T. Heat Transfer Laboratory.

Heat input was determined by three separate methods for the heated runs, and it was required that the heat balance agree within five percent for the data to be accepted. For most runs, however, agreement was within two percent.

Local and average values for the important parameters were determined. A linear variation in bulk temperature from the inlet to the exit of the heated length was assumed, and a linear variation in pressure from the inlet to the exit pressure tap was also assumed.

Since the pressure taps were on the tube wall within the swirl channel, the pressure they read would include the swirl contribution to the total static pressure; hence, the saturation temperature presented for a given point reflects the saturation temperature at the tube wall.

The tube wall temperature drop was calculated considering the variations of the tube properties with temperature in the manner recommended by Kreith and Summerfield (34). Details on the determination of the nickel tube property variations with temperature are presented in Appendix 2.

The heat flux, (q/A), used to calculate the heat transfer coefficient, h, was based on the total inside surface area of the tube as has been done in all previous swirl flow investigations. It is shown in Appendix 5 that this is a reasonable engineering approximation. The heat generated in the tape was always a very small percent of the total heat transfer to the fluid (under 3%).

A detailed error analysis is presented in Appendix 3. Using the 2nd power error determination method recommended by Kline and McClintock (35), the maximum probable error likely to exist for a data point on the conventional forced convection coordinates of $(Nu/Pr^{0.4})_{i,b}$ versus $Re_{i,b}$ is 5%, while on boiling coordinates of q/A versus ΔT_{sat} it is 4%.

2.5.2 Cooling Runs

Data for the cooling runs was reduced by hand with the aid of a slide rule and desk calculator. A heat balance was made by

comparing the First Law expressions, Eq. (2.9) for the two fluid streams. Since the temperature difference of the cooling water was generally small, agreement of the two expressions within eight percent was required in order for the run to be considered valid.

The overall heat transfer coefficient was determined from the expression

$$U = \frac{q/\pi D_i L_h}{\Delta T_{lm}}$$

A plot was then constructed, Fig. 6, in the manner recommended by Wilson (36) in order to determine the inside swirl flow heat transfer coefficient. The effect on h_s of variations in the fluid properties with temperature were accounted for by assuming $h_s \propto Re^{0.8}$. The value of h_s was then computed from

$$\frac{1}{h_s} = \frac{1}{U} - \text{Constant}$$

where the constant is the ordinate intersection of the curve in Fig. 6.

Chapter III

PRESENTATION AND DISCUSSION OF NON-BOILING FORCED CONVECTION HEAT TRANSFER RESULTS

3.1 Observed Effects

The experimental forced convection heat transfer results are presented in Figs. 9-12 on the coordinates of $Nu_i/Pr^{0.4}$ versus Re_i. These coordinates were based on the inside tube diameter rather than the hydraulic diameter in order to best show the improvement obtainable with swirl flow over a comparable empty tube flow. If Nu and Re were based on the hydraulic diameter, they would, for the swirl tubes, be but 57% of the values presented. The straight line on each plot, $Nu/Pr^{0.4} = 0.023\ Re^{0.8}$, is the familiar McAdams adaptation (44) of the equation originally presented by Dittus and Boelter (47) for predicting straight tube heat transfer coefficients for turbulent flows. The observed effects will now be discussed.

3.1.1 Tape Twist Effect on the Heat Transfer Coefficient

It is apparent from these figures that tighter tape twists (lower y values) produce an increase in the heat transfer rate. It may also be observed that h_s varies essentially as $Re^{0.8}$. This would lead one to attempt a linearized correlation, similar to Eq. (4) as presented by Gambill. For the heated forced convection data of this investigation, the following equation correlates the data with a deviation of 25%:

$$\frac{h_s}{h_a} = 2.26\, y^{-0.248} \qquad (10)$$

Equation (10), like Eq. (4), should only be used to predict heat transfer coefficients when the geometry and operating conditions of the system of interest are identical to those upon which the equation is based.

3.1.2 Effect of Variations in ΔT_f on the Heat Transfer Coefficient

The swirl and empty tube data of Fig. 9 were obtained for a variation in ΔT_f of up to 120°F. This wide variation in ΔT_f created a substantial change in the swirl flow heat transfer coefficients for a constant Re,but caused much less variation in the corresponding straight tube h. This is in line with the earlier results of Bergles and Rohsenow (32) who recommended that the McAdams correlation be used for predicting straight tube heat transfer coefficients for low temperature water (below 200°F) at high ΔT_f.

The data for Fig. 10 were obtained with little variation in ΔT_f and the spread in the data for a given y and Re was noticeably less. Figure 13 shows more clearly how the local heat transfer coefficient varies with ΔT_f at various flow rates. The inlet temperature was varied in order to maintain a constant bulk temperature and Re for these runs. It can be seen that the increase in h_s is greater for the higher flows and thus increases the probability that centrifugal convection is an important swirl flow heat transfer mechanism.

3.1.3 Difference Between Average and Local Nusselt Numbers

Figures 9 and 10 are based on the average values of Nu, Pr, and Re existing for a particular run, while Fig. 11 is based on the local values. A comparison of the data on Figs. 9 and 11 for y = 3.15 clearly show that there is a negligible difference between the average and local Nu values. There is also very little entrance effect present for the swirl flow. Thermocouple No. 1 is 12 diameters from the beginning of the heated length, yet even for the low flow rates, the local h at this point was approximately the same as that at the end of the tube for a constant Re. This is not surprising when one considers the increased mixing caused by the tape. Both the average and local Nu versus Re values presented for the swirl flow cooling data in Fig. 12 are also in close agreement. Since the variation in Re and Nu with length for the empty tube was noticeably less, a single line was drawn to represent this variation rather than plotting the separate points. It can be seen in Fig. 11 that with the empty tube, the inlet h, even for the higher flow rates, tends to be greater than a comparable h further downstream. Comparison of these swirl and empty tube data thus indicate entrance effects are more pronounced in straight flow.

3.1.4 Effect on the Heat Transfer of Heating Versus Cooling

The same test section was used to obtain the heating and cooling data presented for y = 3.15 in order to accurately determine the difference in h_s existing for the two modes. Comparison of the data in

Figs. 9, 11, and 12 shows that for the same Reynolds number, the heat transfer coefficient is generally 25% less for cooling than for heating; however, improvements over the empty tube case were still present for all cooling runs.

3.1.5 Fin Effect of the Tape

An indication of the fin effect of the tape for the heated runs may be obtained by plotting, for a constant Re and ΔT_f, the ratio h_s/h_a versus $1/y$ and noting the intercept for $1/y = 0$. This intercept is then indicative of the asymptote that h_s/h_a would approach as y goes to infinity, i.e., a straight tape. This was done for three Reynolds numbers and the results are shown in Fig. 14. The fin effect ranges from 7 to 17% with the greatest variation occurring in the rather limited range of Re_i from 10^4 to 2.5×10^4. These results agree quite favorably with an analytical solution for the tape fin effect shown in Fig. 15 that was predicted by the equations derived in Appendix 4. In this analytical approach, the thermal contact resistance between the tape and the tube wall was assumed to be negligible, and both the tube wall and the tape were assumed to act as fins. For further substantiation of the tape fin effect, heat transfer data were obtained for an insulated tape test section. The resulting Nusselt numbers are compared in Fig. 16 to those obtained at the same conditions from a tube containing a non-insulated Inconel tape of the same twist. It can be seen that the insulated tape results are from 7-12% less than for the corresponding non-insulated case.

For the prediction method that will be developed later in this chapter, we need to know the percent of the total heat transfer that is attributed to the fin effect of the tape. As a result of the rather good agreement between these theoretical and experimental fin effect determinations, it was presumed that the fin heat transfer was 9% of the total for Re_i above 3×10^4 and 12% for Re_i less than 3×10^4.

3.1.6 Tube Wall Temperature Variation with Length

The designer of any heat transfer device is generally interested in the manner in which the wall temperature varies with length as well as the absolute value of that temperature. The rate of this increase (dT_w/dx) is readily predicted from the First Law of Thermodynamics for these constant heat flux test sections. The bulk temperature at any point, x, can be found from

$$T_x = \frac{(q/A)\pi D_i x}{w c_p} + T_{in} \qquad (11)$$

The wall temperature at x can then be determined by the equation

$$T_{w,x} = \frac{q/A}{h_x} + \frac{(q/A)\pi D_i x}{w c_p} + T_{b,in} \qquad (12)$$

Differentiation of Eq. 12 considering the variations in h with x yields

$$\frac{d T_{w,x}}{d x} = -\frac{q/A}{h_x^2} \cdot \frac{d h_x}{d x} + \frac{(q/A)\pi D_i}{w c_p} \qquad (13)$$

For this case, it will be assumed that Eq. (10) applies and that the straight tube h can be predicted by

$$h_{x,a} = 0.023 \frac{k}{D} Pr_x^{0.4} \left(\frac{GD}{\mu_x}\right)^{0.8} \tag{14}$$

The following functional relations are assumed to exist for a given flow rate and tube geometry

$$h_x = f(\mu_x, Pr_x),\ Pr_x = f(T_x),\ \mu_x = f(T_x) \tag{15}$$

Then, by the chain rule, one may write

$$\frac{dh_x}{dx} = \frac{\partial h_x}{\partial \mu_x} \cdot \frac{d\mu_x}{dx} + \frac{\partial h_x}{\partial Pr_x} \cdot \frac{dPr_x}{dx} \tag{16}$$

we also know that

$$\frac{d\mu_x}{dx} = \frac{d\mu_x}{dT_x} \cdot \frac{dT_x}{dx} \tag{17}$$

and

$$\frac{dPr_x}{dx} = \frac{dPr_x}{dT_x} \cdot \frac{dT_x}{dx} \tag{18}$$

Effecting the differentiation of Eq. (11) indicated by Eqs. (17) and (18) and then combining the results with Eq. (14) and (16), one obtains for the desired slope (19)

$$\frac{dT_{w,x}}{dx} = \frac{(q/A)\pi D_i}{w\, c_p} \left\{ 1 - \left[\frac{q/A}{h_x} \cdot \frac{0.4}{Pr_x} \left(\frac{dPr_x}{dT_x}\right) - \frac{0.8}{\mu_x} \left(\frac{d\mu_x}{dT_x}\right) \right] \right\}$$

The values for (dPr_x/dT_x) and $(d\mu_x/dT_x)$ are obtainable from plots of these properties versus temperature or by differentiation of a polynomial which represents these properties in the desired temperature range.

In order to further ascertain the accuracy of the data and to assist in determining the boiling inception points, plots of the tube wall temperature versus length were made. A typical plot showing the variation in tube wall temperature with length for a constant flow rate and variable heat flux is shown in Fig. 17. One may observe that for the low heat flux, non-boiling runs, the increase in wall temperature with length is linear. This would be expected considering the negligible end effects on h_s as indicated by Fig. 11 for this same tube. For this case Eq. (19) will accurately predict the temperature variation with length if the average bulk temperature existing in the test section is used to evaluate the heat transfer coefficients and fluid properties. This was done for several cases and as shown in Fig. 17 the predicted slope was generally within 1 to 2% of the experimentally obtained values. If entrance effects are present or the bulk temperature change in the heated length is large, as they may be for low flows, Eq. (19) will predict a lesser slope than actual if the average bulk temperature is used for property evaluations. This is because of the increased variation in h with length, and the non-linearity in $\mu(T)$ and Pr(T) which exist for a large bulk temperature variation.

For the higher heat flux, surface boiling runs, the wall temperature profile is nearly flat for that region of the tube in fully developed surface boiling. The slight temperature decrease with length observed for q/A's greater than 2.5×10^6 Btu/hr ft^2 may be explained by the

pressure drop with length and consequent decrease in the saturation temperature. Assuming that the wall superheat required for the surface boiling is constant, the wall temperature must also decrease.

3.2 Formulation of Prediction Method

Analysis of the early experimental results of this investigation and consideration of the experiences of previous investigators led to the belief that the swirl flow heat transfer was due primarily to three effects:

1) The heat transferred by conventional forced convection mechanisms as a result of the turbulent flow in the spiral channel. This contribution would be present for all tape generated swirl flows, and should be predictable from the conventional straight tube correlations, such as Eq. (14), if one accounts for the increased velocity at the tube wall caused by the tape insertion and the spiralling flow path. The heat transferred by this mechanism will be referred to as the spiral convection heat transfer.

2) The heat transferred by a centrifugal convection effect. It is theorized that the low density warmer fluid at the tube wall is being continually forced into the cooler main stream as a result of the high centrifugal body force acting on the fluid particles. On this basis, this effect would only be present for swirl flows with heat addition.

3) The heat transferred by the tape acting as a fin. This contribution would be present for both heating and cooling, but its

magnitude would depend on the contact between the tube and tape, tape material, flow characteristics, and the size of both the tube and tape.

It was then assumed that the total heat transfer could be expressed as the sum of these three effects.

$$q_{total} = q_{sc} + q_{cc} + q_f \tag{20}$$

It was also assumed that the heat transferred by the tape could be expressed as a certain fraction of the heat transferred in the tube wall. That is

$$\gamma = \frac{q_f}{q_{total}} \tag{21}$$

If

$$q_{wall} = q_{sc} + q_{cc} \tag{22}$$

then

$$q_{total} = \left[\frac{1}{1 - \gamma}\right] q_{wall} = F q_{wall} \tag{23}$$

where

$$F = \frac{1}{1 - \gamma} \tag{24}$$

For this discussion, the heat transfer coefficient is defined as

$$h_{total} = \frac{q_{total}}{(T_w - T_b)\pi D_i L_h} = \frac{F q_{wall}}{(T_w - T_b)\pi D_i L_h} \tag{25}$$

Similarly

$$h_{sc} = \frac{q_{sc}}{(T_w - T_b)\pi D_i L_h} \tag{26}$$

and

$$h_{cc} = \frac{q_{cc}}{(T_w - T_b)\pi D_i L_h}$$

Then

$$h_{total} = F(h_{sc} + h_{cc}) \tag{27}$$

The spiral convection heat transfer mechanism is thought to be very similar to conventional straight tube heat transfer; hence, the same type equations should predict its magnitude. The increased velocity due to the tape insertion is accounted for by defining the mass velocity as

$$G = \frac{w}{\pi D_i^2/4 - \delta_f D_i} \tag{28}$$

The velocity increase due to the twist can be predicted by a vector summation of the axial and tangential velocity components assuming a rotating, slug flow model describes the flow pattern (see Appendix 1). The flow field analysis of Smithberg and Landis (10, 11), substantiates that the magnitude of the tangential component is accurately predicted by the equation

$$V_t = V_a \frac{\pi}{2y} \cdot \frac{r}{r_i} \tag{1.5}$$

Near the tube wall, the agreement of Eq. (1.5) with the observed values was especially good. It was shown by Evans and Sarjant (3) that the turbulence in swirl flow tends to promote, as one would expect, a more uniform radial temperature profile than found in straight flow. Therefore, the radial temperature gradient is confined to the thinner thermal boundary layer at the tube wall. Since the thermal boundary layer, which depends on the velocity profile, is the controlling heat transfer parameter, it seems reasonable that the resultant velocity

at the tube wall would be of dominant interest in predicting the spiral convection contribution. This resultant velocity can be expressed in terms of the axial or straight tape velocity by (see Appendix 1)

$$\alpha = \frac{V_s}{V_a} = \frac{1}{2y}\left(4y^2 + \pi^2\right)^{0.5} \tag{1.7}$$

The hydraulic diameter should also be used in predicting q_{sc} in that it is more representative of the boundary layer thickness in swirl flow. Tape insertion creates a smaller flow passage and hence, the heat transfer should increase. A similar convention was adopted by Smithberg (11) in calculating a comparable axial flow heat transfer contribution.

Combining these assumptions with the conventional straight flow prediction of McAdams, Eq. (14), h_{sc} would be predicted by

$$h_{sc} = 0.023 \left[\frac{\alpha G D_h}{\mu}\right]^{0.8} Pr^{0.4} \frac{k}{D_h} \tag{29}$$

Although the empty tube heating data of this investigation were approximately 10% above the prediction of Eq. (14), the constant 0.023 was selected for the right hand side of Eq. (29). Exact agreement with predictions are seldom achieved; however, since 0.023 is widely accepted as the correlation coefficient for straight flow, it was felt that the prediction for q_{sc} would also be more widely applicable if it were based on the constant 0.023. If actual empty tube heat transfer performance is known by the designer for a particular system, he could

modify the q_{sc} constant to reflect this information when calculating the improvement available by inserting twisted tapes. Since empty tube heat transfer data were available for this study, the q_{sc} constant was modified accordingly. For Re_i above 1.5×10^4 it was designated as 0.025 and for Re_i below 1.5×10^4 it was 0.0237.

Since the centrifugal convection effect is similar to the natural convection circulation established over a heated plate facing up under the influence of a body force field, the magnitude of the effect should be predictable in a like manner. The applicable Grashof number would be based on the centrifugal acceleration rather than gravitational, however, and as shown previously it can be expressed as

$$Gr = \frac{4.94}{y^2} \cdot Re_h^2 \cdot \frac{D_h}{D_i} \beta \Delta T_f \qquad (2)$$

The expression recommended for predicting h_{cc} on the basis of Eq. (2) is then

$$h_{cc} = \frac{k}{D_h} (0.114) \left[Gr\ Pr\right]^{\frac{1}{3}} \qquad (30)$$

This equation is a modified version of the equation first recommended by Fishenden and Saunders (50) to predict the heat transfer coefficients with turbulent convection for a horizontal hot plate facing up in a normal one gee environment. One may note that it is independent of length.

The heat transfer attributable to the tape fin effect is a variable which must be determined by the designer for each particular system of interest. A theoretical method for predicting the fin effect for the geometry of this system is presented in Appendix 4. This method can be readily adapted to other systems by application of appropriate boundary conditions.

Introducing the expressions in Eqs. (29) and (30) into Eq. (26) yields the final prediction equation. The proposed forms for heating and cooling are as follows:

For heating:

$$h_s = \frac{k}{D_h} \cdot F \left\{ 0.023 \left(\alpha Re_h\right)^{0.8} Pr^{0.4} + 0.193 \left[\left(\frac{Re_h}{y}\right)^2 \left(\frac{D_h}{D_i}\right) \beta \Delta T_f Pr \right]^{\frac{1}{3}} \right\} \quad (31a)$$

For cooling:

$$h_s = 0.023 \, F \, \frac{k}{D_h} \left(\alpha Re_h\right)^{0.8} \quad (31b)$$

The additive manner in which each term contributes to the total heat transfer in Eq. (31) is shown graphically for a typical problem in Fig. 18. The relative importance of each term will vary depending on the geometry and flow conditions; however, it is believed that all previously observed variations in h_s can be predicted by this equation. It is an iterative prediction to the extent that one must assume a ΔT_f, calculate a predicted h, and then check the validity of the assumed ΔT_f. This type of iteration is characteristic of all natural convection problems and presents no real difficulty.

3.3 Application of the Prediction Method

3.3.1 Data of this Investigation

As shown in Fig. 19, Eq. (31) with the modifications to the constant 0.023 discussed previously, was successful in predicting practically all of the 200 forced convection data points of this study within 10%. Of particular interest, is the manner in which it correctly predicts the trends in the data for variations in ΔT_f and centrifugal acceleration as shown in Fig. 13. It was also able to correctly predict the reduced improvement observed with cooling noted in Fig. 12.

3.3.2 Water Data of Other Investigations

The proposed prediction method was applied to the data of several other investigators. Since information on the fin effect, T_b, and ΔT_f are required in order to use Eq. (31), it was only possible to compare it with data which provided this information directly or which provided sufficient information so that reasonable assumptions could be made concerning the value of a particular quantity.

In Fig. 20, the experimental Nusselt numbers for water obtained by Smithberg (11) are compared with the prediction of Eq. (31). For this case, exact values for T_b and ΔT_f were known, and the fin effect was estimated by comparing the predictions of Smithberg made with and without consideration of the fin effect (10, 11). A point by point comparison was made with the assumption that $F = 1.10$. Since ΔT_f was practically a constant for these runs, it was possible to draw a

line through the predicted points as shown. For the tighter tape, $y = 1.81$, all but one of the experimental values agreed within 10% of the prediction of Eq. 31. The sole exception (run #4) was 22.4% higher than predicted. For the looser tape, agreement was within 20% for Re_i above 3×10^4 while the two points at the lower Reynolds numbers were 29% above the predicted value. These low Re_i points also appeared to exhibit the greatest deviation from the prediction of Smithberg and Landis, Eq. (7). As can be seen, at these low Reynolds numbers, the experimental Nusselt number appeared to be independent of tape twist. This independence has not been noted by other investigators nor is it accounted for in the prediction method of Smithberg and Landis. It appears, therefore, that these few points may have been in error.

The form of the data of Gambill et al. (12, 13) made an exact point by point comparison impossible since the Reynolds number corresponding to a given h_s/h_a versus $Gr/Re_{i,a}^2$ point could not be obtained with any degree of certainty. The $Re_{i,a}$ was estimated for four of the data points for water, however, from the $(h_s/h_a)y^{0.09}/2.18$ versus Re_a plot of Reference (12) taking into consideration the manner in which the data were grouped on the two plots. For these four points, the predicted Nu was within 15% of the experimental value. It was not possible to obtain the original Oak Ridge data and further check the validity of the proposed prediction method.

3.3.3 Air Data of Other Investigations

Because of the effect of radial temperature gradients on the heat transfer coefficients obtained for the heating of gases in conventional straight tube flow (51), corrections are generally applied to convert the experimental Nu to isothermal conditions. It is presumed that such corrections are also required for swirl flow, however, the centrifugal convection effect would still be an additional mechanism influencing the total heat transfer. For typical gas flow operating conditions, the evaluation of Eq. (1.23) of Appendix 1, which represents the radial density variation due to the centrifugal acceleration, is very close to 1.0, and thus, the centrifugal convection mechanism would not be inhibited for the swirl flow of a gas. To be consistent with the assumption of earlier investigators (8, 11) the multiplying factor $(T_w/T_b)^{0.575}$, (where the T's represent absolute temperature) as presented by Kays and London (52) is recommended to correct the Nusselt numbers obtained with heating to isothermal conditions. For gases, the left hand side of Eq. (31) would then be $(Nu)\,(T_w/T_b)^n$, with n = 0 for cooling and 0.575 for heating.

Comparison of the predicted and experimental Nusselt numbers for the air data of Smithberg and Landis (11) is shown in Fig. 21. A point by point comparison was again made. For this case, however, the straight tape air data, when compared at constant Re_i, with their straight tube data, indicated a negligible fin effect was actually present,

and accordingly, it was assumed F = 1.0. All 24 data points were within 20% of the values predicted by Eq. (31).

The fully turbulent air data of Koch (9) are compared in Fig. 22. It was assumed that the fin effect was negligible for this data since information on his tape fit was not available. The experimental results were all within 13% of the prediction, and as can be seen, agreement was generally within a few percent.

On the basis of the good agreement between the predicted and actual results for the air and water data of previous investigators, as well as for the data of this study, it appears that Eq. (31) correctly accounts for the major effects influencing swirl flow heat transfer.

Chapter IV

PRESENTATION AND DISCUSSION OF SURFACE BOILING HEAT TRANSFER RESULTS

Typical swirl flow surface boiling curves for two different tubes are presented in Figs. 23 and 24, and a compilation of the fully developed boiling data for both swirl and empty tubes is presented in Fig. 25. The trends observed will now be discussed.

4.1 Comparison of Boiling in Swirl and Straight Flow

In Fig. 25, the dashed lines represent an extrapolation into the wall superheat regime of the forced convection heat transfer rate predicted from the data of Fig. 9 for the conditions specified. It is apparent that for the lower wall superheats the heat flux could be accurately determined from the forced convection prediction method previously discussed.

It can also be seen from Figs. 23 and 24 that the general appearance of these swirl flow boiling curves is essentially the same as found for conventional straight flow boiling (32, 48, 49). Three regimes appear to be present. For the low wall superheats, the heat transfer is by forced convection and a relatively small increase in heat flux occurs for a small increase in the wall superheat. For higher wall superheats, however, a large increase in heat flux occurs for a correspondingly small increase in wall superheat. As with straight tube

boiling, the data for a particular tube at all velocities appeared to be asymptotic to a "fully developed" boiling line in the high superheat region.

The presence of this asymptotic effect can also be inferred from the variation in wall temperature with length shown in Fig. 17. In this figure, one can see that the tube wall temperature remains essentially constant as boiling progresses up the tube. As we approach and enter the fully developed boiling regime at a point, the increase in wall temperature becomes successively less for each incremental increase in heat flux. An intermediate regime was also present where the data begin to deviate from the forced convection prediction and approach the fully developed state.

This similarity between swirl and straight flow surface boiling has not been noted in previous investigations. Complete boiling curves for a given velocity and subcooling were not presented in the earlier investigation of Gambill et al. (12) and as pointed out previously, the data of Feinstein and Lundberg were in error.

4.2 Inception of Boiling

To accurately determine the point of incipient boiling, the visual exit section described previously and shown in Fig. 3 was employed to determine the conditions at which the first vapor was observed. A Strobotac was used in conjunction with this test section in order to better observe the bubble size and their trajectories. The first

bubbles were observed in the visual exit at the points indicated in Fig. 23 for that particular tube. These initial bubbles, as well as all subsequent bubbles for higher heat flux or lower subcooling, were very small in size and barely discernible. Several microflash photographs were taken, but because of the very small bubble size and distortion created by the glass, they were not of high enough quality to permit enlargement and reproduction for this report. It can be seen in Fig. 23 that the first visually observed bubbles occurred very close to the predicted inception point of Bergles and Rohsenow (48), which is given by

$$(q/A)_{inc} = 15.60\, P^{1.156}\, (T_w - T_{sat})\, P^{\frac{2.30}{0.0234}} \qquad (32)$$

This equation is based on the thermodynamic requirements for bubble growth, and it accurately predicts the incipient boiling point for a considerable amount of both high and low pressure straight tube data. Since the heat flux required for stable bubble growth at a given wall superheat is dependent primarily on the pressure, it is not surprising that Eq. (32) also preducts with rather close accuracy the incipient points for swirl flow. The early work of Merte and Clark (55) also indicated that the inception point was essentially the same for pool boiling in an accelerating and non-accelerating system, and is, therefore, in agreement with the present results.

4.3 Effect of Peripheral Pressure Variations on Inception

Since the inception of boiling occurs at the heated wall, the pressure at the wall is of primary interest when applying Eq. (32). For this study, the pressure taps were within the swirl channel, and therefore, their readings include the centrifugal contribution due to the swirl expressed by Eq. (1.20). Since the pressure in an actual system is generally measured at an inlet or exit header, the designer must apply appropriate corrections to determine the actual pressure existing in the swirl channel. The form of these corrections is discussed in the next chapter.

In order to determine the magnitude of the peripheral variation in static pressure and thus check on the probability of inception occurring at some preferential low pressure point on the tube wall, an isothermal survey of the static pressure existing at ten different circumferential points relative to a twisted tape was made. The results from this survey also assist in determining the secondary flow pattern present with isothermal swirl flow. The pressure taps were spaced axially on a 0.75 in. I. D. plexiglas tube so as to provide circumferential pressure readings at 24° increments relative to a tape of twist, $y = 3.60$. The pressure differences between each tap and a given reference tap were determined by recording the output of a differential pressure transducer on a Sanborn, Model 321 Dual Channel Recorder. For the maximum velocity attainable, the peripheral

variations were less than 0.04 psi for this study. Assuming this variation is proportional to the velocity squared, the probable variation in peripheral pressure with the heated smaller diameter tubes would still be less than 1.0 psi for high velocity runs. It is believed that such a small variation would have a minor effect on the boiling pattern at the tube wall. Fig. 26 is a plot of the typical pressure variations observed in this manner. If it is presumed that the higher pressure points represent stagnation points for the radial secondary flows, a radial outflow is probable as indicated. This would tend, therefore, to substantiate the existence of a double vortex secondary flow pattern superimposed on the primary spiralling motion as observed by Smithberg and Landis (10) for air. A more detailed, higher velocity study would be required to firmly establish the secondary flow patterns for both isothermal and heated flows, since the very small pressure variations currently observed do not permit definite conclusions to be drawn.

4.4 Transition to Fully Developed Boiling

As shown in Fig. 23, the transition from incipient to fully developed boiling for a constant flow rate, i.e. the knee generally present on a q/A versus ΔT_{sat} boiling curve, can also be predicted for a swirl flow by conventional straight flow methods. The recommended prediction equation of Reference (48) is

$$q/A = (q/A)_{FC}\left\{1 + \left[\frac{(q/A)_B}{(q/A)_{FC}}\left(1 - \frac{(q/A)_{Bi}}{(q/A)_B}\right)\right]^2\right\}^{\frac{1}{2}} \qquad (33)$$

In this equation, $(q/A)_B$ represents the fully developed boiling asymptote. The value for $(q/A)_{Bi}$ is the value of $(q/A)_B$ for the wall superheat, ΔT_{sat}, found at the intersection of $(q/A)_{inc}$ (From Eq. 32) with $(q/A)_{FC}$, for the flow rate of interest.

4.5 Probable Heat Transfer Mechanism with Fully Developed Surface Boiling

As the superheat was increased beyond the inception point and into the fully developed boiling regime, many more bubbles appeared in the visual section. These bubbles were still quite small but they tended to follow a spiral path of a pitch approximately equal to that of the twisted tape. It is theorized that the centrifugal acceleration caused the heavier liquid to force the low density bubble away from the tube wall and towards the tape surface soon after it has formed. The heat removal is, therefore, stimulated by the periodic disruption of the thin thermal boundary layer adjacent to the tube wall caused by the bubble break away and subsequent in flow of cooler liquid from the bulk core.

While many theories have been presented, the exact mechanism responsible for the improvement in heat transfer in conventional straight flow boiling is still open to question. The rather close agreement in Fig. 25 between the fully developed asymptotes for the straight and swirl flow data indicates the heat removal mechanism with surface boiling is perhaps similar for the two cases. The pool boiling results of Costello and Tuthill (56) and Merte and Clark (55) tend to

substantiate this conclusion, since they both observed that the wall superheat required to produce a given heat flux was practically independent of the acceleration for heat fluxes above 50,000 Btu/hr ft^2.

Since in swirl flow the bubbles are removed soon after they are formed and appear to move toward the center of the tube, a bubble pumping or "microconvection" mechanism similar to that proposed by Forster and Grief (53) is perhaps primarily responsible for the improvement in both the swirl and straight flow cases. The probability of thermocapillarity being a dominant mechanism as recently proposed by Brown (54), is negated, however, by the agreement between the straight and swirl data of Fig. 25. The bubbles must remain near the tube wall for this mechanism to play an important role, and this is obviously not the case for swirl flow.

As a result of this study, it is concluded that the general trends for surface boiling of subcooled water in swirl flow are essentially the same as for straight flow. It is important to realize, however, that while the heat flux for a particular wall superheat may be the same for both a swirl and straight flow, the critical heat flux will always be higher and the forced convection contribution greater for the swirl flow case. It is indeed possible that for equal mass velocities and heat removal,the swirl flow could be in a non-boiling regime while a conventional straight flow would be above the critical heat flux point.

Chapter V

PRESENTATION AND DISCUSSION OF PRESSURE DROP RESULTS

5.1 Contributions to the Total Pressure Drop for Swirl Flow

The increased pressure drop which accompanies the use of twisted tapes for generating swirl flows is quite substantial and must be considered when contemplating their use as an augmentative heat transfer technique. The total pressure drop for a swirl tape assembly is determined from four different contributions defined as follows:

ΔP_1 - pressure loss caused by the fluid acceleration upon entry into the swirl channel due to the reduction in flow area.

ΔP_2 - pressure loss due to the initial establishment of the swirl flow pattern.

ΔP_3 - frictional pressure drop for the length of the spiral channel.

ΔP_4 - pressure recovery due to the increase in flow area at the end of the twisted tape.

The total pressure drop across the swirl assembly is then

$$P_{total} = \Delta P_1 + \Delta P_2 + \Delta P_3 - \Delta P_4 \qquad (34)$$

In line with the work of earlier investigators (11, 12, 14) it will be assumed that the loss ΔP_2 associated with the rotational kinetic energy of the fluid, is not recovered upon exit from the swirl channel.

The separate contributions for ΔP_1, ΔP_2, and ΔP_4 are generally very small in comparison to ΔP_3, but they are easily calculated from

the geometry and flow conditions for a particular system. Assuming the density is constant, the pressure variations associated with the area change at the inlet and exit respectively are:

$$\Delta P_1 = \left[G^2/2\rho_{in}\, g_c\right](1 - \sigma^2 + K_c) \tag{35}$$

$$\Delta P_4 = \left[G^2/2\rho_{ex}\, g_c\right](1 - \sigma^2 - K_e) \tag{36}$$

where $\sigma = (\pi r_i^2 - \delta_f D_i) / \pi r_i^2$ and G is given by Eq. (28). The contraction and expansion coefficients are a function of σ and the flow rate. Their values for a particular case may be estimated from the graphs in Kays and London (57). Since σ is generally close to 1.0, a conservative estimate would be to assume $K_e = 0$. In the event significant vapor is generated by boiling in the heated length, the above expression for ΔP_4 would not be directly applicable. The condensing vapor would alter the flow pattern and this pressure change would then be a function of the flow regime and void fraction existing at the exit as well as the usual single phase pressure drop parameters. Information is not presently available on the magnitude of ΔP_4 for such swirl flow quality exit conditions. For the subcooled surface boiling data of the present investigation, however, negligible pressure recovery was observed between the exit from the swirl section and a downstream plenum. It is recommended, therefore, that the pressure recovery, ΔP_4, due to the slight expansion be neglected if subcooled surface boiling occurs in the swirl tube.

As shown by Gambill (12) and Smithberg and Landis (10), the pressure drop ΔP_2 may be expressed by

$$\Delta P_2 = \frac{1}{2\pi r_i^2 g_c} \int_o^{r_i} V_t^2 \, 2\pi r \, d r \tag{37}$$

With V_t given by Eq. (1.5), this integrates to

$$\Delta P_2 = \frac{\pi^2 G^2}{16 \rho_{in} g_c y^2} \tag{38}$$

The pressure drop, ΔP_3, for boiling and non-boiling swirl flows will now be considered separately.

5.2 Non-Boiling Friction Factors

For this investigation, the pressure drop ΔP_3 was experimentally observed and the friction factors presented are all determined from:

$$f = \frac{\Delta P_3}{2} \cdot \frac{D}{L} \cdot \frac{\bar{\rho}}{G^2} \tag{39}$$

The friction factors of previous investigations have either been based on the same type of measured pressure drop or the observed value was corrected for inlet and exit effects to produce an equivalent ΔP. Isothermal and heated friction factors for two values of tape twist are compared in Fig. 27 with similar values obtained for an empty tube. Since the friction factor and Reynolds number are based on D_i, a direct comparison between the pressure drop obtained for a swirl and empty tube at the same G is possible.

For the empty tube, the isothermal data were predictable within 6% by the usual approximation

$$f = 0.046/Re_i^{0.2} \tag{40}$$

The empty tube friction factors obtained with heat addition were best corrected to isothermal conditions by multiplying them by the viscosity ratio (μ_b/μ_w) raised to the 0.35 power. Dormer and Bergles (45) also found in their extensive pressure drop study that the multiplying factor $(\mu_b/\mu_w)^{0.35}$ corrected their forced convection friction factors to isothermal conditions with the least deviation.

One may note in Fig. 27 that even for the relatively loose tape twist (y = 9.2) the pressure drop for the same G is over twice the empty tube value. This is reasonable considering the increased surface area acting on the fluid. If it is assumed that Eq. (40) based on D_h applies for the case of a straight tape, the pressure drop comparison at the same G would be

$$\Delta P_{y=\infty} = \Delta P_{empty} \Big/ (D_h/D_i)^{1.2} \tag{41}$$

The data of Smithberg and Landis (10) indicates that Eq. (41) correctly relates their straight tape and empty tube pressure drops.

The difference between the isothermal and heated friction factors for the swirl flow data was substantially less than the corresponding difference for the empty tube. This is reasonable if one considers the differences in the cross sections of the flow channels. For the swirl tubes, the effective channel size is decreased, but the total peripheral

shear stress is substantially increased. If we assume the viscosity correction represents the effective decrease in this total shear stress due to the decrease in viscosity of the fluid at the heated surfaces, this correction would be equal for the swirl and empty tube cases only if the thermal boundary layer thickness was the same at the tape surface and tube wall. Since the heat transfer from the tape is only a small percent of the total, it is probable that with heat addition the decrease in the shear stress at the tape surface is less than the decrease at the tube wall. The magnitude of the isothermal correction factor required for swirl flow would then also be less. To account for this difference the viscosity ratio exponent used to correct the empty tube heated friction factors to isothermal conditions was multiplied by the ratio (D_h/D_i) in order to correct the swirl data. That is

$$f_{s,iso} = f_s (\mu_b/\mu_w)^{0.35(D_h/D_i)} \qquad (42)$$

It can be seen in Fig. 27 that the data with heating for swirl flow were quite accurately corrected to isothermal conditions through application of Eq. (42). The friction factors with heat addition for the intermediate tape twists of y = 3.15 and 5.26 are not presented in Fig. 27 but they also were correctable to isothermal conditions by Eq. (42). It is not possible to check the validity of this correction method with the data of other investigators since information on their heated friction factors and corresponding viscosity ratios for swirl and straight flow have not been presented separately.

A comparison of the isothermal and swirl flow friction factors for water found in this study and previous studies is presented in Fig. 28. The variation in f with Re is similar for practically all investigations. For Re above 10^4, f decreases for an increase in Re in approximately the same manner as the conventional smooth tube straight flow f. The lower velocity f values of Smithberg and Landis (10) and Viskanta (18) appear to increase for a decrease in Re at a greater rate than the corresponding straight tube values, but this trend is not noted in the data of other investigators. The N-N curve for Gambill is presented to show the apparent roughness effect. For this curve $\epsilon/D_h = 1.7 \times 10^{-3}$ while for all others $\epsilon/D_h < 3 \times 10^{-4}$.

As shown in Fig. 29, the data of this investigation were correlated within 20% by the equation:

$$(f_s/f_a)_h = 2.75\, y^{-0.406} \qquad (43)$$

The smooth tube ($\epsilon/D_h < 3 \times 10^{-4}$) air and water data of several other investigators were also correlated by Eq. (43) within 30%. For comparison the early correlation of Gambill (12) which is based on the increases in the frictional surface area and flow path caused by the tape, Eq. (9), is also presented. However, as can be seen, the prediction of Eq. (9) is generally low for the majority of the data. The only significant deviation from the prediction of Eq. (43) occurred for the roughest tube of Gambill's later data (6) indicating that roughness can significantly effect the swirl flow pressure drop if it is above a

certain level. The magnitude of this roughness effect is still somewhat indeterminate from the data presently available, and a more comprehensive study would be required in order to accurately determine the effect of roughness on both the swirl flow heat transfer and pressure drop.

Considering the rather close agreement of the smooth tube swirl flow data of several investigators with the prediction of Eq. (43), it is recommended that this equation be used to predict the isothermal friction factors for similar smooth tube systems. For rough tubes, Eq. (8) of Gambill and Bundy (13) which was presented earlier is recommended.

An attempt was made to predict the forced convection swirl flow heat transfer coefficients from the corresponding more easily measured friction factors. It was impossible to accurately predict the heat transfer coefficients by a Colburn type analogy, however, because of the importance of the centrifugal convection effect. The pressure drop and friction factor tend to decrease for an increase in ΔT_f while the heat transfer coefficient tends to increase because of the increased centrifugal convection.

5.3 Surface Boiling Pressure Drop

When the heat flux is sufficient to cause the inception of surface boiling for a straight tube flow, the pressure drop will also tend to increase. As the heat flux is increased well beyond the inception point it has been shown by several investigators (45, 61, 62) that the overall

pressure drop will increase quite rapidly. This increase is generally attributed to the increased acceleration created by the non-equilibrium void fraction and the effect of bubble agitation on the overall flow pattern (45).

In Fig. 30 overall surface boiling pressure drop data for swirl flows with various tape twists are presented. Except for the uppermost curve, (y = 2.48, V = 25 ft/sec) all data represent fully developed surface boiling conditions. Comparison of the straight and swirl flow data at the same velocity shows that the percent increase in the overall pressure drop for an incremental rise in heat flux is significantly greater for the straight flows. The absolute pressure drop increase is also greater for the straight flows. This clearly indicates that for surface boiling with swirl flow the net pressure loss attributable to the bubble formation is less than for straight flow. This is reasonable, considering the swirl flow bubble observations discussed previously. Since the bubbles tend to leave the heated wall soon after they form, they are smaller than they might be in a comparable straight flow. The non-equilibrium void fraction and consequent pressure drop attributable to the bubbles would, therefore, be less for the swirl flow. The difference is further explained by the fact the bubbles are immediately removed from the wall and thus create less agitation of the velocity boundary layer. This is contrary to the observation of Brown (54) and Hosler (63) who noted that the bubbles remain close to the heated surface for subcooled boiling in

straight flows. If one makes the reasonable assumption that the wall shear stress is increased by the bubble agitation which, in turn, leads to an increased pressure drop, it can be seen that the pressure loss attributable to bubble agitation could also be less for swirl flows.

The difference between the surface boiling pressure drops with swirl and straight flows is more clearly seen in Fig. 31. The non-dimensional coordinates in this figure are a modified form of those originally presented by Dormer and Bergles (45). The abscissa is the ratio of the heat added in the boiling length, L_B, of the heated tube to the heat required to produce saturated exit conditions. It is therefore indicative of the exit subcooling. The ordinate $\Delta P_B / \Delta P_{adb}$, is the ratio of the actual pressure drop in the boiling length to the pressure drop that would exist in a similar adiabatic tube of length L_{sat}. The basic equations used to calculate these ratios are as follows. The non-boiling length, L_{NB}, is given by

$$L_{NB} = \left[T_{w,inc} - T_{in} - \frac{q/A}{h}\right] \frac{w\, c_p}{(q/A)\pi D_i} \qquad (44)$$

where $T_{w,inc}$ is found from Eq. (32) and h is determined from experimental data when available or by an appropriate prediction equation such as Eq. (29) for straight flow water data. The non-boiling pressure drop, ΔP_{NB}, is then calculated by

$$\Delta P_{NB} = 2f\,(L_{NB}/D)\, G^2/\rho \qquad (45)$$

where f is taken from experimental data at a Re based upon an average

temperature in the non-boiling length found from

$$\bar{T}_{NB} = \frac{1}{2}(T_{in} + T_{b,inc}) \tag{46}$$

with

$$T_{b,\,inc} = T_{in} + (q/A)\pi\, DL_{NB}/wc_p \tag{47}$$

If data is not available, f may be predicted by Eq. (42).

The boiling pressure drop is then

$$\Delta P_B = \Delta P_{test\ section} - \Delta P_{NB} \tag{48}$$

Similarly

$$L_B = L_h - L_{NB} \tag{49}$$

In Eqs. (48 and 49) it is assumed that the heated length coincides with the distance between the pressure taps. The heat added in the boiling length is now

$$q_B = (q/A)\pi\, DL_B \tag{50}$$

and

$$q_{sat} = w\, c_p\, (T_{sat,\,ex} - T_{in}) - (q/A)\pi DL_{NB} \tag{51}$$

The length from boiling inception to saturation is then

$$L_{sat} = q_{sat}\pi\, D/(q/A) \tag{52}$$

and finally

$$\Delta P_{adb} = 2\, f\, (L_{sat}/D)\, G^2/\rho \tag{53}$$

The evaluation of f and ρ in Eq. 53 is now based on $T_{b,inc}$ given by Eq. (47).

The results from Eqs. (48, 50, 51, and 53) are then used to calculate the desired dimensionless ratios.

Approximately 800 straight flow surface boiling data points of Reference (45) were plotted on these coordinates of $\Delta P_B / \Delta P_{adb}$ versus q_B/q_{sat}. They included a wide range of inlet temperature, flow rate, heat flux, and geometry. Plotted in this manner, it was found that the data could be correlated with a maximum deviation of 50% but an average deviation of approximately 20% by the following expressions:

For $q_B/q_{sat} \leq 0.125 (L_B/D)^{0.38}$

$$\Delta P_B/\Delta P_{adb} = 0.84 (q_B/q_{sat}) \tag{54}$$

For $q_B/q_{sat} > 0.125 (L_B/D)^{0.38}$

$$\Delta P_B/\Delta P_{adb} = \frac{\left[(q_B/q_{sat}) + F \right]^5}{0.142} \tag{55}$$

where $$F = 0.4311 (L_B/D)^{0.076} - 0.125 (L_B/D)^{0.38} \tag{56}$$

Additional work is currently in progress to refine the above correlations and apply them to the pressure drop data of other investigators. On the basis of the work done thus far, however, it is apparent that two regions are of interest for straight tube flows. The first which is predicted by Eq. (54) represents the moderate increase in ΔP for bubble agitation, while the second, Eq. (55), accounts for the more significant increase due to the non-equilibrium voids created by the bubbles. The (L_B/D) criteria for selection of the particular regime of importance is indicative of the effect of heat flux on the surface boiling ΔP.

In Fig. 31 it is apparent that the swirl data do not exhibit the dramatic increase in ΔP at the high heat flux levels, characteristic of the straight flow data. Burnout was reached for the highest q_B/q_{sat} point for $y = 2.48$, but the increase in pressure drop was still quite small.

It may be concluded on the basis of this comparison that the increase in pressure drop for swirl flow surface boiling is significantly less than that normally obtained with straight flows at the same exit subcooling. The reason for the difference appears to be due primarily to the smaller non-equilibrium void fraction present with the swirl flow which in turn will create less acceleration pressure drop. It may also be due in part to decreased boundary layer bubble agitation with swirl flow surface boiling.

Chapter VI

CONSTANT PUMPING POWER COMPARISON

The net benefit obtainable with a tape generated swirl flow can be found by comparing the swirl flow heat transfer coefficient for a given flow rate to the heat transfer coefficient in an empty tube of the same geometry whose velocity has been increased so that the pumping power requirements are the same. This will be referred to as a constant pumping power comparison. The equations required for this type of comparison will now be derived.

For constant pumping power

$$(Q \Delta P)_s = (Q \Delta P)_o \tag{57}$$

and

$$(A V \Delta P)_s = (A V \Delta P)_o \tag{58}$$

Introducing the definition of the friction factor given by Eq. (35) into Eq. (58) and cancelling like terms, we obtain

$$(A f_i V^3)_s = (A f_i V^3)_o \tag{59}$$

Equation (51) can also be expressed in terms of Re_i by

$$(A f_i Re_i^3)_s = (A f_i Re_i^3)_o \tag{60}$$

Assuming that $f_{i,o} = 0.046/Re_{i,o}^{0.2}$, Eq. (60) can be rearranged to yield the constant pumping power straight flow Reynolds number, which is

$$Re_{i,o} = \left[21.7 (A_s/A_o)(Re_{i,s})^3 f_{i,s}\right]^{0.357} \tag{61}$$

If the Reynolds number and friction factor are defined on the basis of the hydraulic diameter, the applicable equation for $Re_{i,o}$ would be

$$Re_{i,o} = \left[21.7\,(D_i/D_h)^4\,(A_s/A_o)(Re_{h,s})^3\,f_{h,s}\right]^{0.357} \qquad (62)$$

The Reynolds number found from Eq. (61) or (62) is then employed in the conventional straight tube correlation, Eq. (14), to calculate the desired constant pumping power straight flow heat transfer coefficient, h_o.

The h_s/h_o ratios for the forced convection heating data of this investigation (ΔT_f approximately constant and equal to 80°F) are plotted against the constant pumping power Reynolds number, Re_o, in Fig. 32. These data indicate that from 10 to 35% improvement in heat transfer is possible with swirl flow for a given pumping power. The tighter tape twists in the range y = 2.5 to 3.2 appear to yield improvement of at least 25% on this comparison basis. This is reasonable upon consideration of the improvement in h versus the increase in f as indicated by Figs. 9 and 29. It was shown in Chapter III that the heat transfer could be accurately predicted by Eq. (31). The q_{sc} contribution then varies as $\alpha^{0.8}$ (α is given by Eq. (1.7)) or approximately as 1/y and the q_{cc} contribution varies as $1/y^{0.67}$. For both terms the improvement will be significantly greater for a decrease in y below 3 than for a similar increase. The friction factor, however, appeared to vary as $1/y^{0.406}$, hence the net variation in f is less for a corresponding perturbation in y about 3.

The improvement for a given tape twist is reasonably constant with Reynolds number variations. An increase in ΔT_f will produce

a corresponding increase in h_s/h_o above the mean line which is drawn through the data points for each tape twist. This is caused by the increase in h_s due to the centrifugal convection without a corresponding increase in f. The data points for y = 3.15, which are above the mean line for y = 2.48 at $Re_o \approx 1.2 \times 10^5$, were in fact obtained with ΔT_f approximately 30°F above the mean values for the y = 2.48 data at this same Reynolds number. This points out that loose tape twists may be more effective than a tight twist if the ΔT_f is higher for the case of the loose twist.

In Fig. 33, a constant power comparison of the data of other investigators is presented. The higher Reynolds number data of Gambill et al. (6, 12) indicate approximately a 10% greater improvement in h_s at constant pumping power than observed in this investigation. The apparent improvement may be explainable by the fact the pressure drops, hence the friction factors were erroneously low for these early Gambill et al. data (12). Their later summary report (6) presented the amount by which their previous data differed from their more comprehensive correlation, Eq. (8). Corrections accounting for this difference were applied to their early friction factor data when computing the curves for Fig. 32, but it is possible that the actual values would have been different. Information on ΔT_f for these data of Gambill et al. is not available, but possible variations could perhaps account for the close grouping of the curves for the various tape twists.

The curves representing the data of Smithberg and Landis (10) indicate a decrease in improvement is noted for an increase in Re_o. For their very loose tape, y = 11, the rather large improvement at lower Re_o values is due to their high h's observed at these lower flows which was discussed earlier. Their very tight tape, y = 1.18, indicates an average improvement of approximately 15% occurs. This is somewhat less than that observed in the present study but the trend of the variation is not significantly different.

As a result of this comparison it is apparent that improvement in heat transfer is generally noted for a tape generated swirl flow over an equivalent constant power straight tube flow. The magnitude of the improvement appears to be dependent on the ΔT_f existing as well as the tape twist, and for a given tube, it is relatively insensitive to variations in the velocity level. Improvements of at least 25% seem probable for the tighter tape twists of y less than 3.2. With the inception of surface boiling, the constant power comparison would also show an improvement for swirl flows, since, as mentioned earlier, the pressure drop increase is significantly less for a surface boiling swirl flow than for a straight flow.

Chapter VII

CONCLUSIONS

The conclusions of this investigation on tape generated swirl flow can be summarized as follows:

7.1 Non-Boiling

1. The non-boiling heat transfer rate was shown to be a function of the tape twist, direction of heat transfer, and fin effect of the tape. The heat transfer coefficients obtained in this and other swirl flow investigations were accurately predicted by Eq. (31) which appears to account for all present and previously observed trends.

2. The improvement in heat transfer is greater with heating than with cooling. This difference appears to be due to the additional circulation, and resulting increase in heat removal, created by the centrifugal body force and favorable density gradient that are present only with heating. The temperature difference, ΔT_f, is, therefore, an important parameter in predicting the h for the heating of swirl flows. The results of a recent investigation by Thorsen (65) which were received too late for detailed analysis and inclusion in this report, are also in agreement with this conclusion.

3. The use of a Colburn type analogy to predict h on the basis of a known friction factor is not feasible for swirl flows.

4. For equal flow rates, twisted tapes increased the heat transfer above the empty tube value by as much as 85%. On the basis of constant

pumping power, the improvement was up to 35% with the tighter tape twists ($y < 3.2$) appearing to yield at least a 25% improvement.

5. The percent decrease in the pressure drop with heat addition is slightly less for a swirl flow than for a comparable empty tube flow.

7.2 Surface Boiling

1. The surface boiling heat transfer characteristics of the present swirl flows do not differ significantly from those observed with empty tube flows. The point of incipient boiling and the transition to fully developed boiling are predictable by conventional empty tube equations.

2. The bubbles generated in surface boiling swirl flow were observed to be very small and move away from the tube wall soon after they are formed which is different than comparable empty tube observations. Since the net improvement in heat transfer is similar for the two cases, however, this indicates that the dominant surface boiling heat transfer mechanism for both swirl and straight flows is similar.

3. The increase in pressure drop with surface boiling in swirl flow is substantially less than that normally observed with a comparable empty tube flow.

REFERENCES

1 Bergles, A. E., and Morton, H. L., "Survey and Evaluation of Techniques to Augment Convective Heat Transfer," M.I.T. Department of Mechanical Engineering, Report No. 5382-34, February 1965.

2 Gambill, W. R., and Greene, N. D., "Boiling Burnout with Water in Vortex Flow," Chem. Eng. Progress, vol. 54, October 1958, p. 68.

3 Evans, S. I., and Sarjant, R. J., "Heat Transfer and Turbulence in Gases Flowing Inside Tubes," Journal of the Institute of Fuel, vol. 24, September 1951, pp. 216-227.

4 Blum, H. A., and Oliver, L. R., "Heat Transfer in a Decaying Vortex System," ASME Paper No. 66-WA/HT-62, 1963.

5 Royds, R., Heat Transmission by Radiation, Conduction, and Convection, Constable and Co: London, England, First Edition, 1921.

6 Gambill, W. R., and Bundy, R. D., "An Evaluation of the Present Status of Swirl-Flow Heat Transfer," ORNL 61-4-61, April 24, 1961. Also ASME Paper No. 62-HT-42, 1962.

7 Colburn, A. P., and King, W. J., "Heat Transfer and Pressure Drop in Empty, Baffled, and Packed Tubes," Industrial and Engineering Chemistry, vol. 23, No. 8, 1931, pp. 910-923.

8 Kreith, F. and Margolis, D., "Heat Transfer and Friction in Turbulent Vortex Flow," Applied Scientific Research, Sect. A, vol. 8, No. 6, pp. 457-473, 1959.

9 Koch, R., "Pressure Loss and Heat Transfer for Turbulent Flow," VDI Forschungsheft, vol. 24, Series B, No. 469, 1958, pp. 1-44.

10 Smithberg, E., and Landis, F., "Friction and Forced Convection Heat Transfer Characteristics in Tubes With Twisted Tape Swirl Generators," ASME Paper No. 62-WA-176, 1962, also Journal of Heat Transfer, Trans. ASME, vol. 86, 1964, pp. 39-49.

11 Smithberg, E., "An Investigation Into the Heat Transfer and Friction Characteristics of Round Tubes With Twisted Tape Swirl Promoters," D. Eng. Sc. Thesis, Department of Mechanical Engineering, New York University, May 1961.

12 Gambill, W. R., Bundy, R. D., and Wansbrough, R. W., "Heat Transfer, Burnout, and Pressure Drop for Water in Swirl Flow Through Tubes With Internal Twisted Tapes, " ORNL-2911, March 1960.

13 Gambill, W. R., and Bundy, R. D., "High-Flux Heat Transfer Characteristics of Pure Ethylene Glycol in Axial and Swirl Flow," A.I.Ch.E. Journal, January 1963, pp. 55-59.

14 Feinstein, L., and Lundberg, R. E., "Fluid Friction and Boiling Heat Transfer With Water in Vortex Flow in Tubes Containing an Internal Twisted Tape," Stanford Research Institute, Menlo Park, California, RADC-TRR-63-451; Defense Documentation Center A.D. 430889, June 1963.

15 Ibragimov, M. H., Nomopfilov, E. F., and Subbotin, "Heat Transfer and Hydraulic Resistance with the Swirl-Type Motion of Liquid in the Pipe," Teploenergetika, No. 7, 1961.

16 Blatt, F. A., and Adt., R. R. Jr., "The Effects of Twisted Tape Swirl Generators on the Heat Transfer Rate and Pressure Drop of Boiling Freon II and Water," ASME Paper No. 63-WA-42, 1963.

17 Girnwalda, K., Blatt, T. A., and Bilger, R. W., "Engineering Study of Vapor Cycle Cooling Components for Space Vehicles," Technical Report No. ASD-TDR-63-582, September 1963.

18 Viskanta, R., Argonne National Lab., private communication to W. R. Gambill cited in Ref. (12) from J. F. Marchaterre (ANL), May 26, 1959.

19 Seymour, E. V., "A note on the Improvement in Performance Obtainable From Fitting Twisted-Tape Turbulence-Promoters to Tubular Heat Exchangers," Transactions Instn Chem Engrs, vol. 41, 1963, pp. 159-162.

20 International Nickel Company Technical Bulletin T-38, "Engineering Properties of Inconel Alloy X-750," 1963.

21 Powell, R. W., Tye, R. P., and Hickman, M. J., "The Thermal Conductivity of Nickel," International Journal of Heat and Mass Transfer, vol. 8, 1965, pp. 679-688.

22 International Nickel Company, Technical Bulletin T-15, "Engineering Properties of Nickel 200 and 201," 1964.

23 Kogan, C. L., Bell Aircraft Report No. 56-982-010.

24 Rohsenow , W. M., Somma, E. H., and Osborn, P. V., "Construction and Operation of Apparatus for Study of Heat Transfer with Surface Boiling," M.I.T. Technical Report No. 2, D.I.C. 6627, July 1, 1950. Personal Communication from the International Nickel Co.

25 Judd, R. L., Canadian General Electric Co. Ltd., Private Communication to W. R. Gambill cited in Ref. (12) above, Oct. 27, 1959.

26 Margolis, D., "The Effect of Turbulence Promoters on the Rate of Heat Transfer and the Pressure Drop in Straight Tubes," M. S. thesis, Lehigh University, 1957.

27 Viskanta, R., "Critical Heat Flux for Water in Swirling Flow," Nuclear Science and Engineering, vol. 10, 1961, pp. 202-203.

28 Goldman, K., "Improved Heat Transfer by Application of Centrifugal Forces," Nuclear Development Corporation of America, NDA2-79, June 1958.

29 "Swirl Flows and Critical Fluxes in Boiling Water at 70 Bars," SNECMA Special Report No. 16, EURAEC-900, 1963.

30 Rosuel, A., Sourioux, G., Dolle, J., Tournier, G., and Beghnin, A., "Escoulements Giratories Dans L'Eau Bouillante," SNECMA, Rapport Euraton No. 26, August 1966.

31 Gambill, W. R., "Generalized Prediction of Burnout Heat Flux for Flowing, Subcooled Wetting Liquids," A.I.Ch.E. Preprint No. 17, presented at the Fifth National Heat Transfer Conference, A.I.Ch.E. - A.S.M.E., Houston, Texas, August, 1962.

32 Bergles, A. E., and Rohsenow, W. M., "Forced-Convection Surface-Boiling Heat Transfer and Pressure Drop in Tubes of Small Diameter," M.I.T. Department of Mechanical Engineering, Report No. 8767-21, May 25, 1962.

33 Maulbetsch, J. S., and Griffith, P., "A Study of System Induced Instabilities in Forced Convection Flows with Subcooled Boiling," M.I.T. Department of Mechanical Engineering, Report No. 5382-35, April 15, 1965.

34 Kreith, F., and Summerfield, M., "Investigation of Heat Transfer at High Heat Flux Densities: Experimental Study with Water of Friction Drop with and without Surface Boiling in Tubes," Jet Propulsion Lab., C.I.T., Progress Report No. 4-68, 1948.

35 Kline, S. J., McClintock, F. A., "Describing Uncertainties in Single Sample Experiments," Mechanical Engineering, January 1953, pp. 3-8.

36 Wilson, E. E., "A Basis for Rational Design of Heat Transfer Apparatus," ASME Transactions, vol. 37, 1915, p. 47.

37 Ewing, C. T., Walker, B. E., Grand J. A., and Miller, R. R., "Thermal Conductivity of Metals," Liquid Metals Technology Chemical Engineering Progress Symposium Series, vol. 53, No. 20, 1957, pp. 19-24.

38 Powell, R. W., "Correlation of Metallic Thermal and Electrical Conductivities for Both Solid and Liquid Phases," International Journal of Heat and Mass Transfer, vol. 8, 1965, pp. 1033-1045.

39 Fine, M. E., "Correlation Between Electrical and Thermal Conductivity in Nickel and Nickel Alloys," Journal of Metals, vol. 188, p. 951, 1950.

40 International Nickel Company, Technical Bulletin T-7, "Engineering Properties of Inconel Alloy 600," 1964.

41 Powell, R. W., and Tye, R. P., "Thermal and Electrical Conductivities of Nickel-Chronium (Nimonic) Alloys, The Engineer, April 29, 1960, pp. 729-732.

42 Keenan, J. H., and Keyes, F. G., Thermodynamic Properties of Steam, John Wiley and Sons Inc: New York, First Edition, 1936.

43 Wellman and Sibbitt, "Heat Transfer Properties of Water," Combustion, April 1955.

44 McAdams, W. H., Heat Transmission, McGraw-Hill Book Co. Inc: New York, New York, Third Edition, 1954, p. 219.

45 Dormer, T., Jr., and Bergles, A. E., "Pressure Drop With Surface Boiling in Small Diameter Tubes," M.I.T. Department of Mechanical Engineering Report No. 8767-31, September 1, 1964.

46 Kreith, F., Principles of Heat Transfer, International Textbook Company: Scranton, Pennsylvania, Second Edition, 1965.

47 Dittus, F. W., and Boelter, L. M. K., "Heat Transfer in Automobile Radiators of the Tubular Type," University of California Publications in Engineering, vol. 2, No. 13, 1930, pp. 443-461.

48 Bergles, A. E., Rohsenow, W. M., "The Determination of Forced-Convection Surface-Boiling Heat Transfer," ASME Paper No. 63-HT-22, 1963, also Journal of Heat Transfer, Trans. ASME, August 1964, pp. 365-372.

49 McAdams, W. H., et al., "Heat Transfer at High Rates to Water with Surface Boiling," Industrial and Engineering Chemistry, vol. 41, 1949, pp. 1945-1953.

50 Fishenden, M., and Sanders, O. A., An Introduction to Heat Transfer, Oxford Press: New York, New York, 1950, pp. 180-182.

51 Desman, L. G., and Sans, E. W., NACA Research Memorandum, RME. 50H23, November, 1950.

52 Kays, W. M., and London, A. L., Compact Heat Exchangers, The National Press: Palo Alto, California, 1955, p. 41.

53 Forster, K. E., and Grief, R., "Heat Transfer to Boiling Liquid - Mechanism and Correlations," Transactions ASME, Journal of Heat Transfer, vol. 81, February 1959, pp. 43-53.

54 Brown, W. T., Jr., "A Study of Flow Surface Boiling," Ph. D. Thesis, Mech. Eng. Dept., M.I.T., February, 1967.

55 Merte, H., Jr., and Clark, J. A., "Pool Boiling in an Accelerating System," ASME Paper No. 60-HT-22, 1960.

56 Costello, C. P., and Tuthill, W. E., "Effects of Acceleration on Nucleate Pool Boiling," Paper No. 60, Chem. Eng. Progress Symposium Series, vol. 57, No. 32, 1961, pp. 189-196.

57 Kays, W. M., and London, A. L., Compact Heat Exchangers, McGraw-Hill Book Co., Inc: New York, New York, Second Edition, 1964, pp. 93-95.

58 Dorsey, N. E., Properties of Ordinary Water Substance, Reinhold Publishing Co: New York, New York, 1940.

59 Eckert, E. R. G., and Diagula, A. J., "Convective Heat Transfer - Flow Through Tubes," Trans. ASME, vol. 75, 1954, pp. 497 - 504.

60 Rohsenow, W. M., and Choi, H. Y., Heat, Mass, and Momentum Transfer, Prentice-Hall, Inc: Englewood Cliffs, New Jersey, 1961.

61 Owens, W. L., and Schrock, V. E., "Local Pressure Gradients for Subcooled Boiling of Water in Vertical Tubes," ASME Paper No. 60-WA-249, 1960.

62 Reynolds, J. B., "Local Boiling Pressure Drop," Argonne National Laboratory Report 5178, March, 1954.

63 Hosler, E. R., "Visual Study of Boiling at High Pressure," Chemical Engineering Progress Symposium Series, vol. 61, No. 57, 1965, pp. 269-279.

64 Eubank, O. C., and Proctor, W. S., SM Thesis, Mech. Eng. Dept., M.I.T., 1951.

65 Thorsen, Richard S., "Friction and Heat Transfer Characteristics in Turbulent Swirl-Flow Subjected to Large Transverse Temperature Gradients," Ph. D. Thesis, New York University, January, 1967.

APPENDIX

APPENDIX I

BASIC SWIRL FLOW EQUATIONS

The following equations were used to describe the flow in a twisted tape swirl channel

$$D_h = \frac{4\,(\text{Flow Area})}{\text{Wetted Perimeter}} = \frac{4\left(\pi D_i^2/4 - \delta_f D_i\right)}{\pi D_i + 2 D_i - 2\delta_f}$$

or

$$D_h = \frac{\pi D_i + 4\delta_f}{\pi + 2\,(1 - \delta_f/D_i)} \tag{1.1}$$

The difference between the hydraulic diameter and the inside tube diameter is then expressed by

$$\frac{D_h}{D_i} = \frac{1 - \frac{4\delta_f}{\pi D_i}}{1 + \frac{2}{\pi}\left(1 - \frac{\delta_f}{D_i}\right)} \tag{1.2}$$

Equation (1.2) may also be used to convert Reynolds numbers and friction factors based upon D_h to corresponding values based upon D_i. That is

$$\frac{D_h}{D_i} = \frac{Re_h}{Re_i} = \frac{f_h}{f_i} \tag{1.3}$$

The length of the spiral edge of the twisted tape, L_s, in a given axial length, L_a, is found from geometric considerations to be

$$L_s = \frac{L_a}{2y}\left(4y^2 + \pi^2\right)^{1/2} \tag{1.4}$$

Where y = Inside diameters/180° tape twist

A rotating slug flow model as first proposed by Gambill et al., (12) was used in this study to estimate the total velocity of the fluid at the wall and resulting centrifugal acceleration. The tangential velocity component with this model is then

$$V_t = V_a \frac{\pi}{2y} \quad \frac{r}{r_i} \tag{1.5}$$

The resultant velocity at the tube wall is then the vector sum of the tangential and axial flow components at the wall.

$$V_s = \left[V_a^2 + \left(\frac{V_a \pi}{2y} \right)^2 \right]^{\frac{1}{2}}$$

or

$$V_s = \frac{V_a}{2y} \left(4y^2 + \pi^2 \right)^{1/2} \tag{1.6}$$

Eq. (1.6) could have been obtained directly from Eq. (1.4) by merely observing that a particle of fluid at the tube wall for swirl flow must traverse a greater distance in a given time period. The ratio of the swirl velocity and flow path to the corresponding straight tube quantities is then

$$\alpha \equiv \frac{L_s}{L_a} = \frac{V_s}{V_a} = \frac{(4y^2 + \pi^2)^{1/2}}{2y} \tag{1.7}$$

The centrifugal acceleration at any point is

$$a_t = \frac{V_t^2}{r} = \left(\frac{V_a \pi}{2y} \right)^2 \cdot \frac{r}{r_i^2} \tag{1.8}$$

At the wall, this is

$$a_s = \frac{1}{2 D_i}\left(\frac{V_a \pi}{y}\right)^2 \tag{1.9}$$

The conventional Grashof number based upon the hydraulic diameter as the characteristic length is

$$Gr = \frac{g \beta \Delta T_f D_h^{\ 3}}{\nu^2} \tag{1.10}$$

If the g in Eq. (1.9) is replaced by the expression for a_s, we obtain

$$Gr = \frac{\pi^2}{2 y^2}\left(\frac{V_a D_h}{\nu}\right)^2 \cdot \frac{D_h}{D_i} \cdot \beta \Delta T_f \tag{1.11}$$

or equivalently

$$Gr = \frac{4.94}{2 y^2} \cdot Re_h^{\ 2} \cdot \frac{D_h}{D_i} \cdot \beta \Delta T_f \tag{1.12}$$

The radial pressure gradient for an inviscid, isothermal fluid in swirl flow may be found by application of Euler's equation normal to a streamline with the tangential velocity expressed by Eq. (1.5) or by a force balance on a differential element. Smithberg and Landis (10, 11) elected to use the former method while Gambill et al. (12) used the latter. The final result was the same in both cases.

Using Euler's equation, one may write

$$\frac{\partial P}{\partial r} = \frac{\rho}{g_c} \frac{V_t^{\ 2}}{r} \tag{1.13}$$

or $$\frac{\partial P}{\partial r} = \frac{\rho}{g_c} \cdot \left[\frac{Va \cdot \pi}{2y \cdot r_i}\right]^2 r \qquad (1.14)$$

Hence, $$\int_{P_\ell}^{P_w} dP = \int_0^{r_i} \frac{\rho}{g_c} \cdot \left[\frac{Va\ \pi}{2y\ r_i}\right]^2 r\ dr \qquad (1.15)$$

For the incompressible case (ρ = constant), this yields upon integration:

$$P_w - P_\ell = \frac{\rho\ Va^2 \pi^2}{8\ y^2\ g_c} \qquad (1.16)$$

For a cylindrical control volume of width dr and unit depth into the paper, 1, the force balance would be

$$dF = dm\ \frac{a_t}{g_c} \qquad (1.17)$$

If $dm = \rho\, r\, \pi\, 1\, dr$

and $A = \pi r\, 1$ (1.18)

Then $$\frac{dF}{A} = \frac{\rho}{g_c}\left(\frac{Va\ \pi}{2y\ r_i}\right)^2 r\ dr \qquad (1.19)$$

Integration of Eq. (1.19) from $r = 0$ to $r = r_i$ will then give

$$P_w - P_\ell = \frac{\rho\ Va^2 \pi^2}{8\ y^2\ g_c} \qquad (1.20)$$

This result is identical to Eq. (1.16) obtained previously.

For compressible fluids such as air which obey the perfect gas relation, $p = \rho R T$, Eq. (1.14) yields upon separation of variables

$$\frac{dP}{P} = \left[\frac{Va^2\ \pi^2}{R\ T\ g_c\ 4y^2\ r_i^2}\right] r\ dr \qquad (1.21)$$

Integration of Eq. (1.21) yields

$$\ln P = \frac{Va^2 \pi^2 \quad r^2}{8\, y^2 \quad g_c \quad r_i^2 \quad R\, T} + \ln C \tag{1.22}$$

The radial pressure and density ratios for this case are then

$$\frac{P_w}{P_\ell} = \frac{\rho_w}{\rho_\ell} = \exp\left[\frac{Va^2 \pi^2}{8\, y^2 \quad g_c \, R\, T}\right] \tag{1.23}$$

APPENDIX 2

DETAILS OF DATA CALCULATION PROCEDURE

The experimental data for all isothermal and heated runs were reduced by a computer program on the IBM 7094. The equations and computational methods used by this program are outlined in this appendix, and Fig. 5 is a printout of the results for a typical run.

Input Information

The test section input information was as follows: D_i, D_o, k, α_k, ρ_o, α_ρ, L_h, y, axial length of each tube wall thermocouple from the beginning of the heated length, and location of the pressure taps relative to the heated length.

The run input information consisted of run number, date, T_{in}, T_{ex}, w, P_{ex}, Δ P, E, I, and $T_{ow(1-6)}$.

Tube Wall Temperature Drop

The tube wall temperature drop was calculated for each wall thermocouple by the Kreith and Summerfield series solution (34) to the equation

$$\frac{d}{dr}\left(k(T)r\ \frac{dT}{dr}\right) + rW_i = 0 \qquad (2.1)$$

With boundary conditions of

$$\text{at } r = 0, \quad \frac{\partial T}{\partial r} = 0, \quad T = T_{ow} \qquad (2.2)$$

and assumed linear variation in tube properties of the forms

$$\rho = \rho_o (1 + \alpha_\rho T) \tag{2.3}$$

$$k = k_o (1 + \alpha_k T) \tag{2.4}$$

The first few terms of the solution, which accounts for the variations in both ρ and k of the tube are

(2.5)

$$T_{iw} = T_{ow} - \frac{m (D_o - D_i)^2}{4 (1 + \alpha_\rho T_{ow})(1 + \alpha_k T_{ow})} - \frac{m(D_o - D_i)^3}{12 D_o (1 + \alpha_\rho T_{ow})(1 + \alpha_k T_{ow})}$$

$$- \frac{(D_o - D_i)^4}{16} \left[\frac{m^2 (3\alpha_k + 4\alpha_\rho \alpha_k T_{ow} + \alpha_\rho)}{6 (1 + \alpha_\rho T_{ow})^3 (1 + \alpha_k T_{ow})^3} + \frac{m}{D_o^2 (1 + \alpha_\rho T_{ow})(1 + \alpha_k T_{ow})} \right] \ldots,$$

where $$m = \frac{8 \times 3.413 \, \bar{\rho}^2 I^2}{\rho_o k_o \pi^2 (D_o^2 - D_i^2)^2}$$

The variation in resistivity with temperature was found experimentally for the tubes used in this study. It was determined by measuring the voltage drop which occurred as a result of passing a known current through a carefully measured test section held at different temperatures in a constant temperature oven. The results are shown in Fig. 3, and it can be seen that very close agreement exists between this present data and that of other investigators. The equations shown on Fig. 7 were used to represent the ρ variation in Eq. (2.5).

A survey of the experimental and theoretical predictions for the variation with temperature of the thermal conductivity of nickel was made, and the results are shown in Fig. 8. A rather high degree of scatter is apparent. This is characteristic of thermal conductivity data,

however, since it is much more difficult to accurately measure than the electrical resistivity. A considerable amount of work has been devoted towards predicting the thermal conductivity from the more easily measured electrical resistivity (37, 38, 39). It was, therefore, appropriate to apply such predictions to the resistivity data of this study. In 1950, Fine (39) presented such a conductivity prediction method especially for nickel and nickel alloys. His recommended correlation equation, which was supposed to be accurate within 20%, is

$$k = \frac{2.13 \times 10^{-8} \times T}{\rho} + 0.084 \qquad (2.6)$$

The units in Eq. (2.6) are: k - watts/cm°C, T -°Kelvin, ρ -ohm-cm. The first term on the right hand side of Eq. (2.6) accounts for the electronic (metallic) conduction while the second accounts for the molecular (nonmetallic) contribution.

Ewing et al. (37) in a later study analyzed over 140 metals and alloys and developed a more generalized correlation. They reasoned, that since resistivity is generally measured under isothermal conditions while a temperature gradient is required for conductivity observations, the mean free path of an electron in the thermal measurement would be less than that in an electrical measurement at the same temperature. This would then reduce the metallic conductivity contribution. Their general equation with a reported over-all average deviation of 5% is

$$k = 2.61 \times 10^{-8}(T/\rho) - 2 \times 10^{-17}(T/\rho)^2 \Big/ c_p d + 97\, c_p\, d^2 \Big/ M\, T \qquad (2.7)$$

The units in this equation are: k-watts/cm°C, T-°Kelvin, ρ -ohm-cm, c_p-calories/gram°C, d-grams/cc, M-average molecular weight.

Considering the close agreement (within 5%) of the prediction of Eq. (2.7) with the experimental data of Powell et al. (21), it was decided to use their results to represent k in Eq. (2.5).

A subroutine was written that evaluated Eq. (2.5) for a six term series. It was an iterative calculation since the mean resistivity, $\bar{\rho}$, is a function of the mean temperature in the tube wall.

Heat Transfer Coefficient

The heat input to the fluid was determined as follows by three different methods, and the results were required to agree within 5%.

$$q = E\ I\ X\ 3.413 \tag{2.8}$$

$$q = wc_p\,(T_{ex} - T_{in}) \tag{2.9}$$

$$q = \frac{I^2 \rho L_h\ X\ 3.413\ X\ 4}{\pi\ (D_o^2 - D_i^2)} \tag{2.10}$$

The heat flux was then defined using the result from Eq. (2.8) as

$$q/A = q/\pi\ D_i\ L_h \tag{2.11}$$

The bulk fluid temperature at each thermocouple location was found by assuming a linear variation in the bulk temperature within the heated length.

The heat transfer coefficient was then found from

$$h = \frac{q/A}{(T_{iw} - T_b)} \tag{2.12}$$

Evaluation of Fluid Properties and Dimensionless Groups

The evaluation of the fluid properties as a function of temperature or pressure and the thermocouple millivolt/temperature conversions were accomplished by a SHARE subroutine entitled "TAINT Code AL., Univariate Table Look-Up and Interpolation for Multiple Arrays," written at the NASA, Ames Research Center, Moffett Field, California. The values for the temperature dependent variables of ρ, μ, k, and β were stored internally at five degree temperature increments and the saturation temperatures corresponding to a given pressure were stored at five pound pressure increments. The TAINT subroutine would effect a polynomial curve fit in order to determine the value of a dependent variable for a given temperature or pressure.

The values of ρ as a function of temperature and of T_{sat} as a function of pressure were found in Keenan and Keyes (42). The values for μ and k as a function of temperature were taken from the data of Wellman and Sibbitt (43), while the variation in β with temperature was determined from the work of Dorsey (58).

The dimensionless groups presented in Fig. 5 were calculated for each wall thermocouple as follows

$$NU = \frac{h D_i}{k} \tag{2.13}$$

$$RE = \frac{G D_i}{\mu} \tag{2.14}$$

where $$G = \frac{w}{\pi D_i^2/4 - \delta_f D_i} \tag{2.15}$$

$$PR = \frac{c_p \mu}{k} \tag{2.16}$$

$$FR = \frac{\Delta P D_i \rho}{2 L_p G^2} \tag{2.17}$$

$$EJ = NU/Pr^{0.4} \tag{2.18}$$

$$UR = (\mu_w/\mu_b) \tag{2.19}$$

$$GR = \frac{g \beta \Delta T_f D_i^3}{\nu^2} \tag{2.20}$$

The average values were calculated by a numerical integration of the curve fit to the local values normalized with respect to the heated length. That is

$$F_{average} = \frac{1}{L_h}\int_1^6 F(x)dx \approx \frac{1}{L_h}\sum_{n=1}^{6} F(n)\,\Delta n \tag{2.21}$$

The Δn's were input variables for a given tube and represented the incremental length associated with each wall thermocouple.

APPENDIX 3

ERROR ANALYSIS

In order to determine the probable error in the presentation of the forced convection and boiling data, an error analysis was made in the manner recommended by Kline and McClintock (35). Uncertainties were assigned to all observed variables and it was presumed that the uncertainty distribution (i.e. the manner in which the observed value varies from the actual) was normal for these variables.

The coordinates for the data presentations are: Forced convection - $(Nu/Pr^{0.4})$ versus Re; Boiling - q/A versus ΔT_{sat}. The functional relations for the results of interest are then

$$q/A = q/A\,(E,\ I,\ D_i,\ L_h)$$

$$T_i = T_i\,(I, \rho,\ k,\ D_o,\ D_i,\ T_o)$$

$$T_{sat} = T_{sat}\,(P_x)$$

$$Nu = Nu\,(q/A,\ T_i,\ T_b,\ D_i,\ k_b)$$

$$Re = Re\,(w,\ A_c,\ \mu_b)$$

The uncertainties in the observable quantities were estimated to be

Observed Variable	W = Uncertainty
T_o	2.0°F
T_b	2.0°F
P	1.0 psi
T_{sat}	3.0°F
D_o and D_i	0.001 in.
L_h	0.01 in.

$\frac{W_{kw}}{k_w}$ = 2.0%, $\frac{W_\rho}{\rho}$ = 10%, $\frac{W_{A_c}}{A_c}$ = 5%,

$$\frac{W_{Pr^{0.4}}}{Pr^{0.4}} = 2.0\%, \qquad \frac{W_{\mu}}{\mu} = \frac{W_k}{k} = \frac{W_w}{w} = 0.5\%$$

The uncertainties in the current and voltage depend on the particular meter scale used to observe their values for a particular run.

The probable error for the quantities in Eq. (3.1) were then found by what is commonly referred to as the second-power equation. For $q/A = E\,I/\pi D_i\,L_h$ the probable uncertainty in q/A would be

$$W_{q/A} = \left[\left(\frac{\partial(q/A)}{\partial E} W_E\right)^2 + \left(\frac{\partial(q/A)}{\partial I} W_I\right)^2 + \left(\frac{\partial(q/A)}{\partial D_i} W_{D_i}\right)^2 + \left(\frac{\partial(q/A)}{\partial L_h} W_{L_h}\right)^2\right]^{\frac{1}{2}} \tag{3.2}$$

This equation can be reduced to

$$\frac{W_{q/A}}{q/A} = \left[\left(\frac{W_E}{E}\right)^2 + \left(\frac{W_I}{I}\right)^2 + \left(\frac{W_{D_i}}{D_i}\right)^2 + \left(\frac{W_L}{L}\right)^2\right]^{\frac{1}{2}} \tag{3.3}$$

For a typical forced convection non-boiling run, the evaluation of Eq. (3.3) is

$$\frac{W_{q/A}}{q/A} = \left[\left(\frac{.05}{6}\right)^2 + \left(\frac{0.03}{11.3}\right)^2 + \left(\frac{0.001}{.193}\right)^2 + \left(\frac{0.01}{14.5}\right)^2\right]^{\frac{1}{2}} = 1.02\% \tag{3.4}$$

With the higher heat flux boiling runs, the probable error in the worst case would be

$$\frac{W_{q/A}}{q/A} = \left[\left(\frac{0.15}{15}\right)^2 + \left(\frac{0.2}{26}\right)^2 + \left(\frac{0.001}{.193}\right)^2 + \left(\frac{.01}{14.5}\right)^2\right]^{\frac{1}{2}} = 1.62\% \tag{3.5}$$

The error in the tube wall temperature drop may be estimated by assuming this drop is given by the exact solution to Eq. (2.1), neglecting the

radial variation in tube properties, which is

$$\Delta T_{wall} = \frac{3.413 I^2 \rho X}{4\pi^2 k} \qquad (3.6)$$

where $$B = \left(\frac{r_i}{r_o}\right)^2 , \quad X = \left[\frac{\ln B}{B-1} - 1\right] \frac{1}{(r_o^2 - r_i^2)}$$

By taking the required partial derivatives, the applicable second power equation for the uncertainty in Eq. (3.6) is found to be

$$\frac{W_{\Delta T_{wall}}}{\Delta T_{wall}} = \left\{\left(\frac{W_\rho}{\rho}\right)^2 + \left(\frac{2W_I}{I}\right)^2 + \left(\frac{W_k}{k}\right)^2 + \left[\frac{W_{r_i}}{X}\left(\frac{2\left(1 + B + \frac{2B}{1-B}\ln B\right)}{r_i r_o^2 (1 - B^2)}\right)\right]^2 + \left[\frac{W_{r_o}}{X}\left(\frac{2}{r_o^2 (1-B)^3}\cdot\left\{2(1-B) + (1-B)\ln B\right\}\right)\right]^2\right\}^{\frac{1}{2}} \qquad (3.7)$$

In the evaluation of the various terms of Eq. (3.7), the probable uncertainty in resistivity and conductivity are the most important error source. The error introduced by the uncertainty in the current is small in comparison, hence, the probable error in ΔT_{wall} is practically independent of heat flux level. The evaluation of Eq. (3.7) for a typical case is

$$\frac{W_{\Delta T_{wall}}}{\Delta T_{wall}} = \left[10^{-2} + .12 \times 10^{-4} + 4 \times 10^{-2} + .576 \times 10^{-2} + .166 \times 10^{2}\right]^{\frac{1}{2}} \qquad (3.8)$$

$$= 23.9\%$$

The net error in the inside wall temperature may then be found from

$$\frac{W_{T_i}}{T_i} = \left[W_{T_o} + \left(\frac{W_{\Delta T_{wall}}}{\Delta T_{wall}}\right)\cdot \Delta T_{wall}\right] \Big/ T_i \qquad (3.9)$$

Evaluation of Eq. (3.6) for a high heat flux surface boiling run yields

$$\frac{W_{T_i}}{T_i} = (2.0 + 0.239 \times 39) \Big/ 358 = 3.18\% \qquad (3.10)$$

For the non-boiling, forced convection runs, the probable error in the inside wall temperature is less. In the worst case, it was found to be

$$\frac{W_{T_i}}{T_i} = (2.0 + 0.239 \times 15) / 260 = 2.15\% \qquad (3.11)$$

While the probable error in the tube wall temperature drop may be large, the error in the calculated inside wall temperature remains small as long as the magnitude of ΔT_{wall} is small. Thin walled, relatively high conductivity nickel tubing was selected for use in this study in order to minimize the tube wall temperature drop and thus negate the probability of large errors being introduced by the uncertainty in tube properties.

The error in the calculated wall superheat, ΔT_{sat} may be expressed by

$$\frac{W_{\Delta T_{sat}}}{\Delta T_{sat}} = \frac{W_{T_i}}{T_i} + \frac{W_{T_{sat}}}{T_{sat}} \qquad (3.12)$$

Using the results of Eq. (3.10) and the estimated uncertainty in T_{sat}, the maximum probable error in ΔT_{sat} on a boiling plot is

$$\frac{W_{\Delta T_{sat}}}{\Delta T_{sat}} = 3.18 + \frac{3 \times 100}{280} = 4.25\% \qquad (3.13)$$

The expression for estimating the error in the calculation of the heat transfer coefficient by Eq. (2.12) is

$$\frac{W_h}{h} = \left[\left(\frac{W_{q/A}}{q/A} \right)^2 + \left(\frac{W_{T_i}}{T_i} + \frac{W_{T_b}}{T_b} \right)^2 \right]^{\frac{1}{2}} \qquad (3.14)$$

Introducing the results from Eqs. (3.4) and (3.11) into Eq. (3.14) yields for a forced convection non-boiling run

$$\frac{W_h}{h} = \left[(1.02)^2 + \left(2.15 + \frac{2 \times 100}{155}\right)^2\right]^{\frac{1}{2}} = 3.58\% \qquad (3.15)$$

The probable error in Nu is then

$$\frac{W_{Nu}}{Nu} = \left[\left(\frac{W_h}{h}\right)^2 + \left(\frac{W_D}{D}\right)^2 + \left(\frac{W_k}{k}\right)^2\right]^{\frac{1}{2}} \qquad (3.16)$$

or

$$\frac{W_{Nu}}{Nu} = \left[3.58^2 + \left(\frac{.1}{.193}\right)^2 + (0.5)^2\right]^{\frac{1}{2}} = 3.64\% \qquad (3.17)$$

The maximum error in the ordinate, $X = (Nu/Pr^{0.4})$, for a forced convection run would then be

$$\frac{W_X}{X} = \left[\left(\frac{W_{Nu}}{Nu}\right)^2 + \left(\frac{W_{Pr^{0.4}}}{Pr^{0.4}}\right)^2\right]^{\frac{1}{2}} = (3.64^2 + 2^2)^{\frac{1}{2}} = 4.17\% \qquad (3.18)$$

The probable error in Re can be found from

$$\frac{W_{Re}}{Re} = \left[\left(\frac{W_G}{G}\right)^2 + \left(\frac{W_{D_i}}{D_i}\right)^2 + \left(\frac{W_\mu}{\mu}\right)^2\right]^{\frac{1}{2}} \qquad (3.19)$$

where

$$\frac{W_G}{G} = \left[\left(\frac{W_w}{w}\right)^2 + \left(\frac{W_{A_c}}{A_c}\right)^2\right]^{\frac{1}{2}} \qquad (3.20)$$

For the typical forced convection run, the probable error in G will then be

$$\frac{W_G}{G} = \left(0.5^2 + 5^2\right)^{\frac{1}{2}} = 5.02\% \qquad (3.21)$$

This in turn leads to a probable error in Re for a typical run of

$$\frac{W_{Re}}{Re} = \left[(5.02)^2 + \left(\frac{.1}{.193}\right)^2 + (0.5)^2\right]^{\frac{1}{2}} = 5.1\% \qquad (3.22)$$

APPENDIX 4

DERIVATION OF FIN EFFECT EQUATIONS

The amount of heat that is transferred by the tape acting as a fin may be estimated by treating both the tube wall and the tape as fins. Since the heat flux is uniform in the tube wall, the presence of the tape can be thought of as creating a circumferential variation in the tube wall temperature, which has the effect of causing the wall to act as a fin. This circumferential temperature variation would be superimposed on the uniform radial temperature drop caused by the electric heating and would in fact be responsible for the additional heat transferred by the tape. Taking into account the symmetry, the problem is modeled as follows:

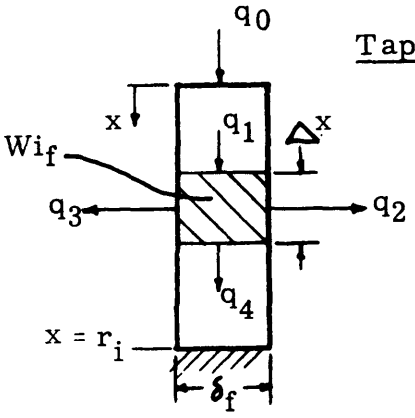

Tape

$T_f = f(x)$

Boundary Conditions

$$\frac{d T_f}{dx} = 0 \quad \text{at} \quad x = r_i \qquad (4.1a)$$

$$q_o = -k_f \delta_f L \frac{d T_f}{dx} \quad \text{at} \quad x = 0 \qquad (4.1b)$$

Tube

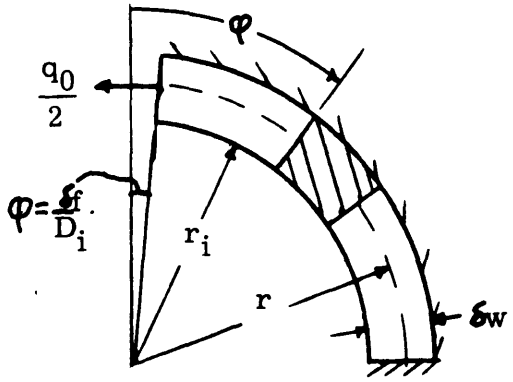

$T_w = f(\varphi)$

$r = \frac{2}{3} r_o + \frac{1}{3} r_i$

Boundary Conditions

$$\frac{d T_w}{d \varphi} = 0 \quad \text{at} \quad \varphi = \frac{\pi}{2} \qquad (4.2a)$$

$$\frac{q_o}{2} = \frac{k_w \ w \ L}{r} \ \frac{d T_w}{d} \ \text{at} \ \varphi = \frac{\delta f}{D_i} \qquad (4.2b)$$

The contact resistance between the tape and tube wall is considered negligible since the tape uniformly penetrated the wall.

A heat balance on a differential element of the tape would be

$$q_1 - q_2 - q_3 - q_4 + Wi_f \delta_f \Delta x \, L = 0 \tag{4.3}$$

$$\text{Define} \quad \Theta = T - T_b \tag{4.4}$$

From the definition of h we know

$$q_2 = q_3 = h \, \Delta x \, L \Theta_f \tag{4.5}$$

Neglecting the higher order terms in the Fourier expression for T_f at $(x + \Delta x)$ we can also write

$$q_1 - q_4 = k_f \delta_f \frac{d^2 T_f}{dx^2} \Delta x \, L \tag{4.6}$$

Introducing these results into Eq. (4.3) and cancelling like terms yields

$$\frac{d^2 \Theta_f}{dx^2} - \frac{2 h \Theta_f}{k_f \delta_f} + \frac{Wi_f}{k_f} = 0 \tag{4.7}$$

This equation can be solved by letting

$$\Theta_f = \lambda + \frac{Wi_f \delta_f}{2 h} \tag{4.8}$$

Then

$$\frac{d^2 \lambda}{dx^2} - \frac{2 h \lambda}{k_f \delta_f} = 0 \tag{4.9}$$

Equation (4.9) may now be solved by letting $\lambda = e^{mx}$. This yields upon substitution in Eq. (4.9) and consideration of Eq. (4.8) the result

$$\Theta_f = K_1 e^{mx} + K_2 e^{-mx} + \frac{Wi_f \delta_f}{2 h_f} \tag{4.10}$$

where

$$m = \sqrt{\frac{2 h_f \delta_f}{k_f}} \tag{4.11}$$

The constants K_1 and K_2 may be solved for by applying to Eq. (4.10) the boundary conditions presented in Eq. (4.1). The final expression for the temperature distribution in the tape is then

$$\theta_f = \frac{q_o \left[e^{mx/\delta_f} + e^{m(D_i - x)/\delta_f} \right]}{k_f L m (e^{m D_i/\delta_f} - 1)} + \frac{Wi_f \delta_f}{2h} \qquad (4.12)$$

The temperature distribution in the tube wall may be found in a similar manner. The differential energy balance in this case yields

$$\frac{d^2\theta_w}{d\varphi^2} - \frac{h r r_i \theta_w}{k_w \delta_w} + \frac{r^2}{k_w} \cdot Wi_w = 0 \qquad (4.13)$$

The solution to Eq. (4.13) can be found by effecting a transformation similar to Eq. (4.8) and following the same procedure which led to Eq. (4.12). The desired temperature distribution in this case is found to be

$$\theta_w = \frac{r q_o \left[e^{B\varphi} + e^{B(\pi - \varphi)} \right]}{L\sqrt{4 k_w \delta_w r r_i h} \left[e^{B\delta_w/D_i} - e^{B(\pi - \delta_w/D_i)} \right]} + \frac{Wi_w \delta_w r}{h r_i} \qquad (4.14)$$

where:

$$B = \sqrt{\frac{h r r_i}{k_w \delta_w}} \qquad (4.15)$$

The heat transferred from the tube wall to the tape, q_o, is solved for by letting $\theta_w (\varphi = 0) = \theta_f (x = 0)$. The resulting expression for q_o is

$$q_o = \frac{1}{\epsilon} \left[\frac{Wi_f \delta_f}{2h} - \frac{Wi_w \delta_w r}{h r_i} \right] \qquad (4.16)$$

where

$$\epsilon = \left[\frac{r\,(1 + e^{B\pi})}{L\sqrt{4\,k_w \delta_w\, r\, r_i\, h_w}\,\left[e^{B\delta_f/D_i} - e^{B(\pi - \delta_f/D_i)}\right]} - \frac{(1 + e^{m\,D_i/\delta_f})}{k_f\, L\, m\,(e^{m\,D_i/\delta_f} - 1)} \right] \tag{4.17}$$

The fraction of the total heat transfer that is attributable to the tape fin effect is

$$\gamma = \frac{q_o + Wi_f \delta_f\, r_i\, L}{Wi_f \delta_f\, r_i\, L + Wi_w \delta_w \pi r\, L} \tag{4.18}$$

Introducing Eqs. (4.16) and (4.17) into Eq. (4.18) yields the desired fin effect

$$\gamma = \frac{1 + \frac{1}{\epsilon}\left[\frac{1}{2\,h\,r_i\,L} - \frac{Wi_w \delta_w\, r}{Wi_f \delta_f\, r_i^{\,2}\, h\, L}\right]}{1 + \frac{Wi_w \delta_w\, L \pi r}{Wi_f \delta_f\, L\, r_i}} \tag{4.19}$$

The ratio (Wi_w/Wi_f) can be expressed in terms of the electrical resistivity if the tape is assumed to be a resistance in parallel with the tube. That is:

$$(I\,R)_f = (I\,R)_w \tag{4.20}$$

or

$$\frac{I_f}{I_w} = \frac{R_w}{R_f} = \left(\frac{\rho\, L}{A_x}\right)_w \left(\frac{A_x}{\rho\, L}\right)_f \tag{4.21}$$

Invoking the definitions of resistivity and internal heat generation yields:

$$\frac{Wi_w}{Wi_f} = \frac{I_w^{\,2} \rho_w}{A_{x,w}(A_{x,w} L)} \cdot \frac{A_{x,f}\,(A_{x,f}\, L)}{I_f^{\,2} \rho_f} \tag{4.22}$$

Introducing Eq. (4.21) into Eq. (4.22) will then give the desired result

$$\frac{Wi_w}{Wi_f} = \frac{\rho_f}{\rho_w} \tag{4.23}$$

The evaluation of the tape fin effect as indicated by Eq. (4.19) for the tubes of this study is presented graphically in Fig. 15. As one would expect the trend of the curve indicates an increase in the fin effect for a decrease in the heat transfer coefficient.

The probable fin effect for an electrically insulated tape may be found directly by taking the limit of γ given by Eq. (4.19) as $Wi_f \longrightarrow 0$. This equation may be rewritten as

$$\gamma = \frac{\frac{Wi_f \delta_f r_i}{Wi_w \delta_w \pi r} + \frac{1}{\epsilon}\left[\frac{Wi_f \delta_f r_i}{2 h r_i L Wi_w \delta_w \pi r} - \frac{1}{\pi h r_i L}\right]}{1 + \frac{Wi_f \delta_f r_i}{Wi_w \delta_w \pi r}} \tag{4.24}$$

$$\lim_{Wi_f \longrightarrow 0} \gamma = \frac{0 + \frac{1}{\epsilon}\left[0 - \frac{1}{\pi h r_i L}\right]}{1 + 0} = -\frac{1}{\epsilon \pi h r_i L} \tag{4.25}$$

Equation (4.25) can also be used to estimate the fin effect for a condensing steam heating system where the total q to the fluid is known and the tube wall temperature drop is small.

APPENDIX 5

A NOTE ON THE DEFINITION OF THE HEAT TRANSFER COEFFICIENT

The wall temperature used in the determination of the heat transfer coefficients for this and most other swirl flow investigations was the measured temperature at the ninety degree point relative to the tape. Taking into consideration the fin effect of the tape and the consequent circumferential heat flow, we see that this is the maximum theoretical temperature likely to exist in the tube wall. The equation used for the calculation of h was (5.1)

$$h = \frac{q}{\pi D_i L_h (T_{w_{max}} - T_b)} = \frac{q}{\pi D_i L_h \theta_{max}}$$

A heat transfer coefficient based on the actual heat transfer area and which takes into consideration the temperature variation in the tape and the tube wall could be defined as follows:

$$h^1 = \frac{q}{\pi D_i L_h \bar{\theta}_w + 2 D_i L \bar{\theta}_f} \qquad (5.2)$$

The ratio of heat transfer coefficients is then

$$\frac{h^1}{h} = \frac{\theta_{w\,max}}{\left(1 - \frac{2\delta_f}{\pi D_i}\right)\bar{\theta}_w + \frac{2}{\pi}\bar{\theta}_f} \qquad (5.3)$$

$\bar{\theta}_w$ and $\bar{\theta}_f$ represent the integrated average temperature difference existing between the tube wall and the tape and the bulk fluid. They are found from

$$\bar{\theta}_w = \frac{2}{\pi r} \int_0^{\frac{\pi}{2}} \theta_w(\varphi)\, r\, d\varphi \qquad (5.4)$$

$$\bar{\theta}_f = \frac{1}{r_i} \int_o^{r_i} \theta_f(x)\, dx \tag{5.5}$$

Using the expressions for the temperature variation in the tube wall and tape which were derived in Appendix 4 and effecting the integrations required by Eqs. (5.4) and (5.5) one obtains

$$\frac{h^1}{h} = \frac{1 + 2 C_2 e^{B\pi/2}}{1 - \frac{2\delta_f}{\pi D_i} - \frac{2}{\pi} \frac{C_2 (1 - e^{B\pi})}{B} + \frac{2}{\pi} C_1 + C_3} \tag{5.6}$$

where

$$C_1 = \frac{\rho_w \delta_f r_i}{2 \rho_f \delta_w r} \tag{5.7}$$

$$C_2 = \frac{C_1 - 1}{\epsilon L \sqrt{4 k_w \delta_w \left(\frac{r_i}{r}\right) h} \left(e^{B\delta_f/D_i} - e^{B(\pi - \delta_f/D_i)} \right)} \tag{5.8}$$

$$C_3 = \frac{2}{\pi} \frac{\delta_f (C_1 - 1)}{m^2 r_i \epsilon L k_f} \tag{5.9}$$

The values for m, B, and ϵ are given by Eq. (4.11), (4.15), and (4.17) respectively.

The evaluation of Eq. (5.6) for the tubes used in this study with $h = 10^4$ Btu/hr ft^2°F yields $h^1/h = 1.01$, and with $h = 10^3$ Btu/hr ft^2°F, $h^1/h = 0.93$. This rather close agreement between h^1 and h for the range of flows of interest in this study substantiates that the reported heat transfer coefficients are indicative of the average heat transfer coefficients existing in the tube. Considering the simplicity of Eq. (5.1) relative to Eq. (5.2) and the coupling which exists in Eq. (5.2) between the actual and calculated average, h^1, it is recommended that Eq. (5.1)

be used for the reporting of all swirl flow heat transfer coefficients.

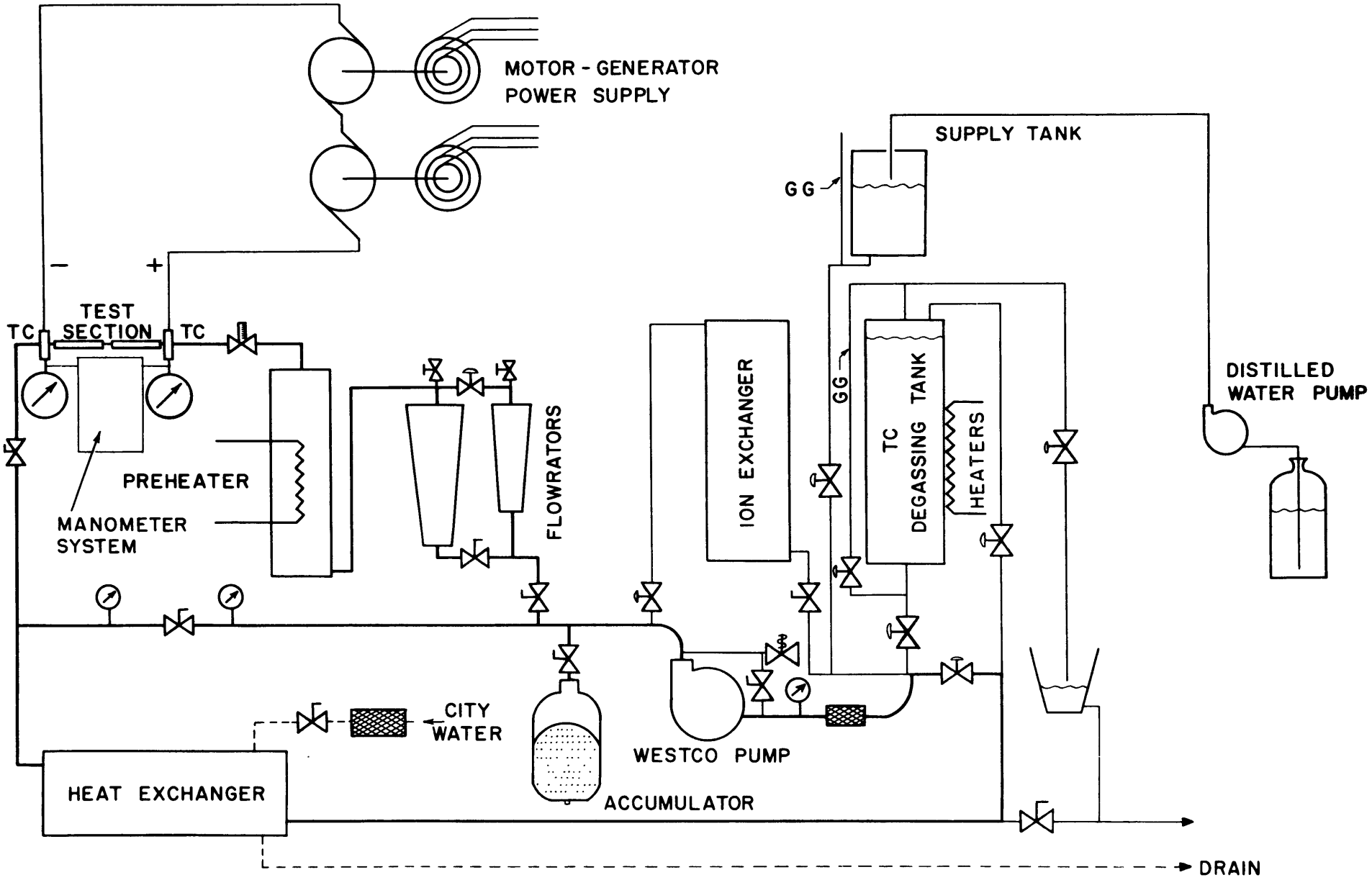

FIG. 1 SCHEMATIC LAYOUT OF EXPERIMENTAL FACILITY

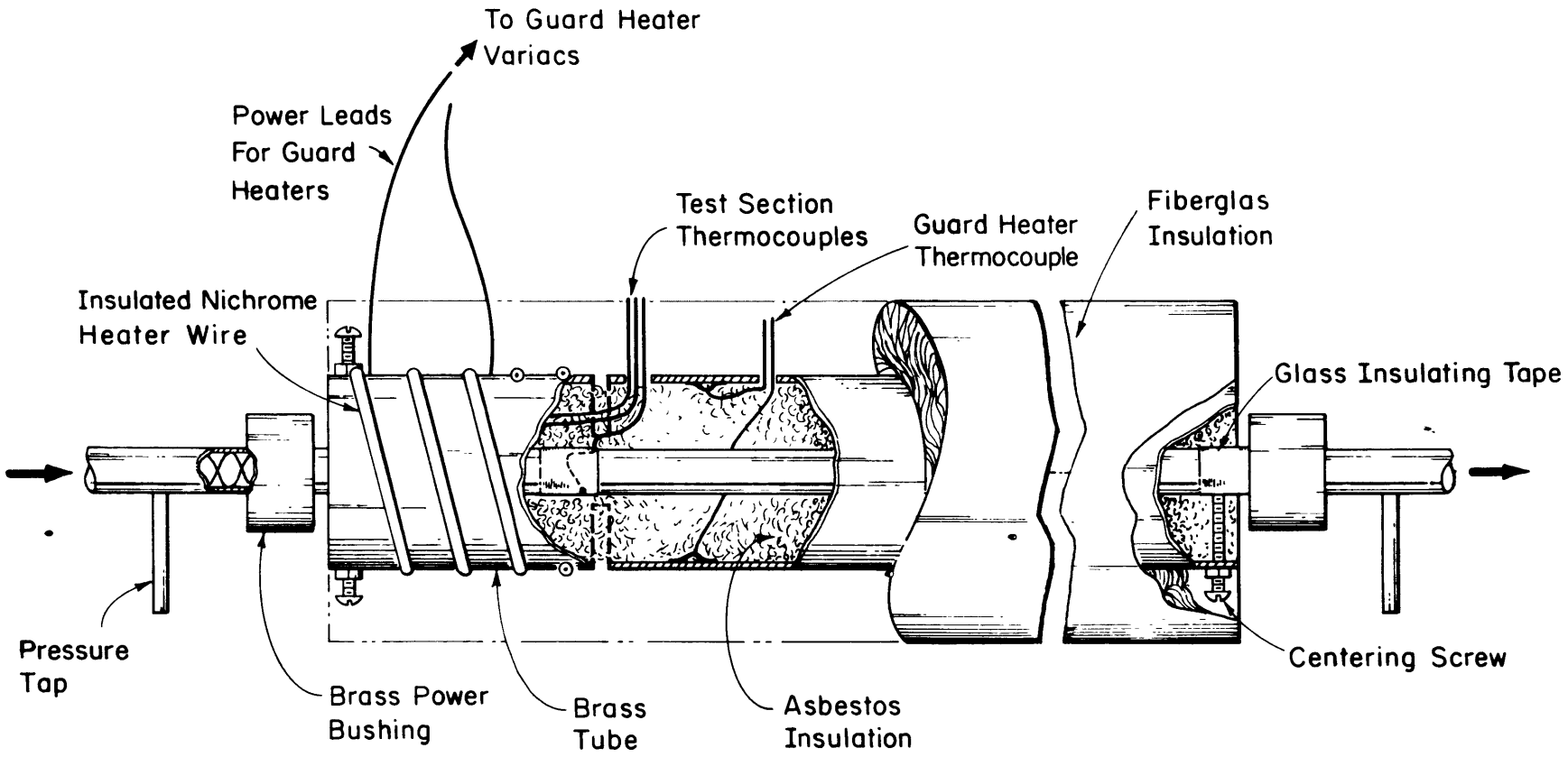

FIG. 2 TYPICAL TEST SECTION FOR THE HEATING OF SWIRL FLOWS.

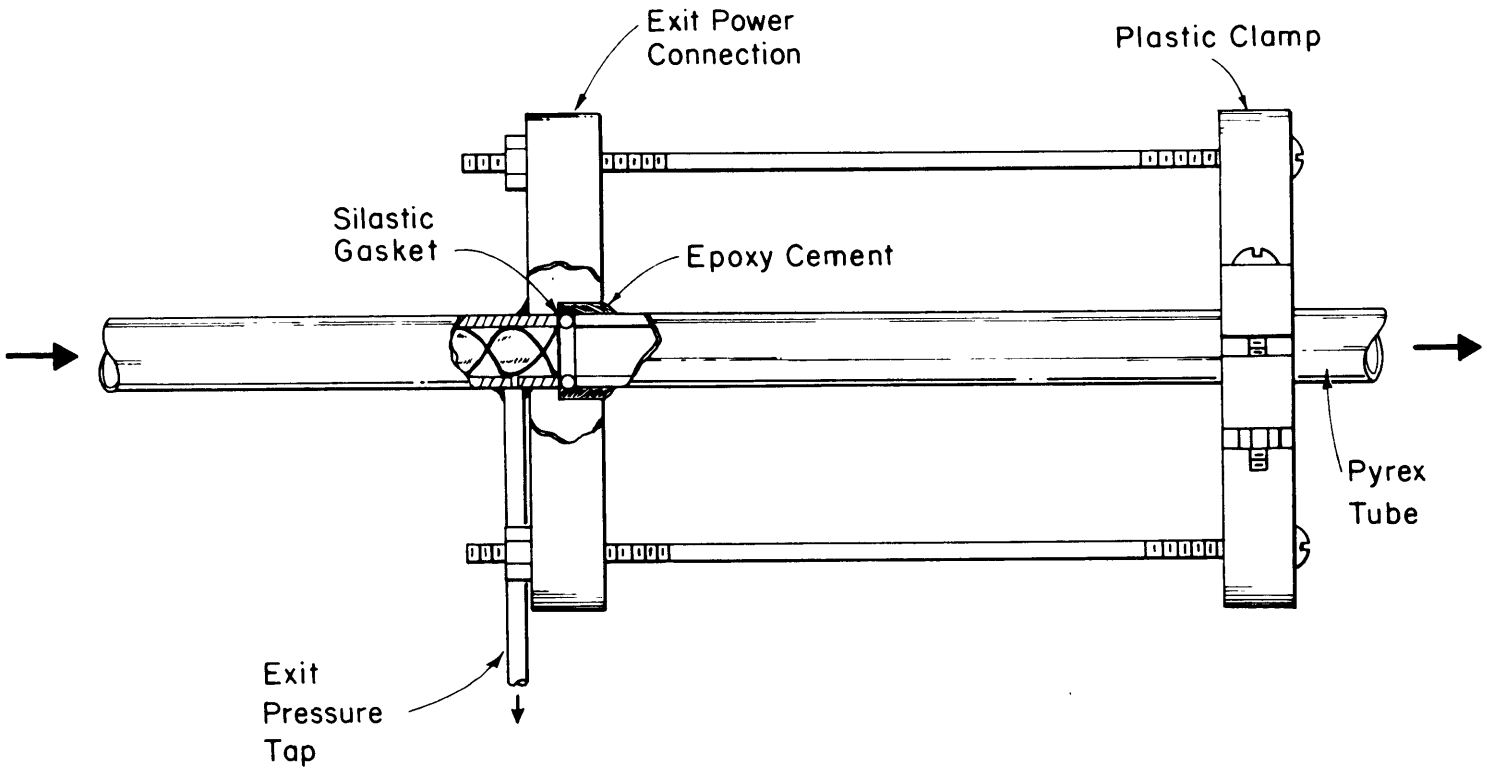

FIG. 3 VISUAL EXIT SECTION FOR SURFACE BOILING OBSERVATIONS.

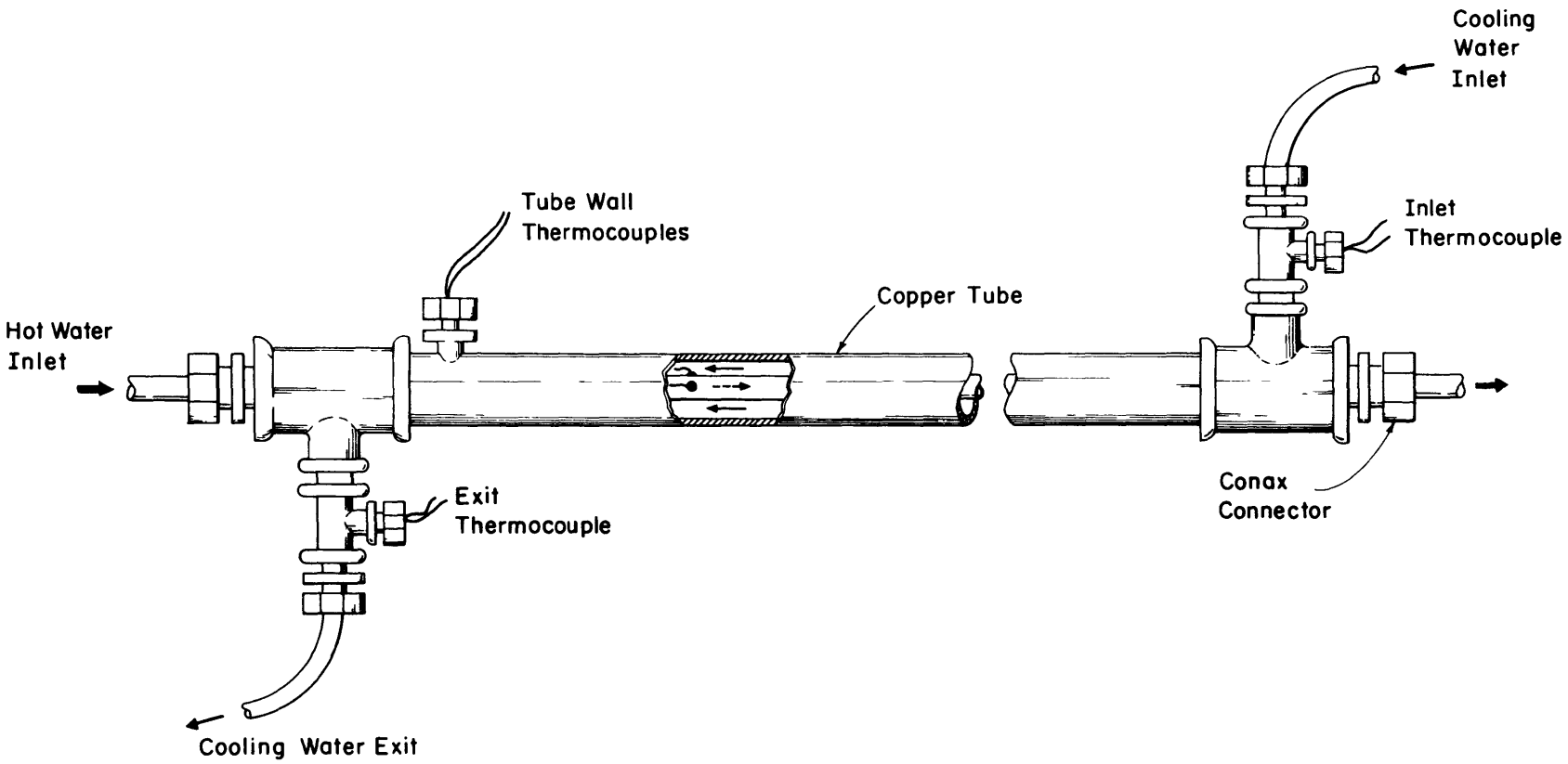

FIG. 4 COUNTERFLOW HEAT EXCHANGER FOR THE COOLING OF SWIRL FLOWS.

H E A T T R A N S F E R L A B O R A T O R Y

TUBULAR OR ANNULAR DATA REDUCTION

RUN INPUT

RUN NO. SWIRL B 81 DATE 9/29/66

IP = 2 AMV = 19.1900 TINMV = .95C0 TOUTMV = 2.1000 V = 10.0000 EMM = 800.0000

TWMV(1 THRU IM) ARE .3440E 01 .351CE 01 .3690E 01 .3780E 01 .3870E 01 .3940E 01 .0000E 00

DP (1 THRU IP) ARE .2920E 02 .CCCCE 00 .00C0E 00 .0000E 00 .0000E 00 PGCUT = .3610E 02

C A L C U L A T E D O U T P U T

A = .11546623E 04 TIN = .75265485E 02 TOUT = .12470833E 03 G = .42993381E 07 PACUT = .50799999E 02

M = .8CCCCCDE 03 QM = .3955428E 05 QV = .3940862E 05 QA = .3950536E 05 QF = .6354789E 06 PAIN= .6408833E 02

T.C.	T	TB	DTF	H	NU	RE	PR
1	.1724697E 03	.8312910E 02	.8934058E 02	.7112993E 04	.3247574E 03	.3451425E 05	.5687348E 01
2	.1751977E 03	.8983581E 02	.8536192E 02	.7444524E 04	.3359741E 03	.3740094E 05	.5187857E 01
3	.1821475E 03	.9654252E 02	.8560495E 02	.7423390E 04	.3315830E 03	.4025400E 05	.4770705E 01
4	.1856200E 03	.1032492E 03	.8237073E 02	.7714863E 04	.3413660E 03	.4311337E 05	.4412469E 01
5	.1890855E 03	.1099559E 03	.7913355E 02	.8030461E 04	.3521856E 03	.4589306E 05	.4108523E 01
6	.1917740E 03	.1166626E 03	.7511133E 02	.8460493E 04	.3682546E 03	.4928250E 05	.3797181E 01
AV				.7714077E 04	.3431138E 03	.4177147E 05	.4675620E 01

	FR	EJ	UR	GR	QL	DTSAT	DTSUB
1	.1456873E-01	.1620299E 03	.4406864E 00	.2472739E 05	.6237551E 06	-.1211973E 03	.2105379E 03
2	.1455073E-01	.1739044E 03	.4687138E 00	.3026883E 05	.6273293E 06	-.1168571E 03	.2022190E 03
3	.1453260E-01	.1774840E 03	.4802570E 00	.3862971E 05	.6364354E 06	-.1082260E 03	.1938309E 03
4	.1451537E-01	.1885157E 03	.5014142E 00	.4613882E 05	.6409857E 06	-.1030721E 03	.1854429E 03
5	.1449423E-01	.2001231E 03	.5199618E 00	.5434880E 05	.6455323E 06	-.9791685E 02	.1770504E 03
6	.1447220E-01	.2159552E 03	.5494359E 00	.6213775E 05	.6490503E 06	-.9342580E 02	.1685371E 03
AV	.1452196E-01	.1868220E 03	.4937136E 00	.4284113E 05	.6370388E 06	-.1068794E 03	.1895910E 03

FIG. 5 COMPUTER PRINTOUT FOR A TYPICAL RUN.

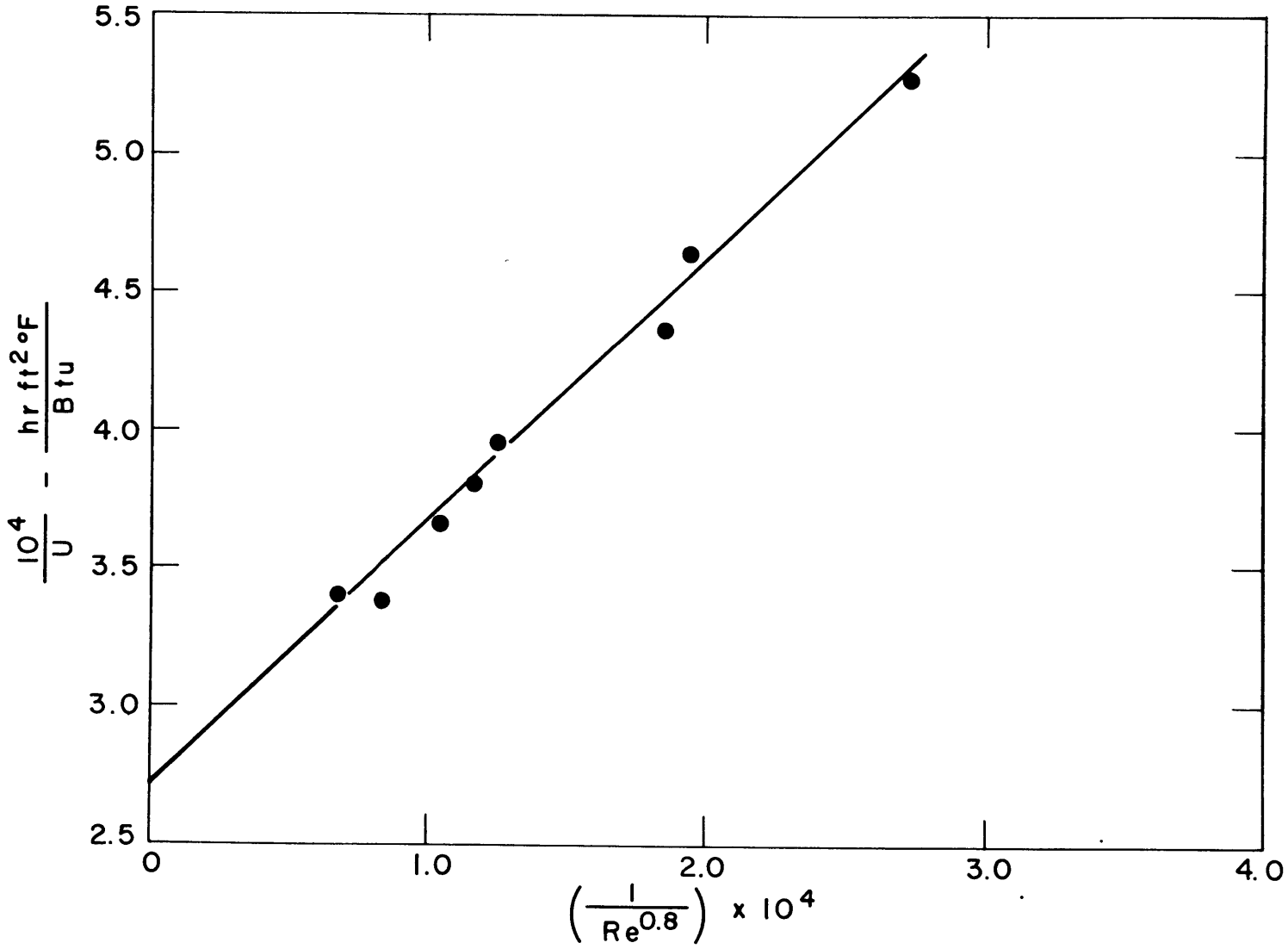

FIG. 6 WILSON PLOT FOR COOLING DATA REDUCTION.

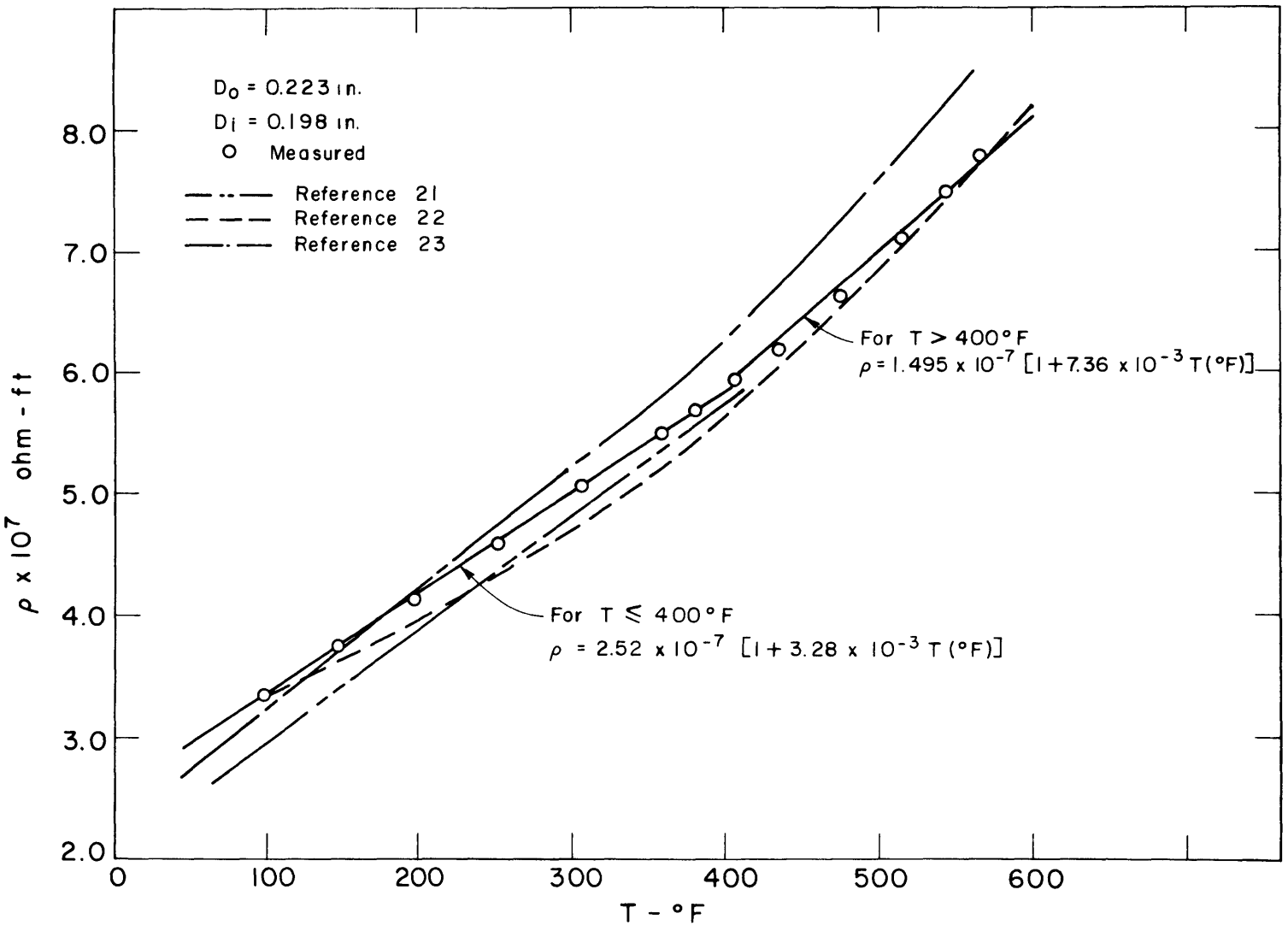

FIG. 7 TEMPERATURE DEPENDENCE OF RESISTIVITY FOR NICKEL TUBING.

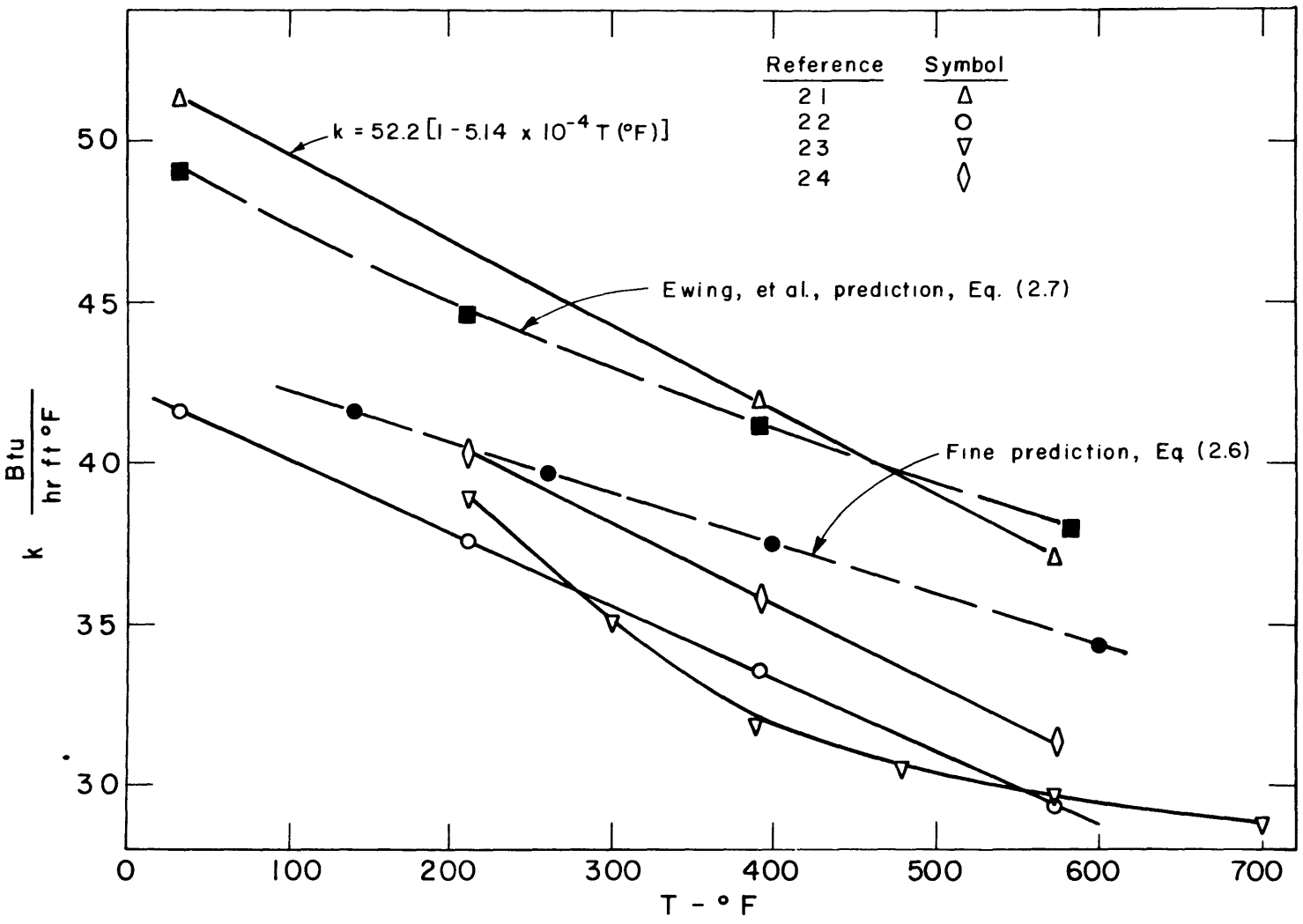

FIG. 8 TEMPERATURE DEPENDENCE OF THERMAL CONDUCTIVITY FOR NICKEL TUBING.

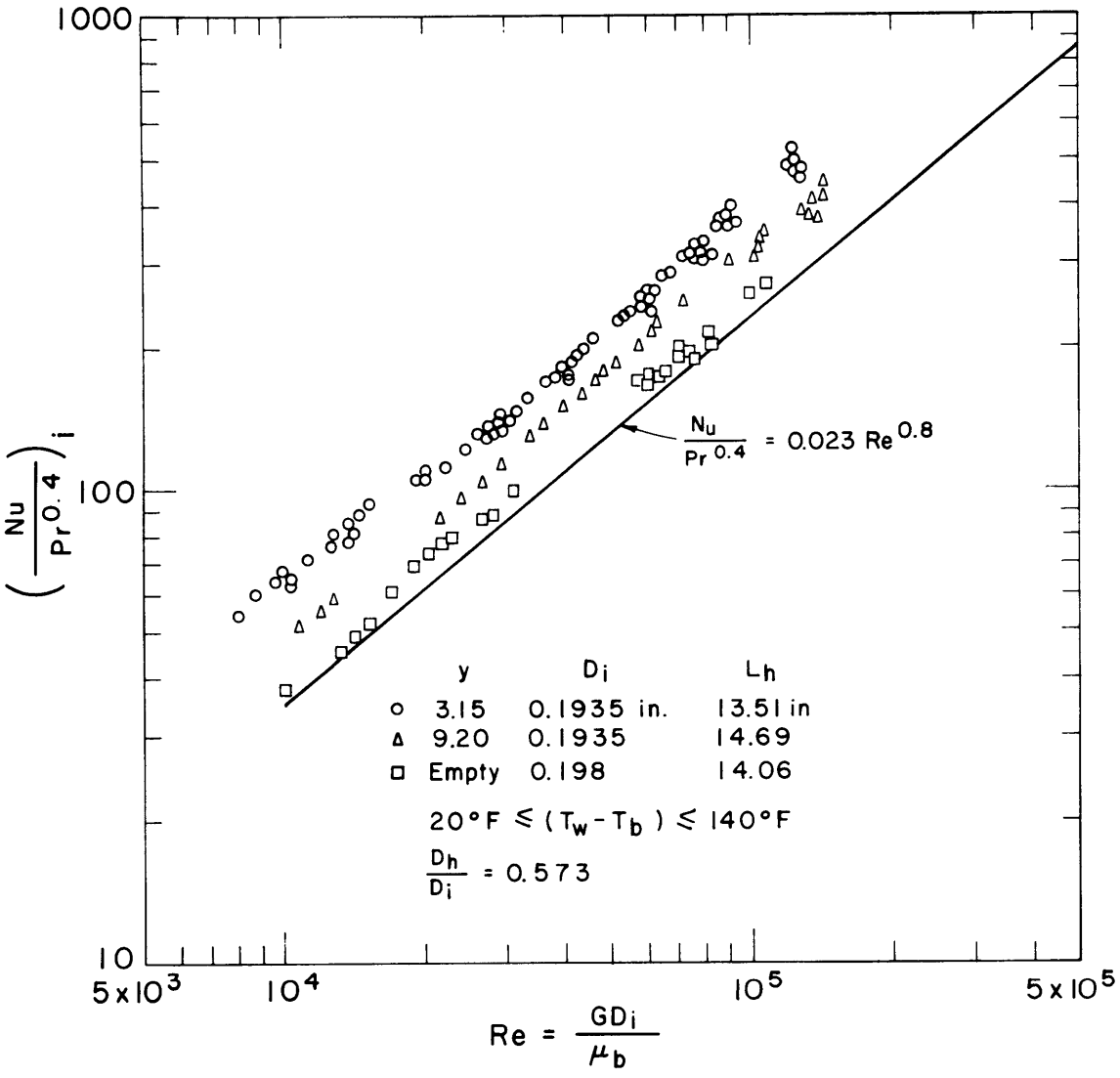

FIG. 9 AVERAGE NUSSELT NUMBERS FOR HEATING WITH SWIRL AND STRAIGHT FLOWS.

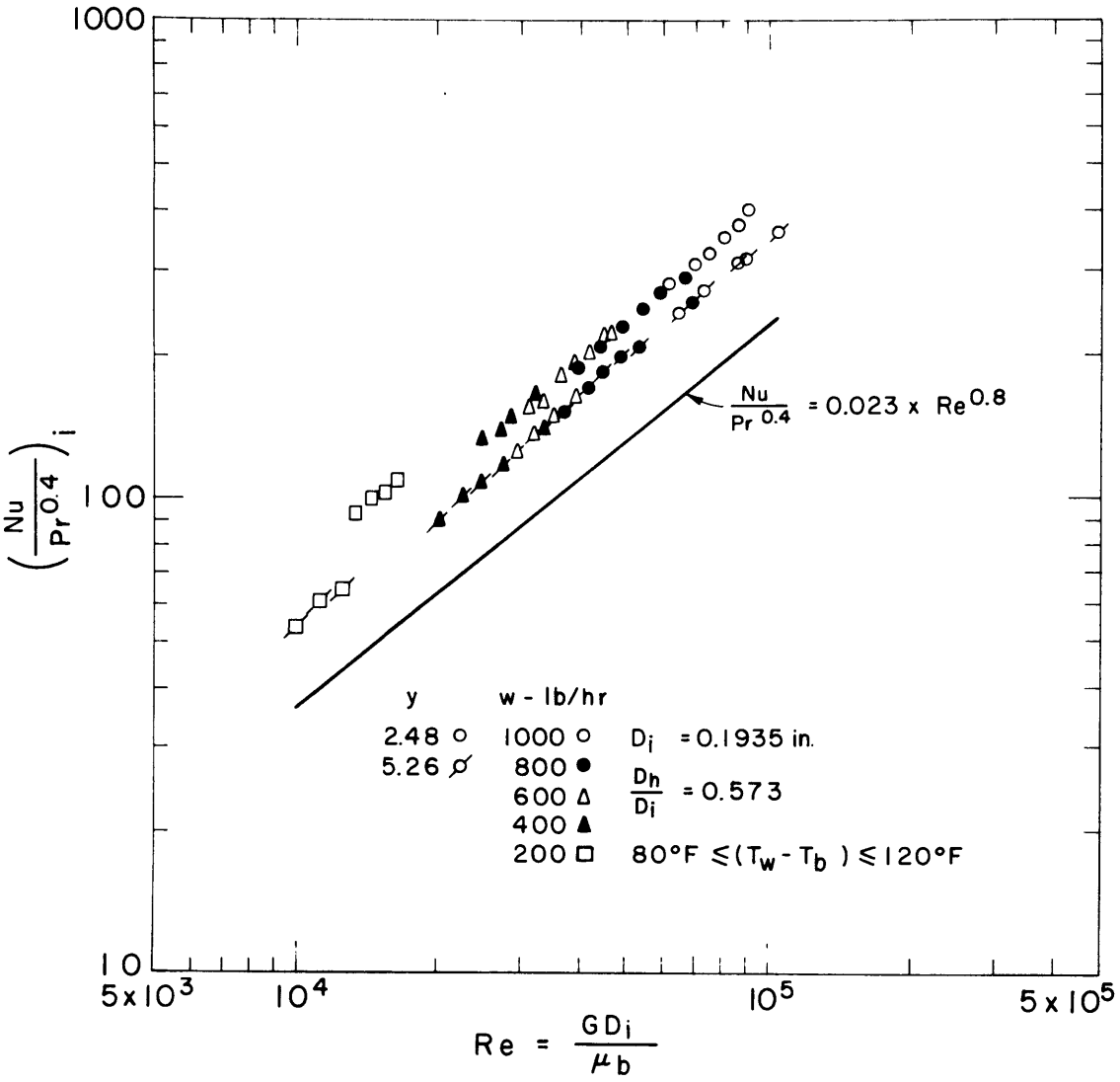

FIG. 10 AVERAGE NUSSELT NUMBERS FOR HEATING WITH SWIRL FLOW.

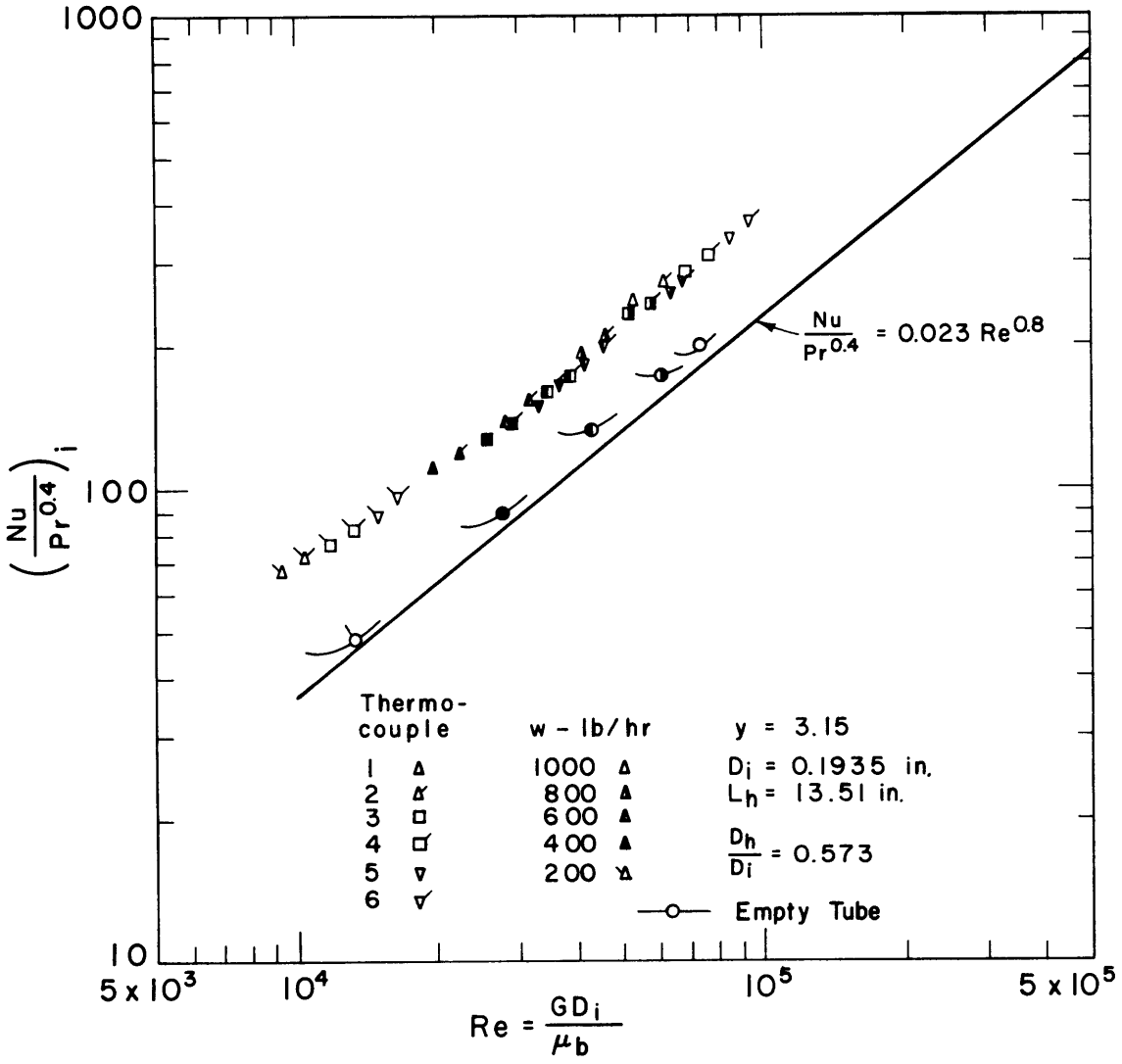

FIG. 11 LOCAL NUSSELT NUMBERS FOR HEATING.

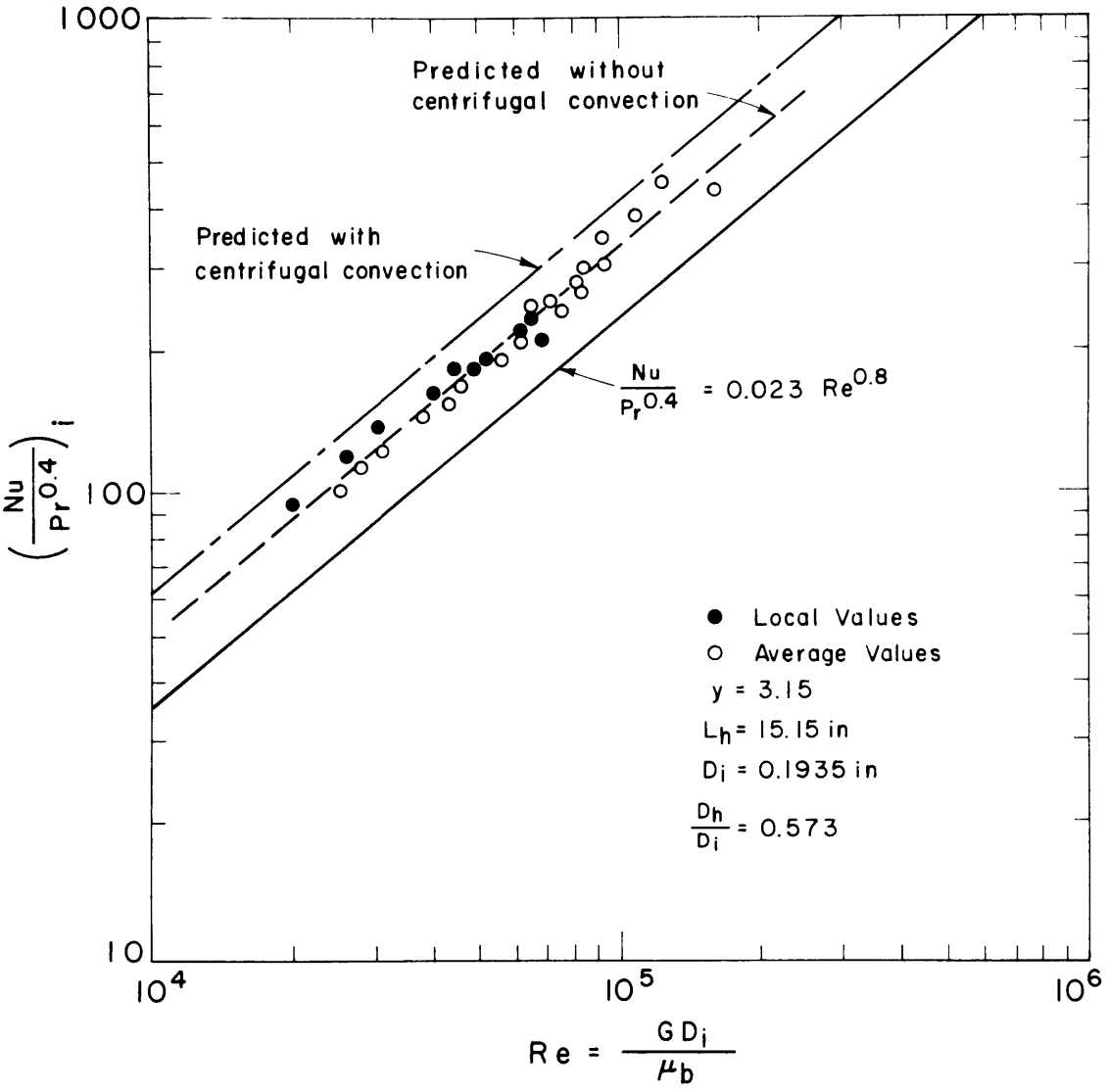

FIG. 12 AVERAGE NUSSELT NUMBERS FOR COOLING.

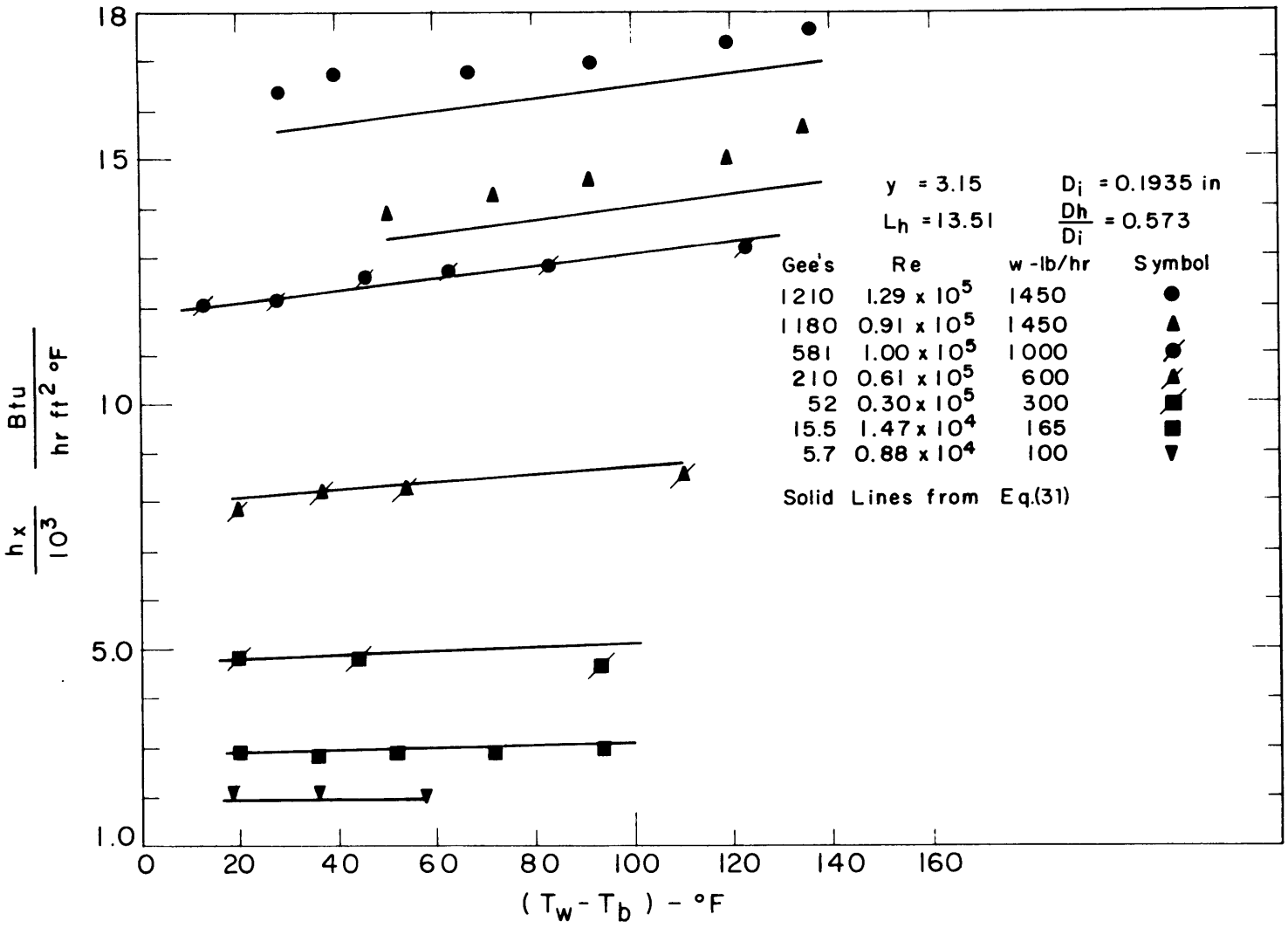

FIG. 13 DEPENDENCE OF HEAT TRANSFER COEFFICIENT ON TEMPERATURE DIFFERENCE.

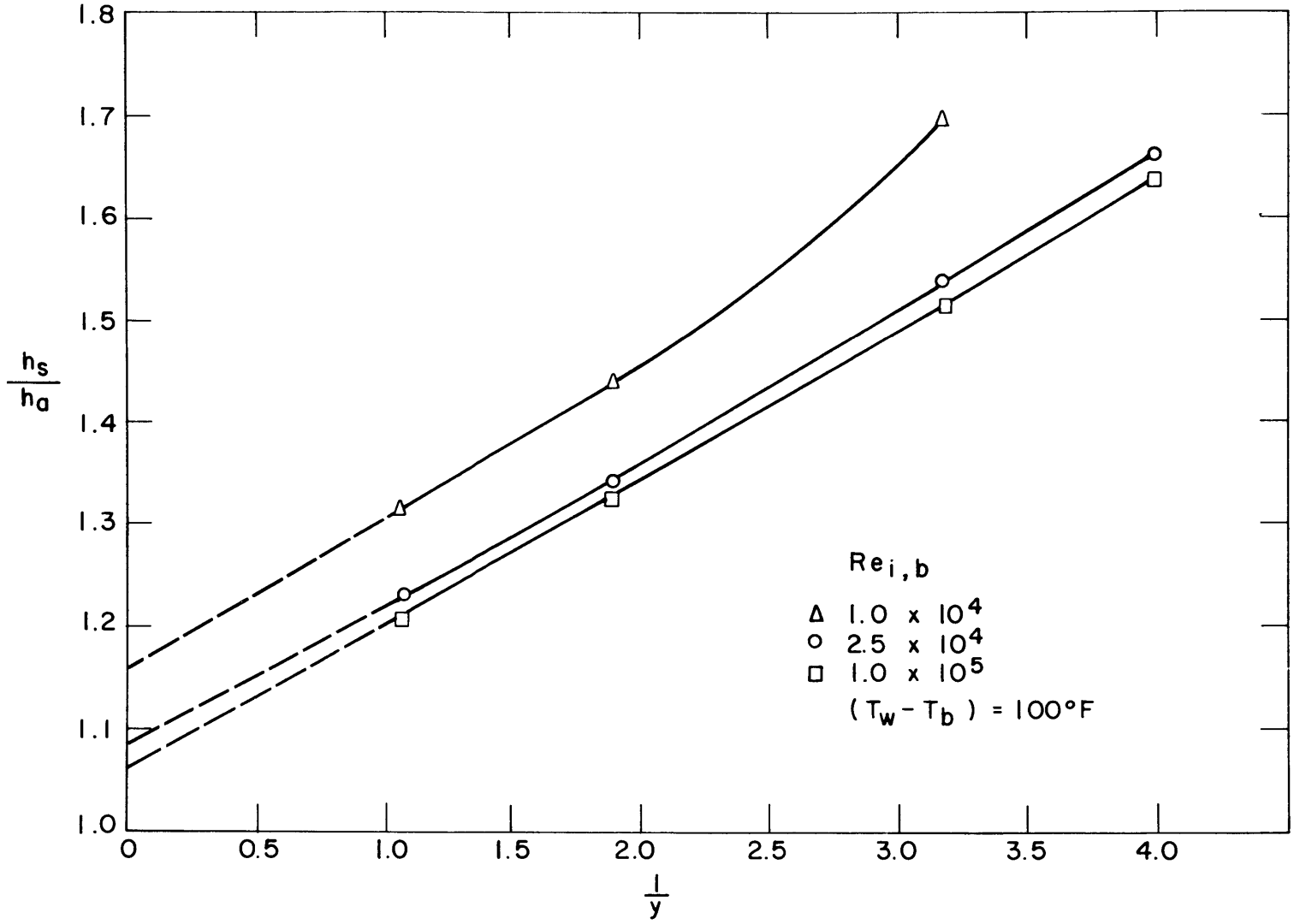

FIG. 14 EXPERIMENTAL DETERMINATION OF THE TAPE FIN EFFECT.

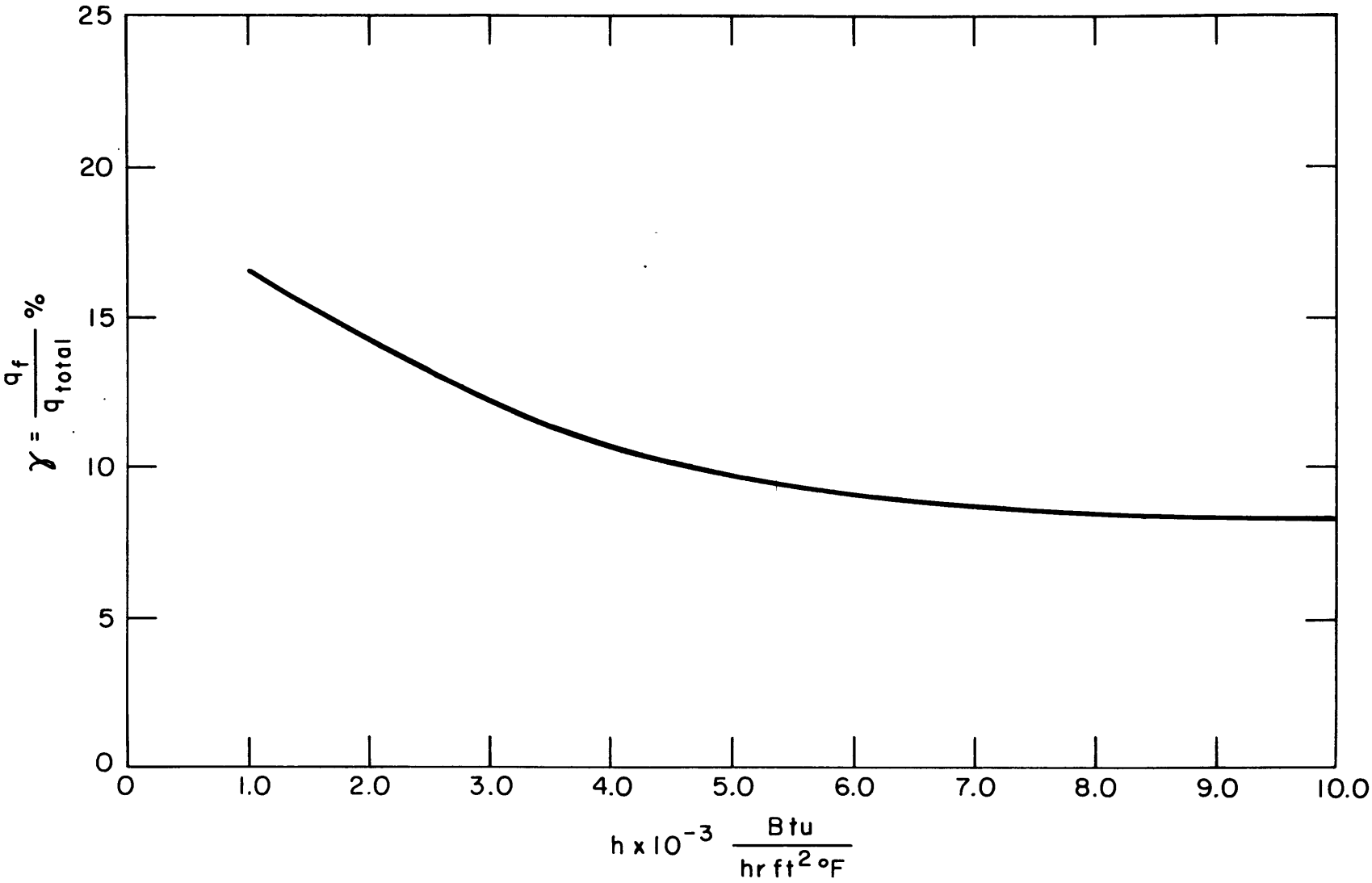

FIG. 15 THEORETICAL PREDICTION OF THE TAPE FIN EFFECT.

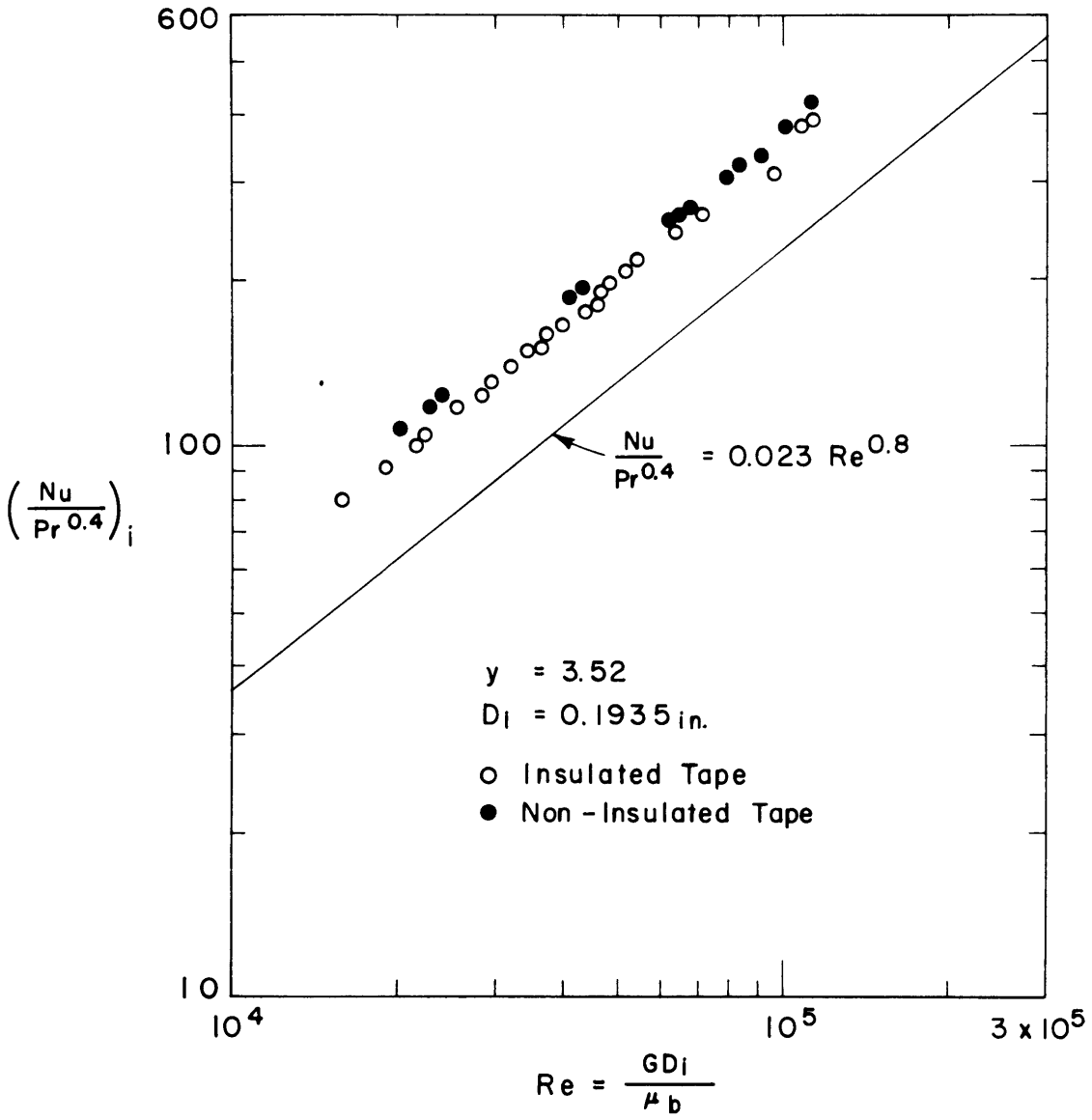

FIG. 16 COMPARISON OF AVERAGE NUSSELT NUMBERS FOR INSULATED AND NON-INSULATED TWISTED TAPES.

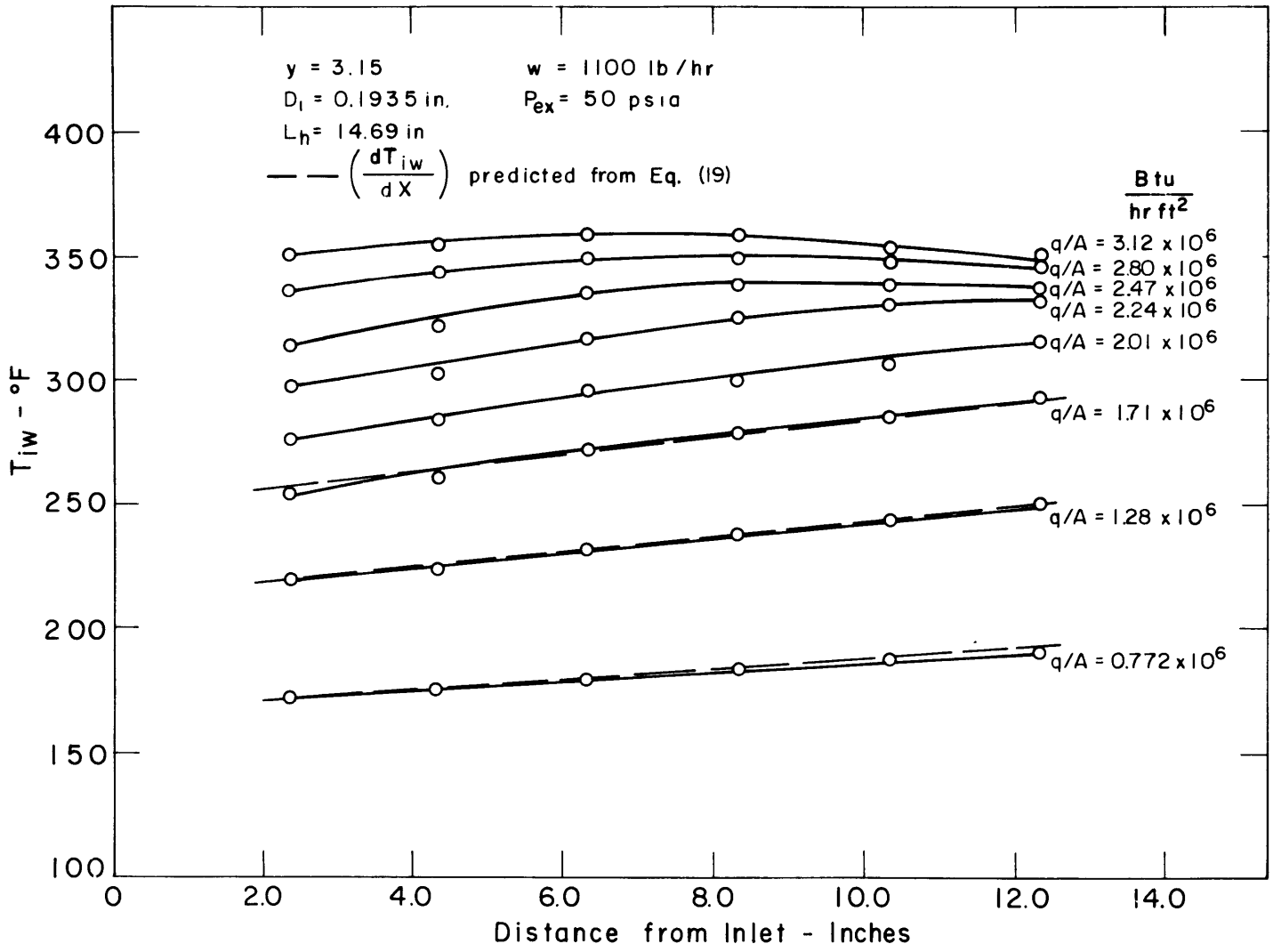

FIG. 17 TUBE WALL TEMPERATURE PROFILES FOR VARIOUS HEAT FLUXES.

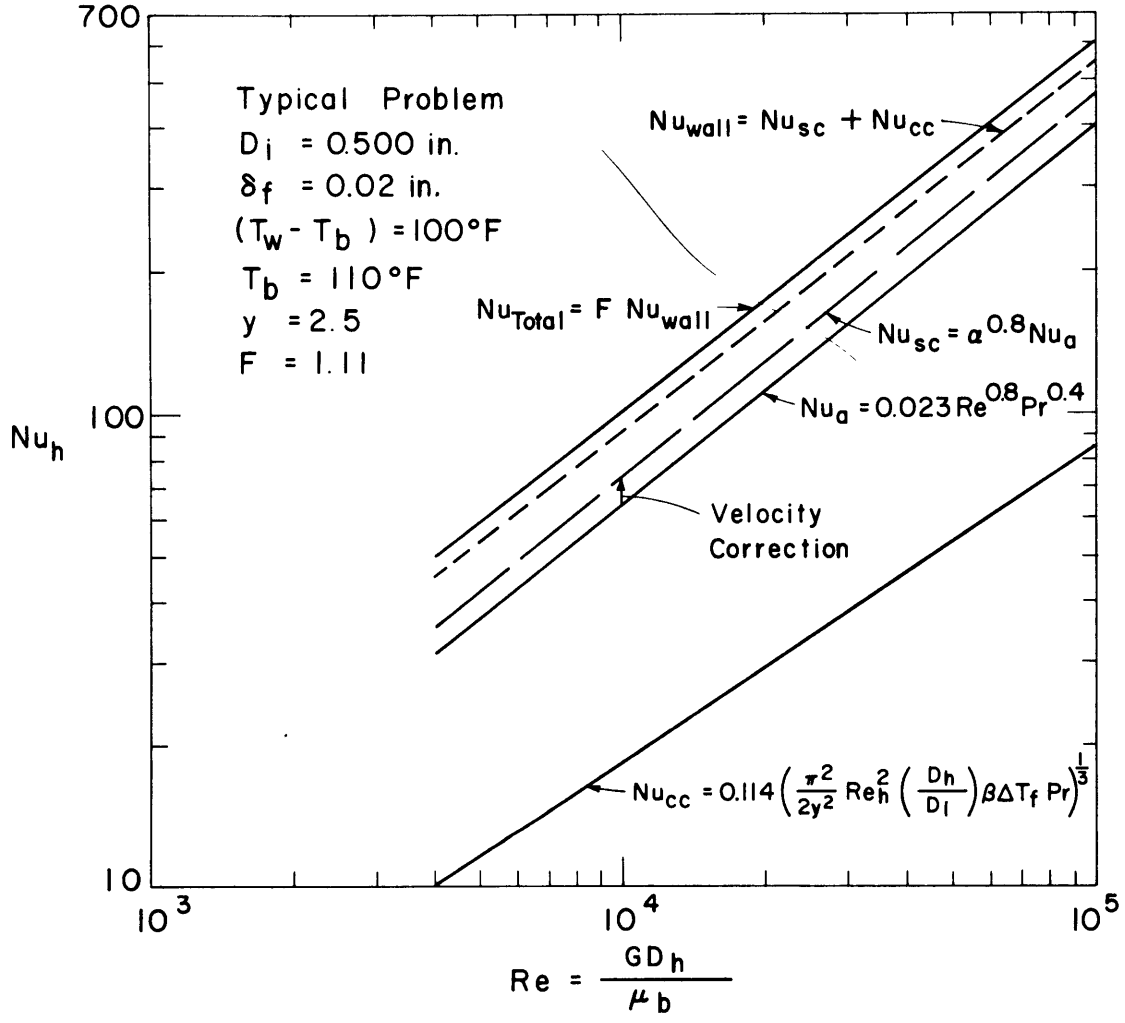

FIG. 18 GRAPHICAL REPRESENTATION OF THE SWIRL FLOW HEAT TRANSFER PREDICTION METHOD.

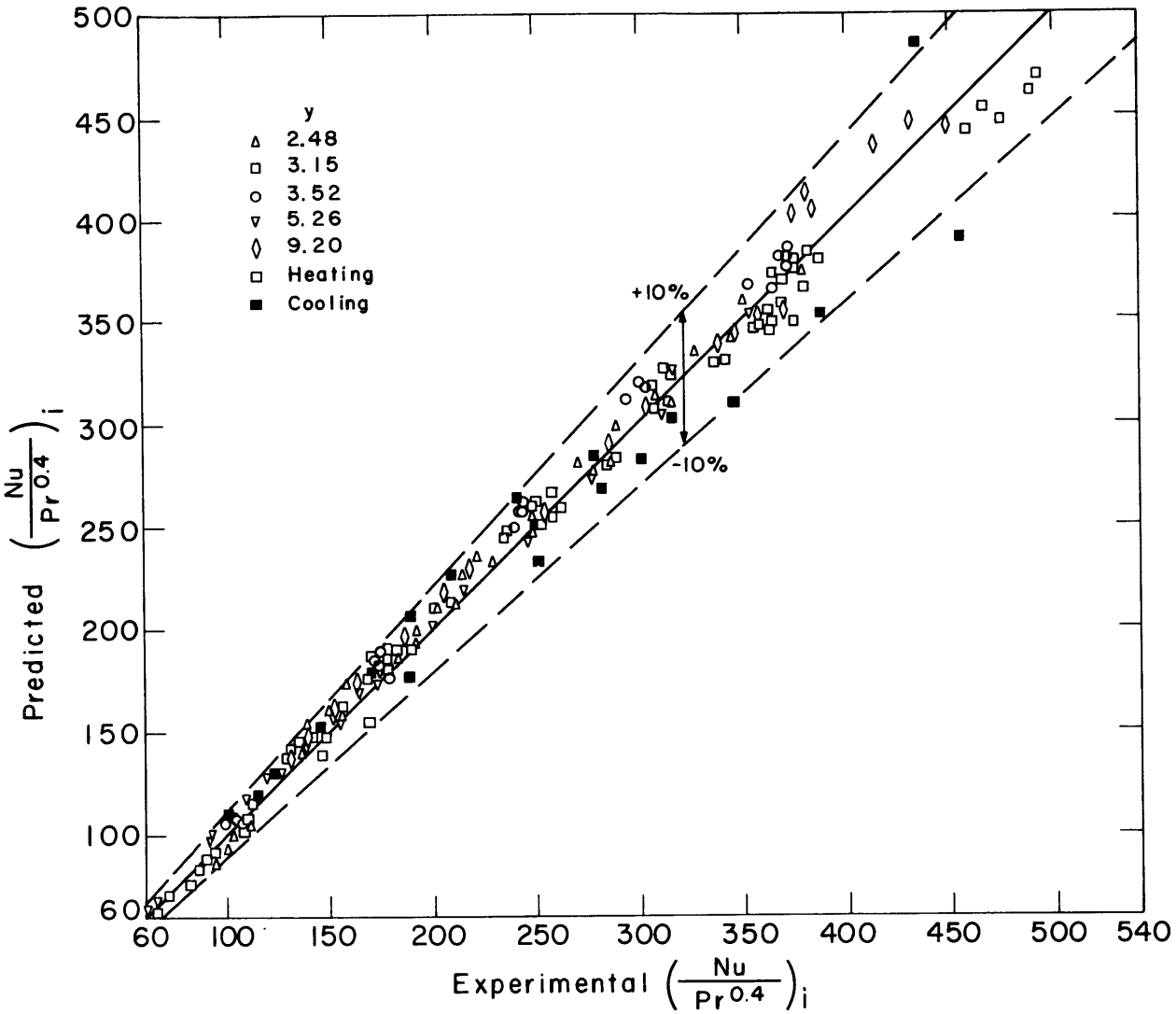

FIG. 19 COMPARISON OF PREDICTED AND OBSERVED AVERAGE NUSSELT NUMBERS.

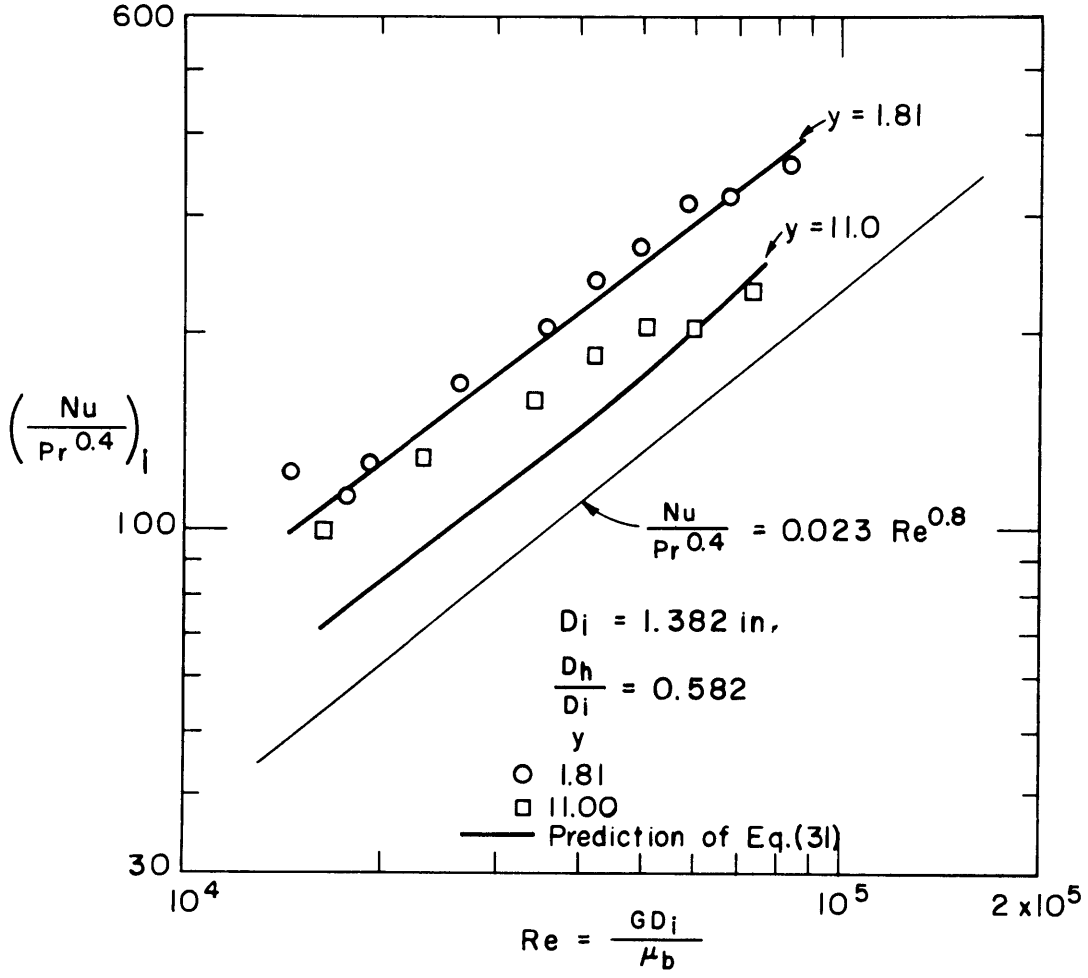

FIG. 20 COMPARISON OF THE EXPERIMENTAL AND PREDICTED NUSSELT NUMBERS FOR THE WATER DATA OF SMITHBERG AND LANDIS (10).

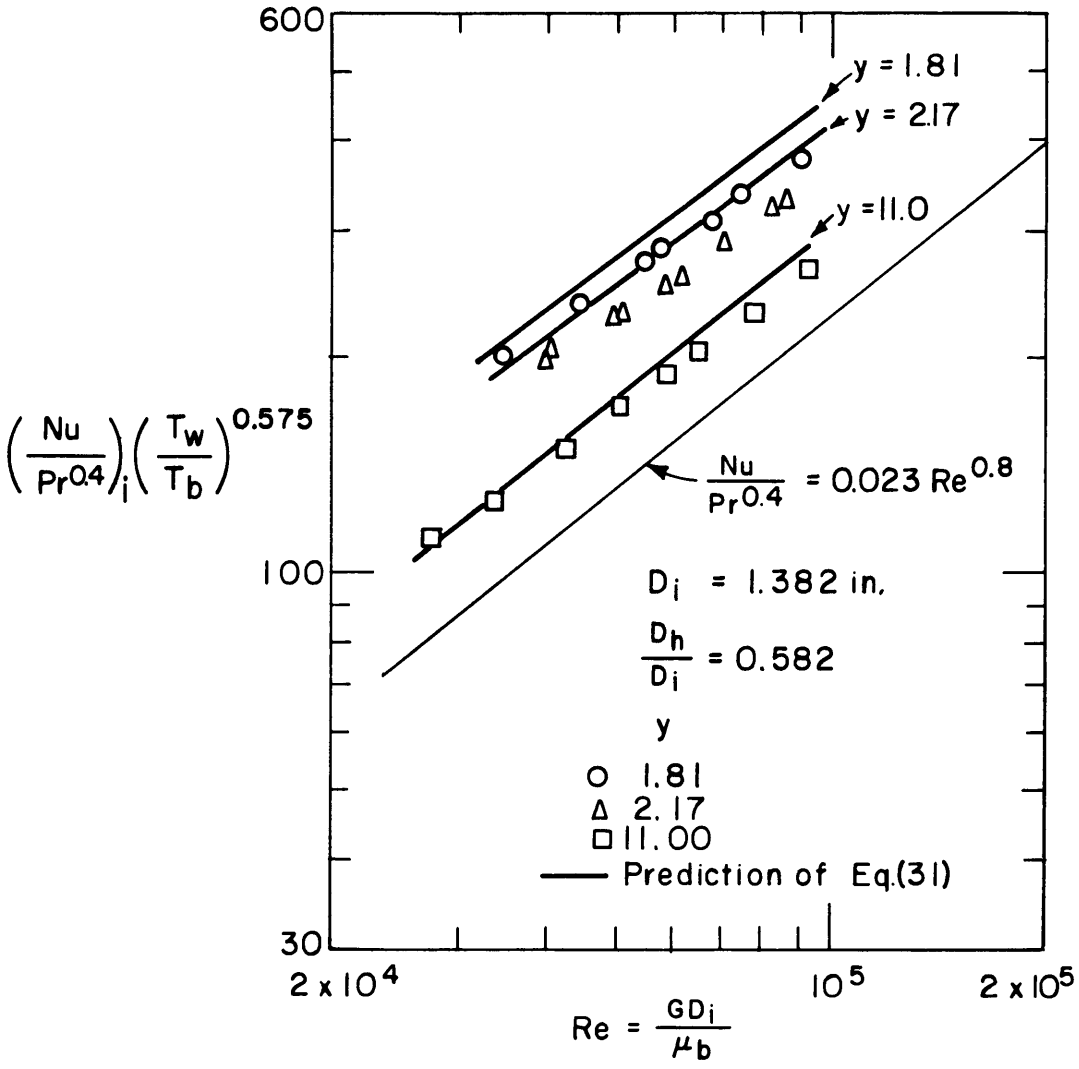

FIG. 21 COMPARISON OF THE EXPERIMENTAL AND PREDICTED NUSSELT NUMBERS FOR THE AIR DATA OF SMITHBERG AND LANDIS (10).

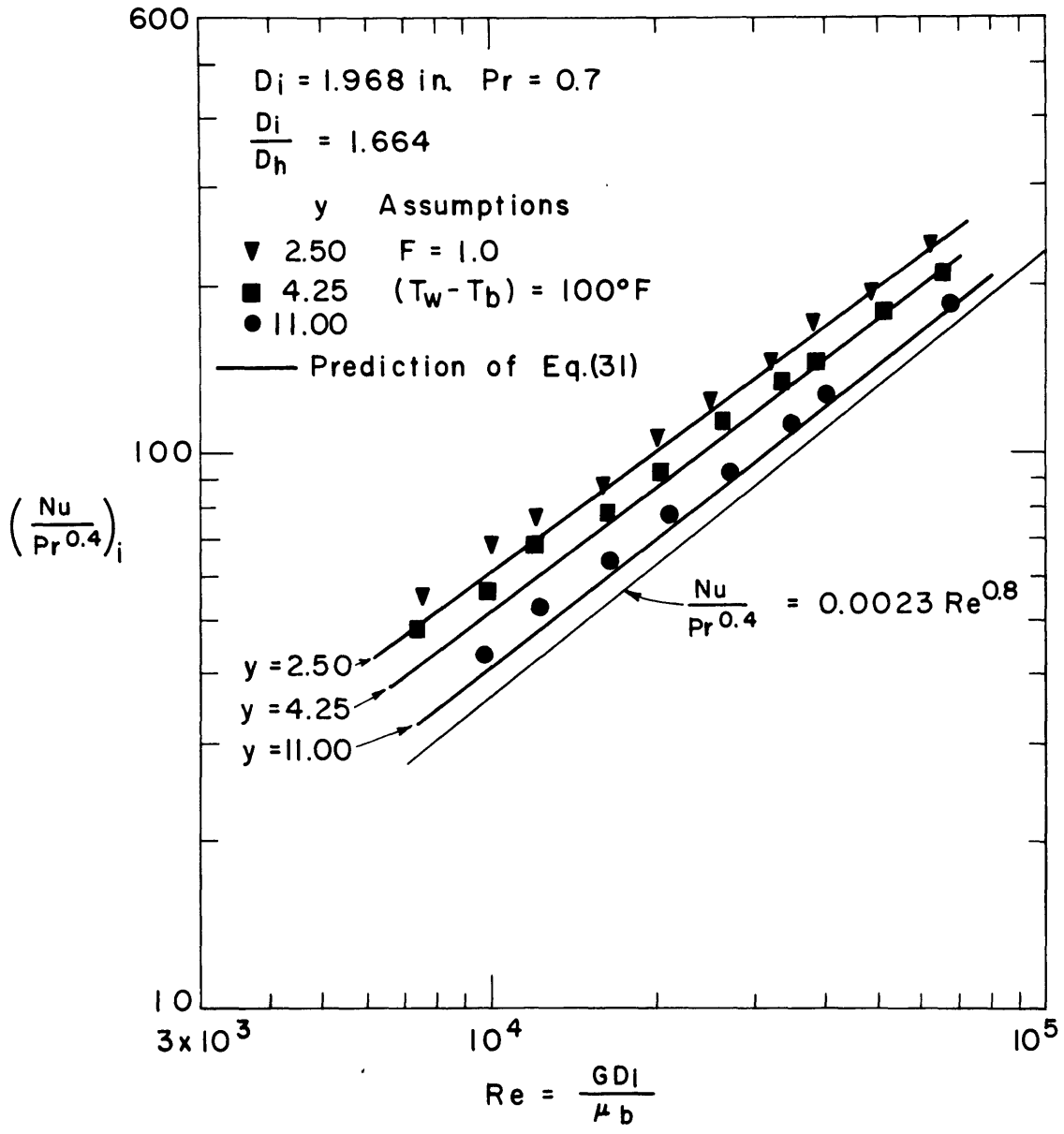

FIG. 22 COMPARISON OF THE EXPERIMENTAL AND PREDICTED NUSSELT NUMBERS FOR THE AIR DATA OF KOCH (9).

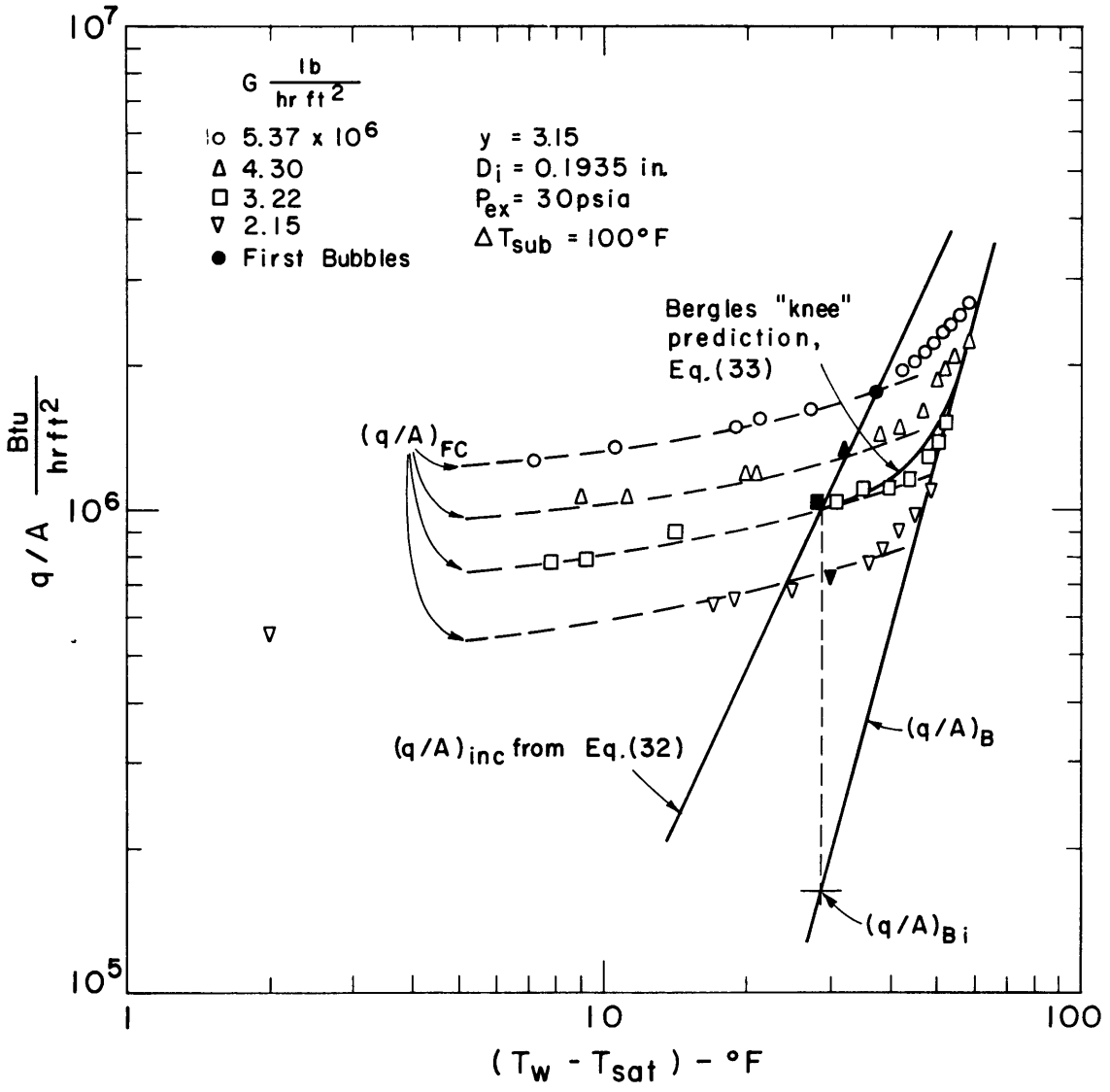

FIG. 23 SURFACE BOILING DATA FOR WATER IN SWIRL FLOW, y = 3.15.

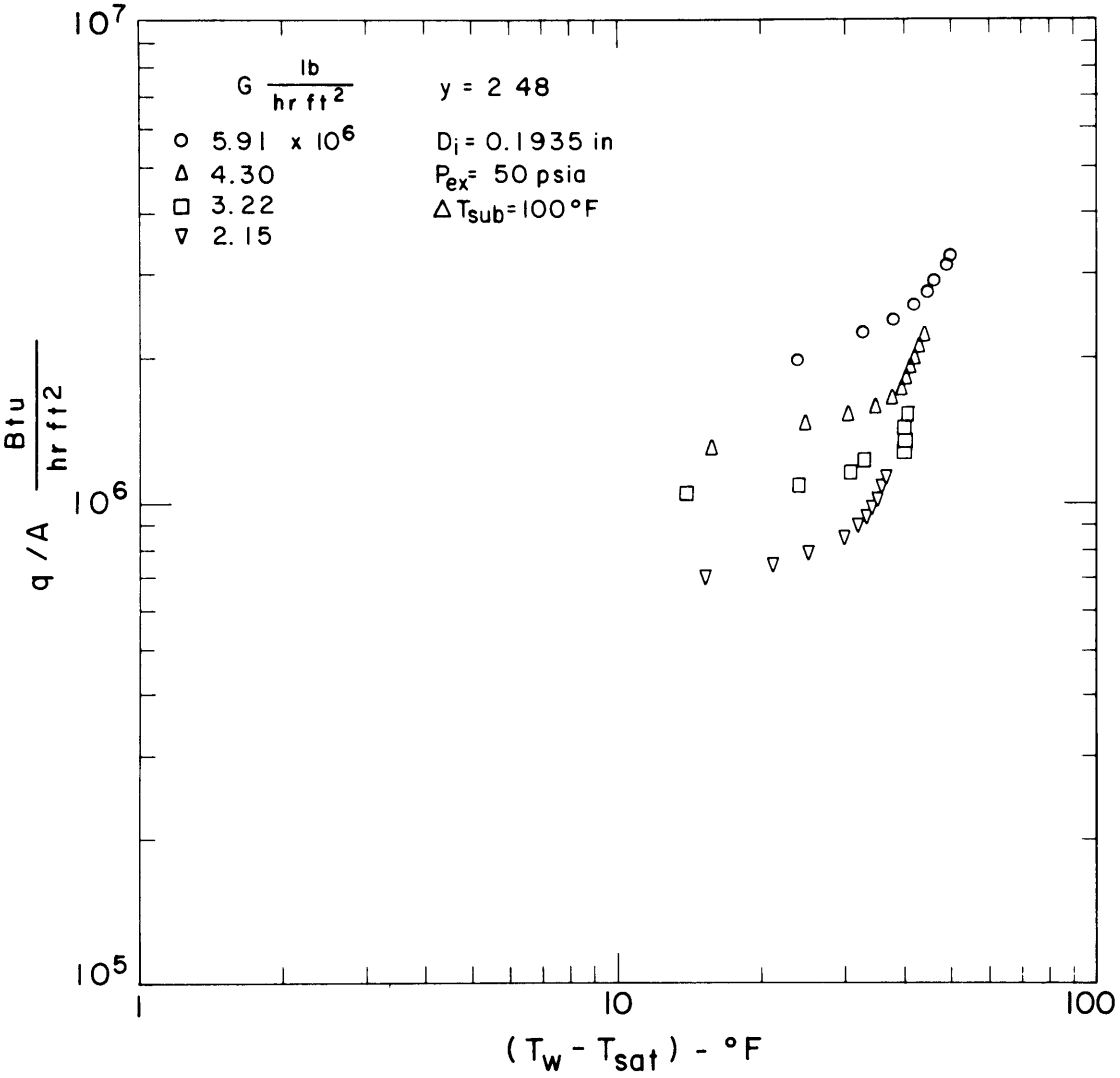

FIG. 24 HEAT FLUX VERSUS WALL SUPERHEAT, y = 2.48.

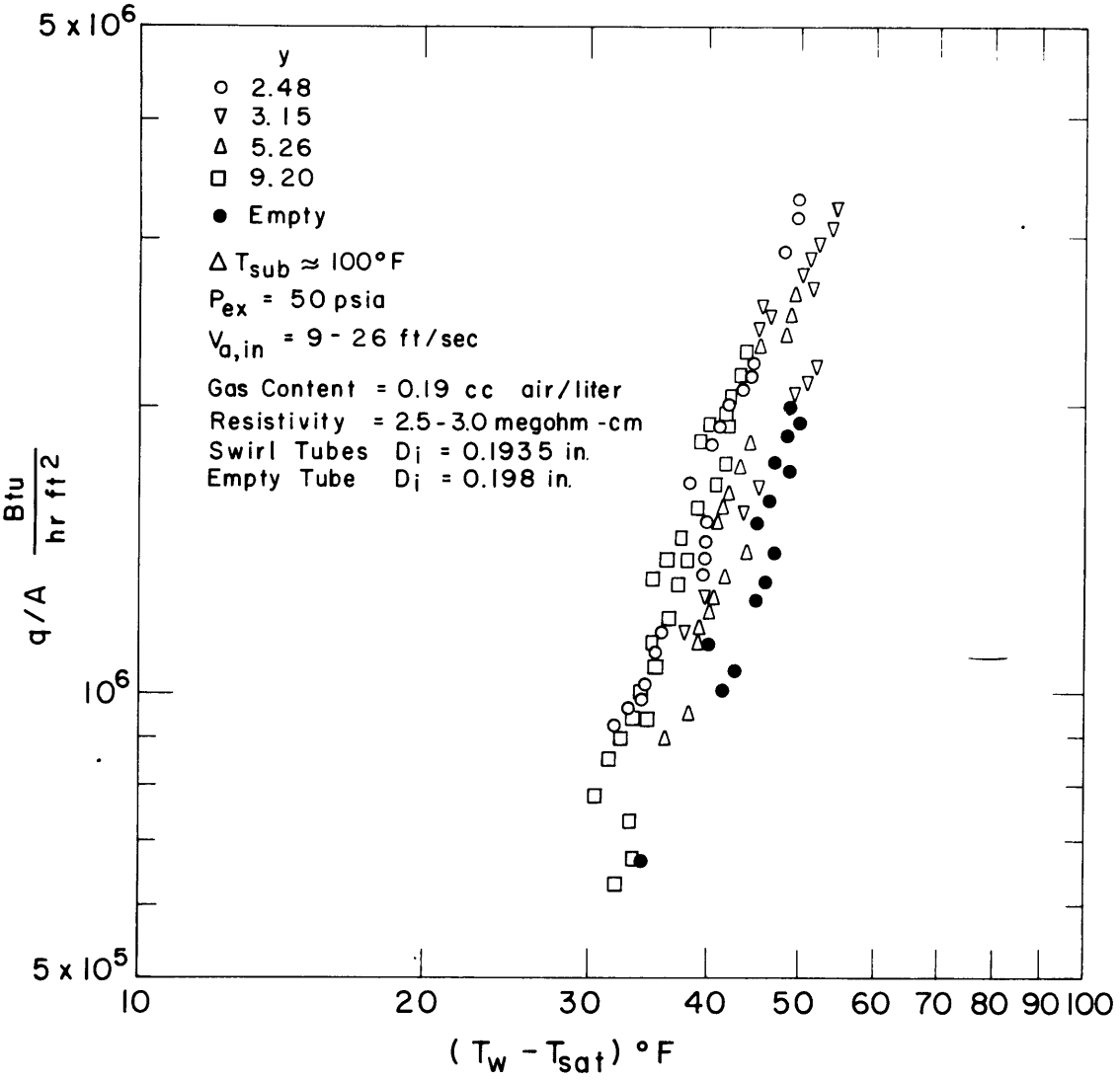

FIG. 25 COMPOSITE OF FULLY DEVELOPED SURFACE BOILING DATA.

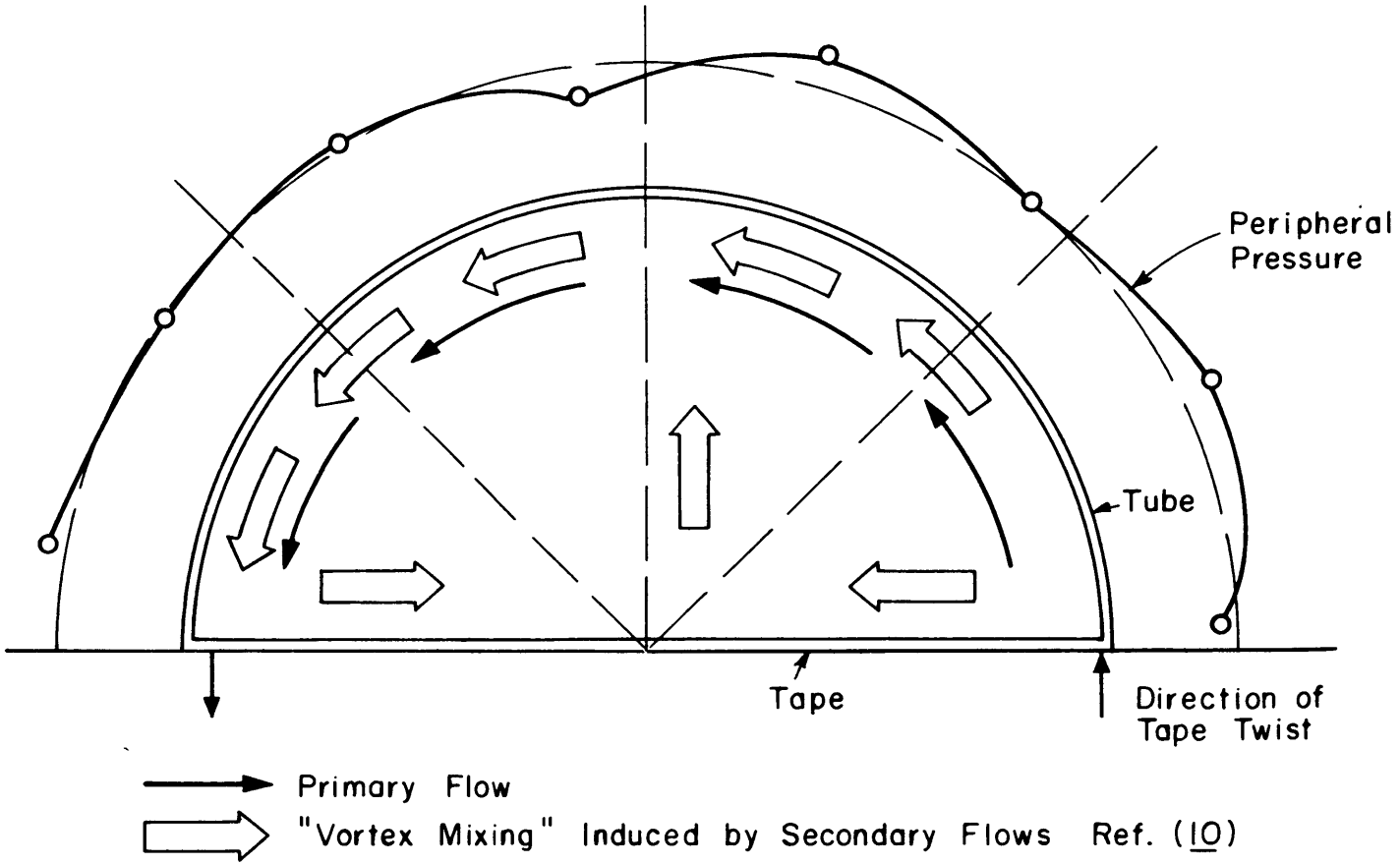

FIG. 26 TYPICAL PERIPHERAL PRESSURE VARIATION.

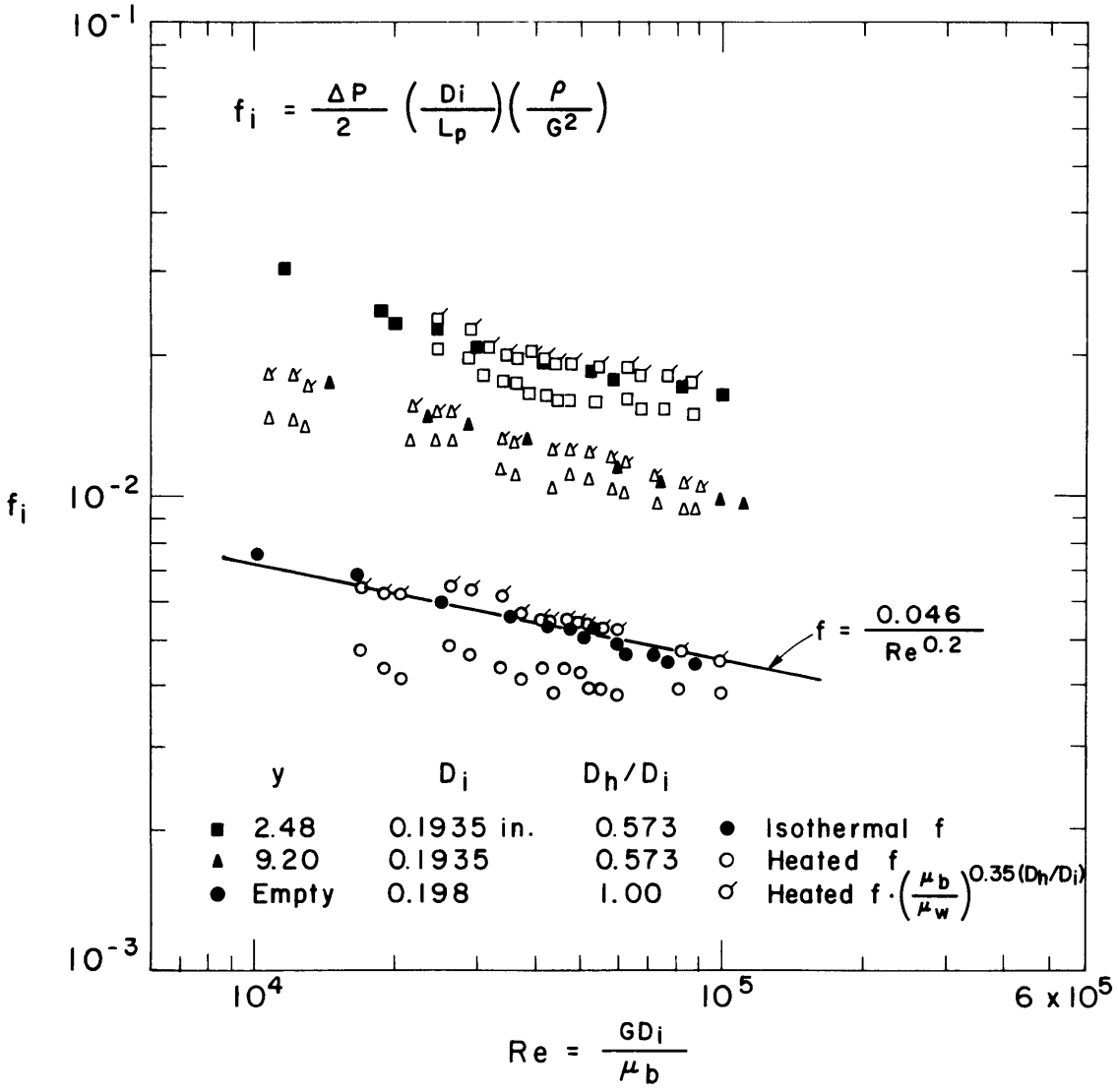

FIG. 27 NON-BOILING FRICTION FACTORS FOR ISOTHERMAL AND HEATED CONDITIONS.

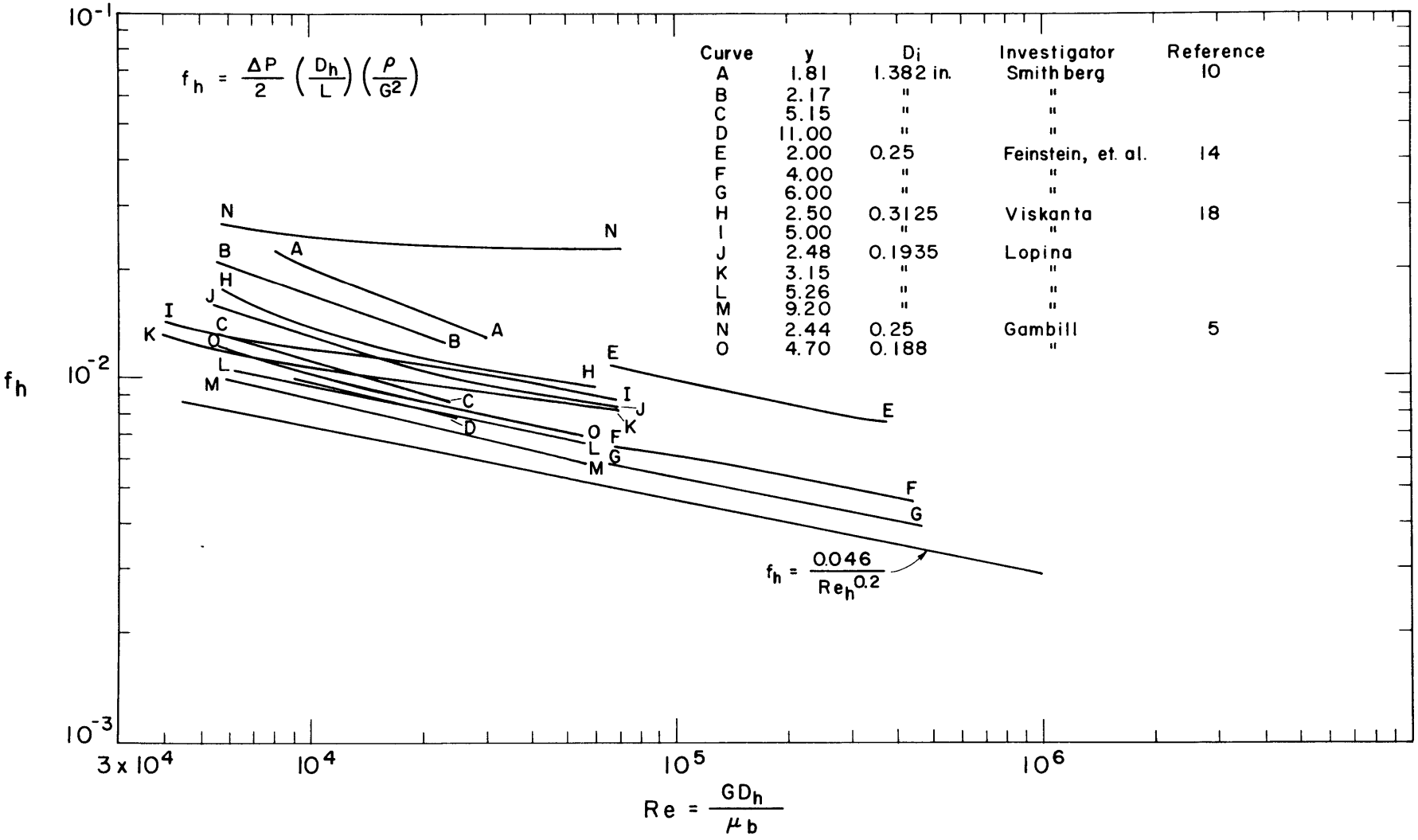

FIG. 28 COMPARISON OF ISOTHERMAL SWIRL FLOW FRICTION FACTORS.

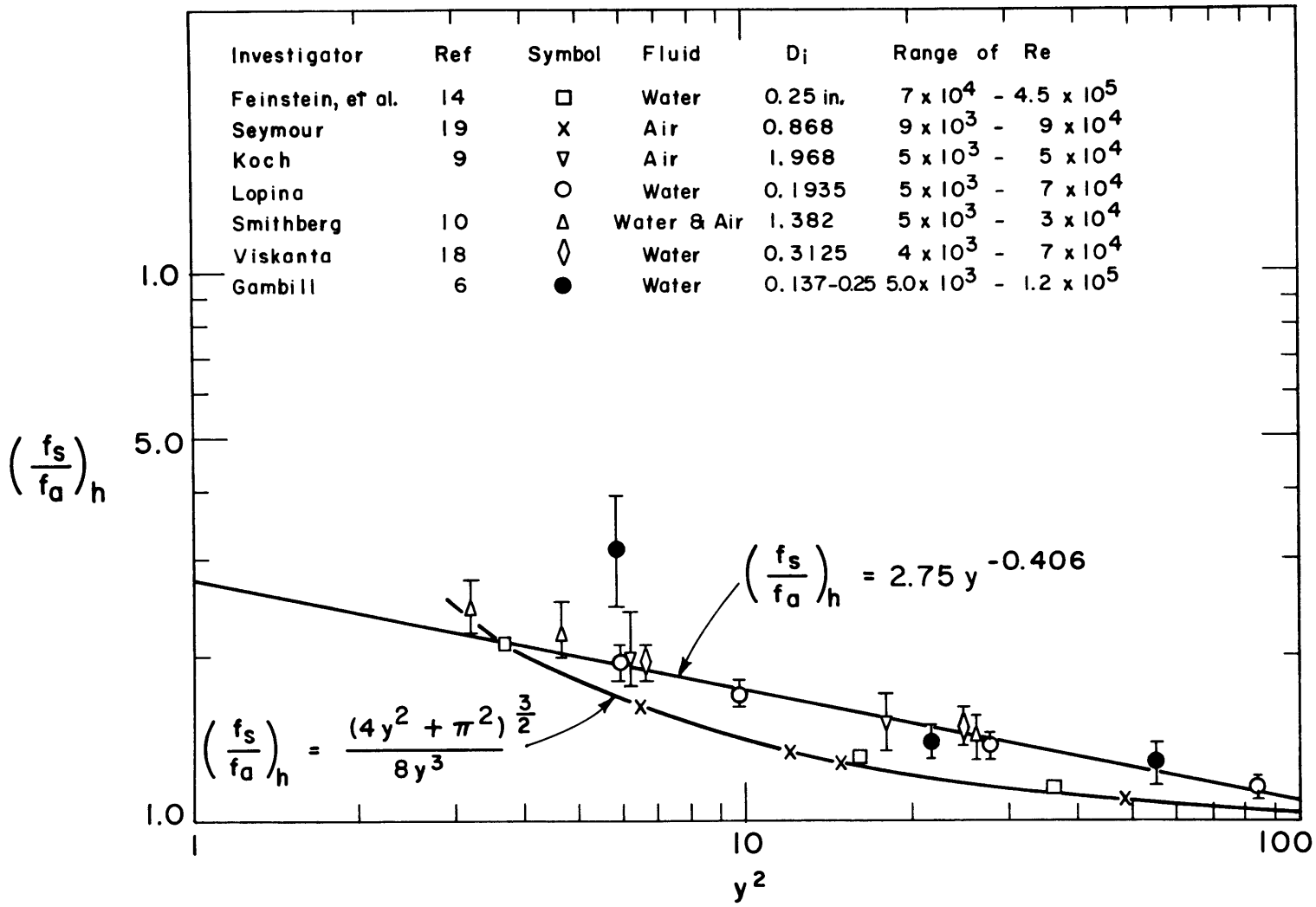

FIG. 29 CORRELATION OF ISOTHERMAL SWIRL FLOW FRICTION FACTORS.

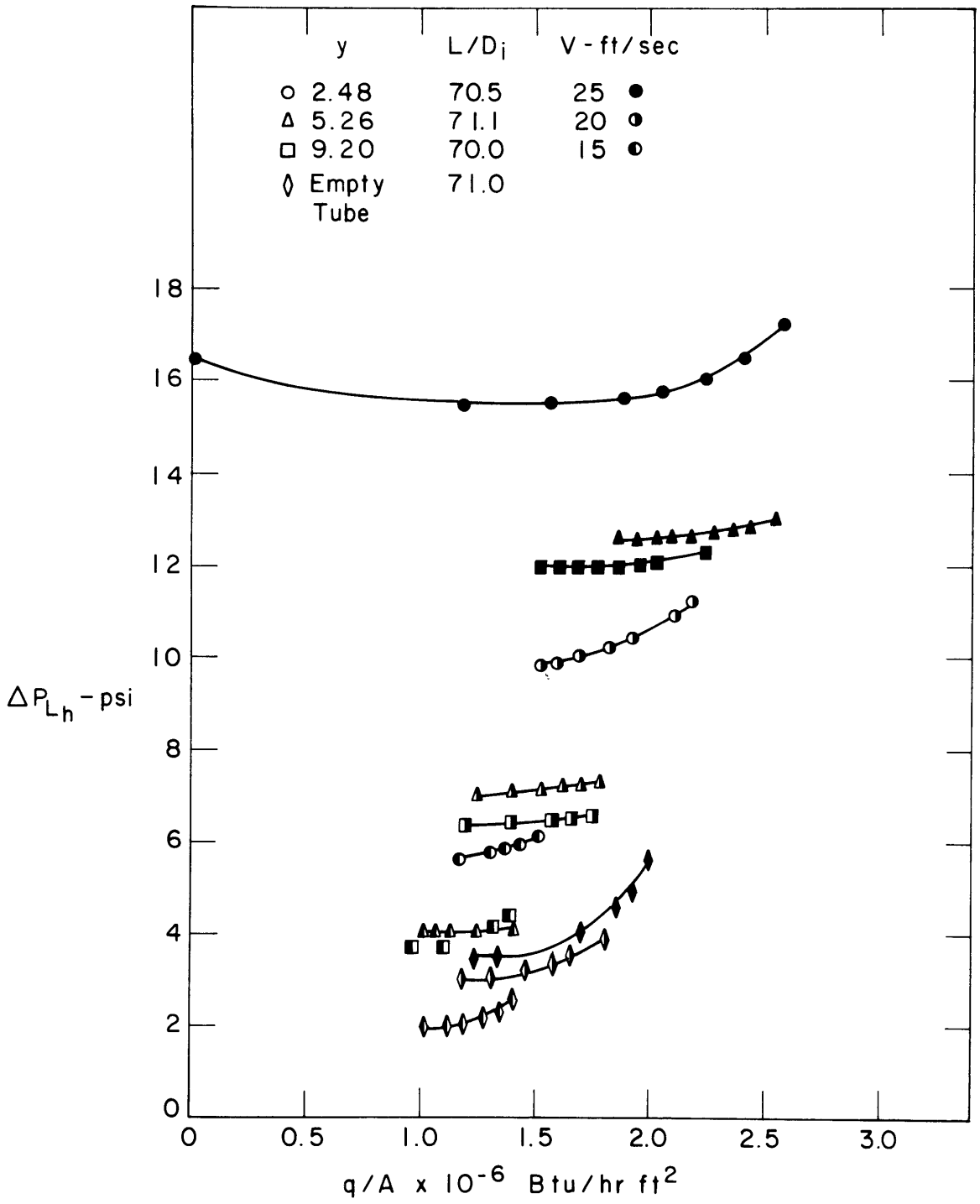

FIG. 30 OVERALL PRESSURE DROP FOR SURFACE BOILING OF WATER IN SWIRL FLOW.

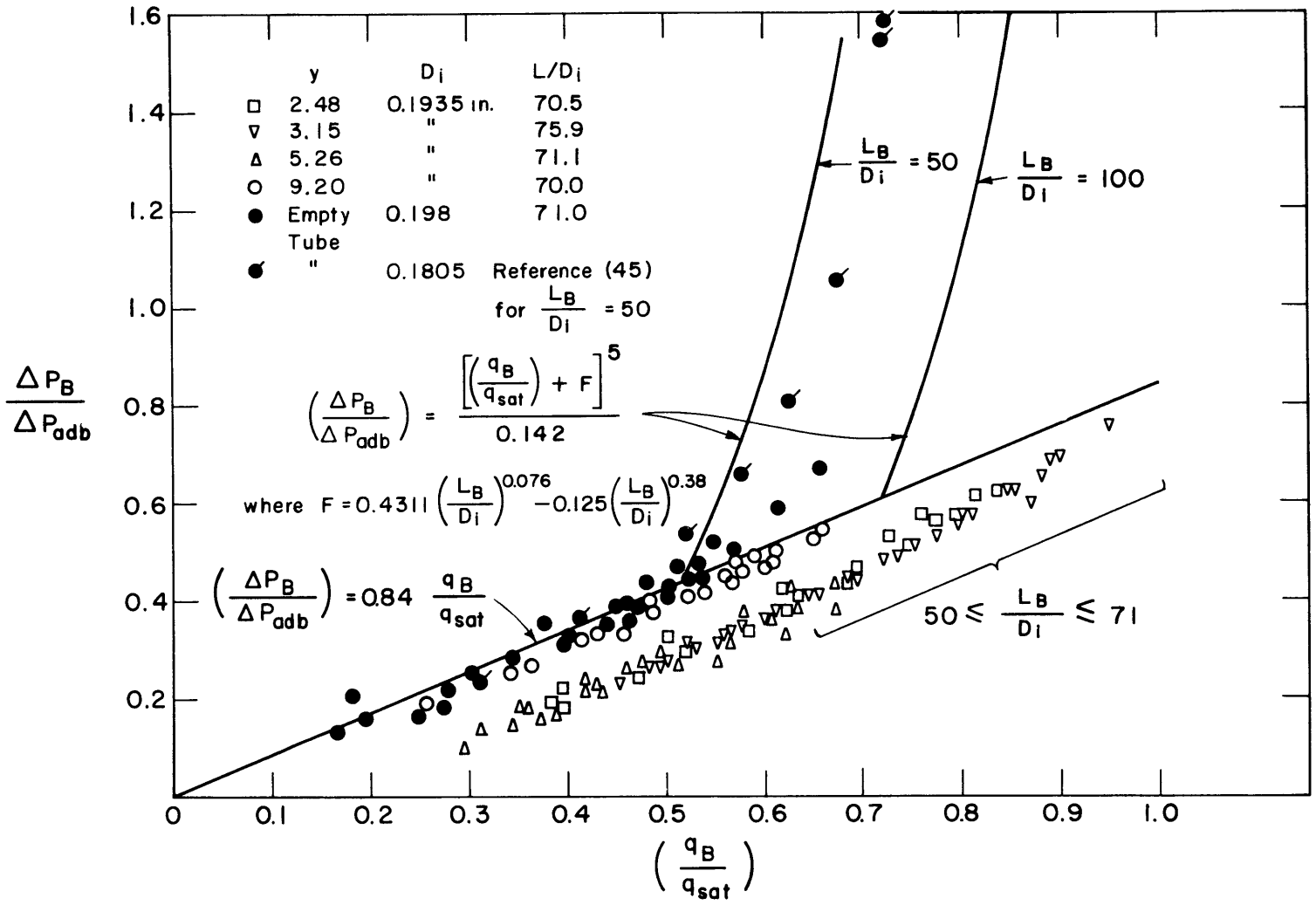

FIG. 31 COMPARISON OF THE SURFACE BOILING PRESSURE DROP FOR SWIRL AND STRAIGHT FLOW.

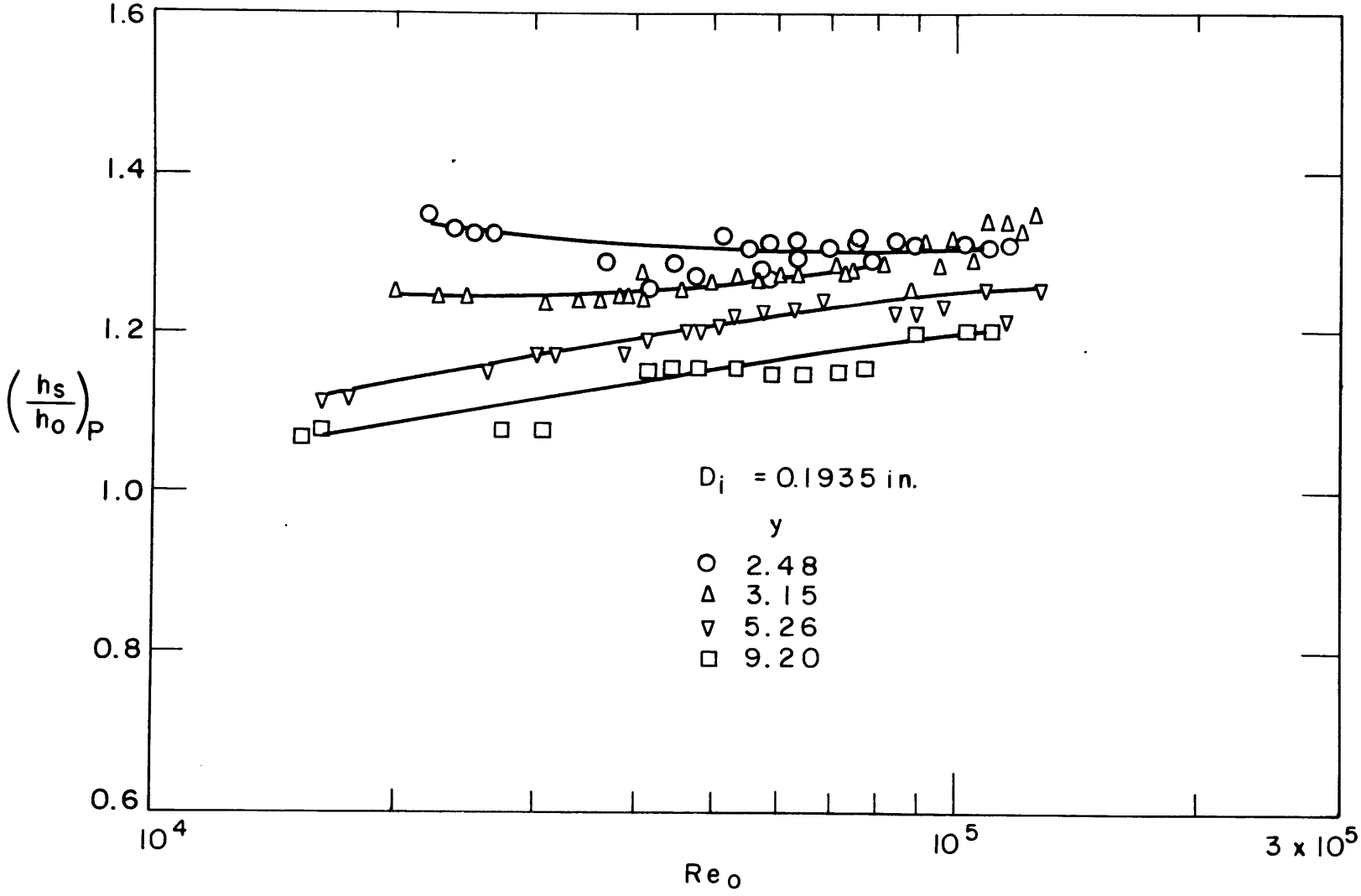

FIG. 32 CONSTANT PUMPING POWER PERFORMANCE OF PRESENT SWIRL FLOW SYSTEMS.

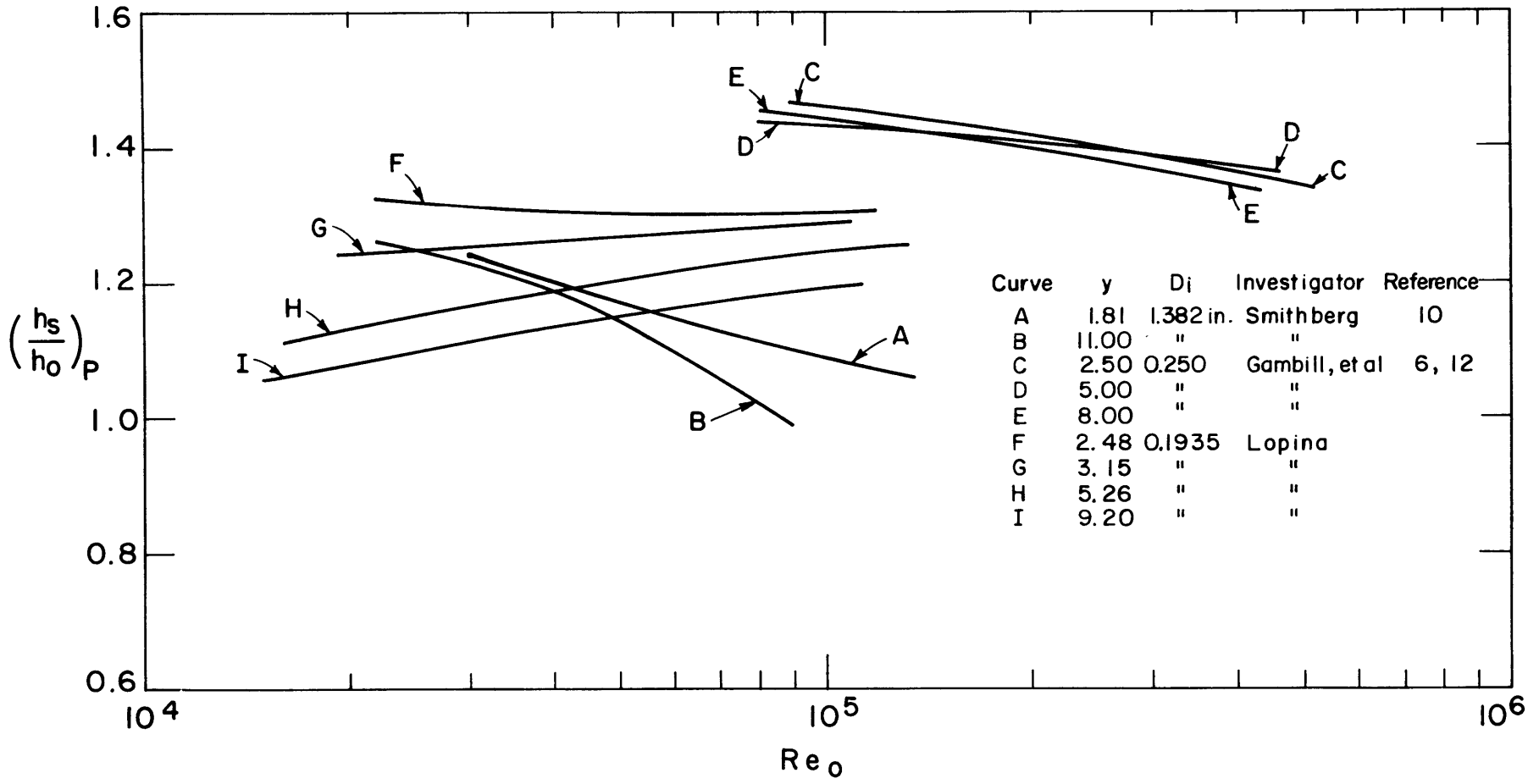

FIG. 33 CONSTANT PUMPING POWER COMPARISON INCLUDING DATA OF PREVIOUS INVESTIGATIONS.